UNIVERSITÀ
DEGLI STUDI
DI PADOVA

Head Office: Università degli Studi di Padova

Department of Civil, Environmental and Architectural Engineering (ICEA)

Ph.D. COURSE IN: Civil and Environmental Engineering Sciences
CURRICULUM: Structural Engineering
SERIES: XXX

LOSS ASSESSMENT MODELS FOR SEISMIC RISK MITIGATION IN STRUCTURES

Coordinator: Prof. Stefano Lanzoni
Supervisor: Prof. Carlo Pellegrino
Co-Supervisor: Dr. Mariano Angelo Zanini

Ph.D. student : Lorenzo Hofer

To my family, with gratitude

ABSTRACT

Seismic risk can be defined as an inclusive term that encompasses the probability of different ground motions and the related consequences, depending on the structural vulnerability. Seismic risk analysis is a general procedure that usually can consider different indicators, for both a specific structure or at territorial level: among others, for civil structures, risk is expressed in terms of monetary losses, i.e. costs to be sustained for repairing seismic damage or loss of revenue. This work wants to contribute to the current seismic risk assessment approaches with original contributions to the analysis of both point-like and territorial assets, focusing on some aspects, that are still not or poorly treated in literature. Regarding seismic risk analysis for a single specific structure, this work focuses on seismic risk analysis of industrial productive processes, with particular reference to business interruption losses. Recent seismic events, as the Emilia-Romagna earthquake in 2012, showed that such type of indirect losses can be very significant, and therefore a model is proposed to fill this lack of models for assessing indirect losses due to business interruption. Furthermore, a financial framework is also set up to assess the optimal seismic retrofit strategy for productive processes. In regard to the seismic risk analysis at territorial level, a seismic risk map of Italy is developed. Some considerations on historical losses and the implementation of specific earthquake catastrophe funds is also discussed. Finally, a deep insight on Catastrophe bonds (CAT bonds), as financial tool for transferring potential losses arising from natural hazards is illustrated. In particular, a novel reliability-based CAT bond pricing framework is developed, and applied to a case study represented by the Italian residential building portfolio.

SOMMARIO

Il rischio sismico può essere definito come un termine riassuntivo che comprende la probabilità del verificarsi in un certo sito di differenti campi di scuotimento, le perdite correlate, considerando la vulnerabilità strutturale. L'analisi di rischio è un metodo generale che può far riferimento a più indicatori in base al problema indagato, sia a livello di struttura specifica, sia a livello territoriale; per strutture civili, spesso si fa riferimento alle perdite monetarie, cioè il costo che deve essere sostenuto per riparare il danno strutturale derivante dal sisma. Questo lavoro approfondisce il rischio sismico sia a livello locale/puntuale, sia a livello territoriale, focalizzandosi su temi ancora poco approfonditi. A livello locale, la tesi si concentra sull'analisi di rischio sismico in ambito industriale con particolare riferimento ai danni da interruzione di esercizio. Recenti eventi sismici, come il terremoto in Emilia del 2012, hanno infatti dimostrato come tale tipologia di perdite possa essere particolarmente significativa; viene quindi sviluppato un modello per il calcolo delle perdite da interruzione di esercizio. Viene inoltre sviluppato un framework per valutare l'ottima strategia di retrofit sismico per la filiera produttiva. Nell'ambito dello studio del rischio sismico su scala territoriale, viene calcolata la mappa di rischio sismico per il territorio italiano. Vengono poi fatte alcune considerazioni sulle perdite causate dai terremoti passati, e sulla possibile implementazione di un fondo catastrofale nazionale. Infine, questo lavoro approfondisce i Catastrophe bond (CAT bond) come strumento finanziario per il trasferimento del rischio da disastri naturali. In particolare, viene sviluppata una procedura matematica rigorosa, basata su un approccio affidabilistico, per il pricing dei CAT bond. Tale procedura viene quindi applicata ad un caso studio e i risultati sono ampiamente discussi.

TABLE OF CONTENTS

List of Figures

List of Tables

Introduction

In recent years, the number of significant losses following natural disasters worldwide has been rapidly growing. Just considering the last thirty years, recent data (Munich RE 2017) show a significant increasing trend of losses due to natural hazards (Figure 0.1).

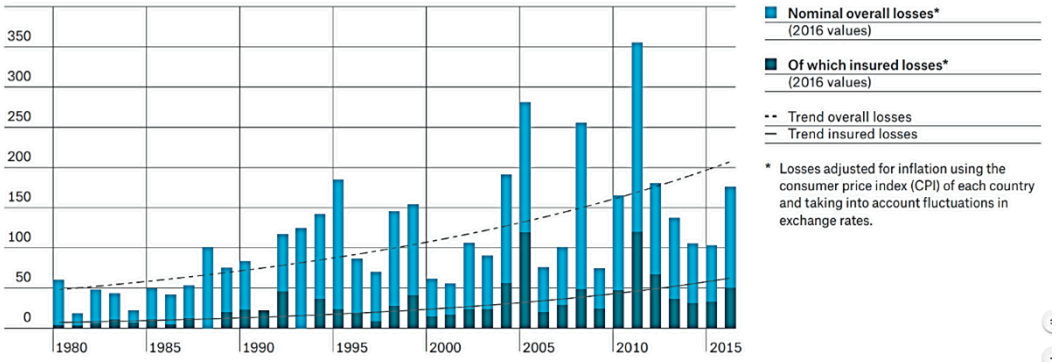

Figure 0.1: Overall losses and insured losses 1980-2016 due to natural disasters (in US$ bn).

This is mainly due to the urbanization, the growing world population and Gross Domestic Product (GDP). These three factors imply a concentration of people and goods, thus increasing their exposure to natural hazards more than in the past (Daniell et al. 2011). In addition, the vulnerability of many structures and infrastructures is still high, since retrofitting and re-building are time and money consuming processes. According to Holtzer and Savage (2013), an increasing in the death toll due to large catastrophic seismic events in the course of the 21st century is expected and it is estimated in 2.57+/-0.64 million. Earthquake represent one of the most destructive natural event that can significantly affect the economy of a region and lead to long-term restoration processes (Cutler et al. 2016). Recent events have shown the importance of taking into account different aspects related to the vulnerability of industrial plants and productive processes, due to the

significant potential losses associated with both property damage and business interruption. In particular, it has been shown how the gross domestic product of an area hit by a seismic events, suffered a significant drop in a short-to-medium term after its occurrence (Fischer 2014, Tokui et al. 2017). For example, the 2011 Tohoku Earthquake and the subsequent tsunami caused a direct economic loss ranging between 479 and 710 *bn* $, and an estimated economic loss between 479-710 *bn* $ (10-15% of the national Gross Domestic Product, Daniell and Vervaeck 2012). For this reason, seismic risk assessment plays a key role for the knowledge of potential damage and consequent economic losses that an industry or an area might suffer in case of earthquake occurrence. At the same time, seismic risk assessment can be used as starting point for developing methodologies aimed at defining cost-benefit approaches for the identification of optimal retrofit strategies when dealing with complex systems.

Overview of seismic risk assessment approaches

Seismic risk can be defined as an inclusive term that encompasses the probability of different ground motions and the related consequences, depending on the structural vulnerability. Seismic risk analysis is a general procedure that usually can consider different indicators, for both a specific structure or at regional level: among others, for civil structures, risk is expressed in terms of monetary losses, i.e., costs to be sustained for repairing seismic damage or loss of revenue. Given its wide applicability, different scientific areas can be involved in the seismic risk assessment, especially seismology, geology, structural and earthquake engineering and economy. Three main components are involved in the calculation of the seismic risk: seismic hazard, representative of the site seismicity; seismic vulnerability, that quantifies the susceptibility of a structure to suffer

seismic damage for different levels of seismic action, and finally the exposure, that characterizes the amount of property/goods and their regional distribution and has to be used for translating physical seismic damage into loss estimates.

In order to perform a seismic risk analysis, these components have to be linked. The best current practice for seismic loss assessment for point-like structures, is the so-called Performance Based Earthquake Engineering methodology (PBEE), based on the calculation of the triple integral equation (Cornell and Krawinkler 2000, Ellingwood et al. 2007). This methodology was developed with the aim to improve the decision making procedures about the seismic performance of constructed facilities. Seismic risk is expressed in terms of the exceeding rate of a decision variable *dv* that can represent a cost, the number of casualties, the length of downtime or any other variable of interest. The main equation is the following:

$$\lambda(dv) = \int_{dm}\int_{edp}\int_{im} G(dv \mid dm)\left|dG(dm \mid edp)\right|\left|dG(edp \mid im)\right|\left|d\lambda(im)\right| \qquad 0.1$$

where $\lambda(dv)$ is mean annual frequency of a decision variable *dv*, being exceeded through the consideration of the range of seismic intensities, *im*, plausible for a given site. Each intensity level considers the integration of probability distributions of a likely decision variable *dv* (usually repair cost, loss ratio, downtime), conditioned on expected damage *dm*, of components within a facility experiencing engineering demands parameters *edp* (e.g., interstory drift or force demands to structural members) for a given intensity level with a corresponding annual rate of exceedance $\lambda(im)$. In Eq. 0.1, $G(x \mid y) = P(X \geq x \mid Y = y)$ is the conditional complementary cumulative distribution function of *X* given *Y* (CCDF) and $dG(x \mid y)$ and $d\lambda(im)$ are the differentials of $G(x \mid y)$ and $\lambda(im)$. Absolute value signs are

required for each of the terms in Eq. 0.1, as some of the derivatives of the CCDF's may be negative. Computation of Eq. 0.1 requires four important stages: *hazard analysis*, *structural analysis*, *damage analysis* and *loss analysis*. In the following a description of every stages is provided; further information regarding the details of the PBEE framework can be found within Cornell and Krawinkler 2000, Ellingwood et al. 2007 and Der Kiureghian 2005.

The *hazard analysis* stage aims to quantify the site hazard characteristics and usually results in an occurrence relationship that describe the frequency of exceedance of a given intensity measure *IM* (e.g., the Peak Ground Acceleration PGA or the first mode spectral acceleration $S_a(T_1)$) of the ground motion at the site of interest ($\lambda(IM)$).

The *structural analysis* stage deals with the modelling of the seismic response of the structure, aiming to obtain useful response quantities (*EDP*). The output of this stage is the probabilistic distributions of *EDPs*; in particular $P[EDP \geq edp \mid IM = im]$ that is the conditional probability that *EPD* exceeds a specific level *epd*, given that *IM=im*.

These *EDPs* are used for estimating damage to various components of a building during the *damage analysis* stage. Output of this stage, $P[DM = dm \mid EDP = edp]$, represents the probability of being in a damage state *dm* given that the *EDP* is equal to a given *edp*. The final stage in this comprehensive framework is the *loss analysis*: here, losses (i.e., the *DVs*) due to the chosen *DMs* are computed. *DMs* are defined at the component level, while *DVs* are defined at system or building level.

Commonly, the Expected Annual Loss (*EAL*) is used as synthetic economic indicator of the seismic risk analysis process herein described. In order to compute *EAL*, all losses (*dv*) has to be integrated over the entire range of probability:

$$EAL = \int_0^{\infty} dv \left| dP(dv) \right| \qquad 0.2$$

EAL is widely used because it allows quantifying benefits associated to a retrofit intervention, but also because it provides a reasonable estimate of the insurance premium that can be expected based on the design or strengthening decision taken (Williams et al. 2009, ATC 2011).

Objectives of the study

Sesmic risk analysis is a consolidated general procedure that can be applied for assessing the risk of several losses associated to seismic hazard. This general methodology can be performed on two different levels: at a local or regional scale. In the first case, the object of the analysis is usually a single building. In the latter case, the analysis can consider an urbanised area, a whole region or nation. In this context, the thesis wants to contribute to the current seismic risk assessment approaches with original contributions to the analysis of both point-like and regional assets, since some aspects are still not or poorly treated in literature.

Regarding the seismic risk analysis of point-like structures, thesis focuses on the development of a detailed model able to assess indirect losses due to business interruption of industrial productive processes. This model considers the fragility of each element of the productive process, its restoration time and the logic scheme of the productive process. For computing monetary losses due to business interruption, data coming from the balance sheet of the analysed company will be used, with the aim to formulate a framework for assessing the *EAL* due to business interruption consequences, that is a relevant component of loss when dealing with businesses. Results are then used for defining a financial framework for

finding the optimal retrofit strategy to be implemented in a productive process.

As regard the seismic risk analysis at regional level, first the thesis focuses on the seismic risk assessment for the Italian territory. The risk map for Italy is developed and the national *EAL*, referring to direct losses on residential buildings, is computed. A historical analysis on past suffered losses, and the behaviour over time of a possible national catastrophe fund, is also provided. Finally, the thesis aims to give a deep insight on Catastrophe bonds (CAT bonds) as financial tool for transferring the risk of significant potential losses arising from natural hazards, to the financial market. In particular, a new reliability-based mathematical framework for CAT bond pricing, is developed and lastly applied to a case study represented by the Italian residential building stock.

Outline of the thesis

A brief thesis outline is herein presented:

- **Chapter 1** describes in detail the model that has been developed for assessing the indirect losses due to business interruption of an industrial process. The model is then applied to a real case study of an Italian cheese factory; at the end of the Chapter, results are widely discussed.
- **Chapter 2** illustrates the proposed financial framework for assessing the optimal retrofit strategy for a productive process, through the use the Actualized Future Cash Flows vs Initial Investment curve (*AFCF-II curve)*. The proposed method is then applied to a case study and results are critically discussed.
- **Chapter 3** shows the vulnerability and exposure of the Italian building stock, at a municipality level. Then the seismic risk map of Italy is computed, and compared with the Italian seismic hazard

map. Some considerations on historical losses and the implementation of specific earthquake catastrophe funds are also included in the Chapter.

- **Chapter 4** presents a mathematical formulation developed for a reliability-based CAT bond pricing. The proposed formulation allows considering uncertainties in model parameters and thus defining the CAT bond price based on a fixed acceptable level of risk.
- **Chapter 5** illustrates a possible CAT bond-based coverage configuration, against earthquake-induced losses, for the Italian territory.

1 Seismic loss estimation for enterprises, including interruption of business

Recent seismic events worldwide have shown how industrial complexes may be significantly vulnerable and suffer high financial losses when an earthquake occurs. Structural damage may also have serious consequences in terms of business interruption, leading in some cases to bankruptcy. Several researchers have studied single cases of loss assessment due to seismic damage and quantification of the resilience of structural systems, but no comprehensive study of seismic risk assessment of businesses has been published.

This chapter proposes a new probabilistic framework for seismic risk assessment of potential non-structural losses to production chains and the consequences of business interruption in all kinds of enterprises. The framework is composed of modules in which seismic hazard, vulnerability, exposure and recovery are stochastically characterized. An application to a case study, a typical Italian cheese-producing facility, is presented and results are discussed. Details can be found in Hofer et al. 2018a.

1.1 Introduction

Earthquakes represent one of the most destructive natural events that can significantly affect the economy of a region and lead to disruptions with associated long-term restoration processes (Cutler et al. 2016). Recent experiences have shown how the gross domestic product of an area hit by a seismic event suffers a significant drop in a short-to-medium term after its occurrence (Dosanjh 2011; Fischer 2014; Tokui et al. 2017). Particularly, productive processes can be negatively affected by seismic events, and damaged enterprises can experience severe financial losses.

Loss estimation is therefore a matter of significant interest in the research on earthquake engineering: in this regard, over the years a probabilistic Performance-Based Earthquake Engineering framework has been developed for considering the size hazard, structural vulnerability and exposure (see Introduction). Uncertainties in seismic hazard, vulnerability, and damage consequences are thus combined through the total probability theorem. The decision variable can represent a direct loss induced to structures, and usually can be assessed through the so-called damage ratios (Mander et al. 2012), commonly derived from datasets of past events (HAZUS-MR4 2003; Dolce and Manfredi 2015). On these bases, Porter et al. (2004) and Williams et al. (2009) defined an average value of loss amount, called Expected Annual Loss (EAL), as synthetic economic indicator. The greatest advantage of EAL is to take into account a wide set of seismic scenarios, with the associated losses and occurrence probabilities, into a single mean value.

Loss estimates can be performed also analyzing indirect consequences associated with earthquake-induced structural damages. In general terms, indirect losses can be viewed as the economic quantification of the time duration of structural system downtime (Cimellaro et al. 2010a). Resilience to seismic events can be adopted as suitable metrics to describe indirect effects of earthquakes on structural systems (Bruneau et al. 2003; Cimellaro et al. 2006; McAllister 2013; Sharma et al. 2017 and Liu et al. 2017).

Recently, some researchers studied the concept of resilience (Xu et al. 2007; Jacques et al. 2014; Biondini et al. 2015; Broccardo et al. 2015) and proposed probabilistic approaches mostly oriented to its inclusion in seismic risk assessment of strategic buildings and urban areas (Cimellaro et al. 2010b; Mieler et al. 2014; Burton et al. 2015). However, no study was performed on the analysis of earthquake–induced consequences on businesses, even though disruption can seriously compromise financial stability of small-to-medium enterprises (Rose 2004).

This chapter provides an original methodological contribution to the existing literature in seismic risk assessment of existing structural systems. In particular, the novelty element regards the subject of the analysis, a business productive process composed by several components. A model for the economic quantification of losses is proposed, starting from the recovery functions of the components of a process and the balance sheet data of the company. An application of the proposed framework is lastly shown on a typical Italian cheese-production facility located in North-Eastern Italy and results are critically discussed.

1.2 Probabilistic seismic risk estimation procedure

Figure 1.1 shows the key steps of the proposed modular procedure, which is made by four main stages. The first is the definition of seismic hazard at the site of interest; then vulnerability of each productive process component is estimated, and non-structural *(NS)* losses to process components are assessed. Lastly, business interruption (*BI*) economic consequences are evaluated. The procedure does not take into account directly the industrial building itself, since recent seismic events evidenced how, especially for new constructions, damage on structures was slight (Bournas et al. 2014). Conversely, significant damage was mostly observed in productive processes components, causing important losses due to business interruption.

The procedure adopts Monte Carlo sampling technique for considering uncertainties in the estimation of ground motions at site, damage states, repair cost ratios and recovery functions of each process component. In the following sections, a description of each main module is given.

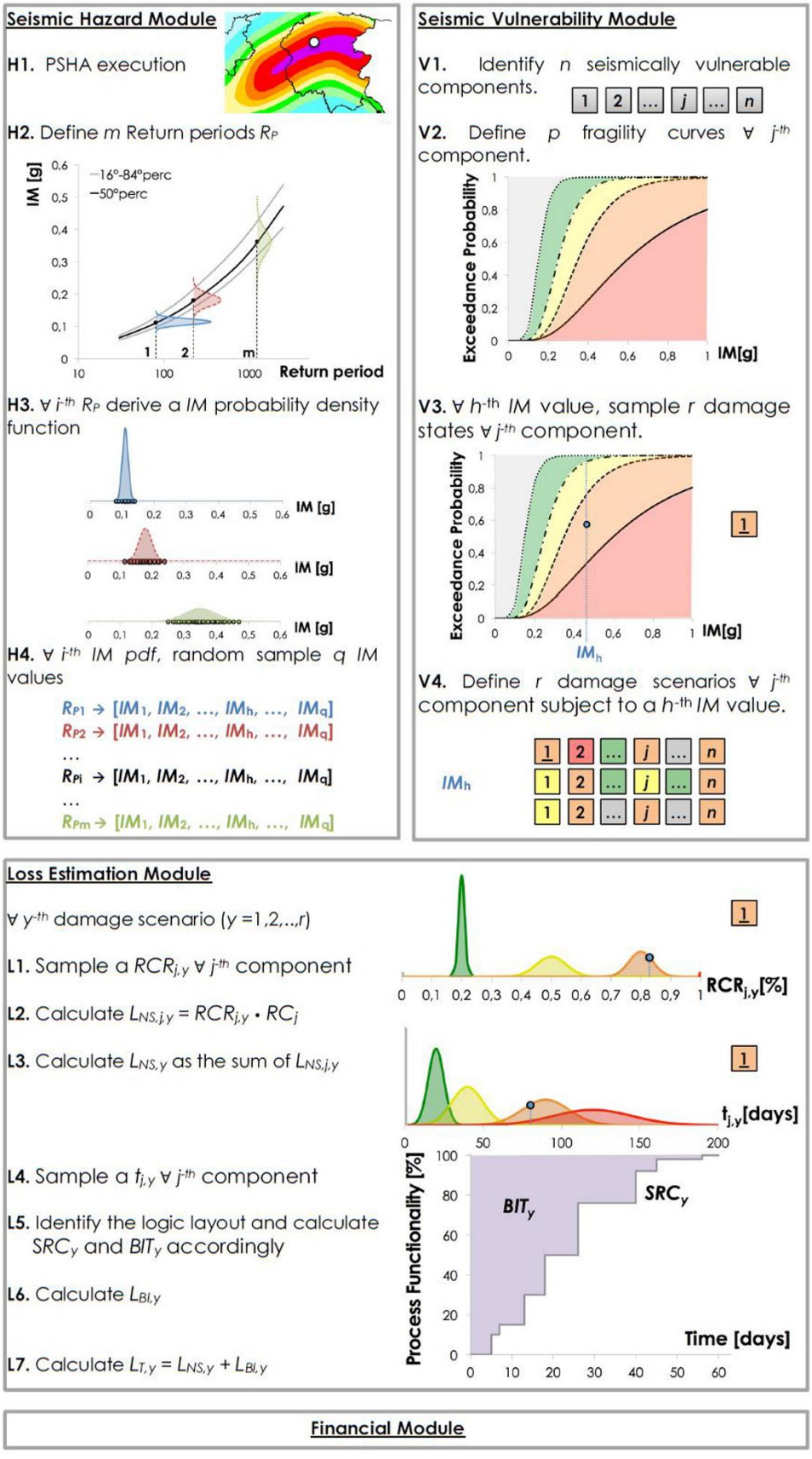

Figure 1.1: Flowchart of the proposed probabilistic seismic risk framework.

1.2.1 Seismic Hazard Module

The first stage of the procedure is the characterization of the seismicity of the site of interest through the definition of a set of intensity measure (*IM*) vectors, which defines ground motion at the site. For this aim, a Probabilistic Seismic Hazard Analysis (PSHA, Cornell 1968) can be performed, leading to define the mean annual rate of exceedance of a specific intensity measure *im*, $\lambda_{TOT}(IM>im)$ for a site subject to a set of seismogenic sources; alternatively, more sophisticated models can be implemented (e.g., Pace et al. 2006; Kumar and Gardoni 2013). The hazard curve allows to quantify the probability of exceeding each value of *IM* in next T years $P(IM>im, T)$ through Eq. 1.1, where the mean annual rate $\lambda_{TOT}(IM>im)$ can be considered according to Eq.1.2:

$$P\left(IM > im, T\right) = 1 - e^{-\lambda_{TOT}\left(IM>im\right)\cdot T} \tag{1.1}$$

$$\lambda_{TOT}\left(IM > im\right) = \frac{1}{R_P\left(IM > im\right)} \tag{1.2}$$

$R_P(IM>im)$ is the mean return period of a design earthquake characterized by a specific value of exceedance probability in fixed time span $P(IM>im,T)$. Hence, for a set of finite exceedance probabilities, it is possible to define the respective *IM* values, given a PSHA curve and fixed an observational time-window *T*. In particular, once defined a set of *i = 1, 2, .. m* exceedance probability values, by substituting Eq. 1.2 in Eq. 1.1, *m* couples of (R_P,IM) values can be derived.

Usually *PSHA* curves provide mean estimates of ground motion, but the calculation can be performed also for other significant percentiles: in this way, an *IM* probability density function *(pdf)* is derived instead of a single value, for each return period R_P. Finally, a vector of *h = 1, 2, .. q IM* values is randomly sampled for each i^{th} return period, according to its *IM pdf*. Every h^{th} *IM* value is then used for seismic vulnerability assessment of productive process components, under the reasonable assumption of uniform ground motion acting on all the productive process components.

1.2.2 Seismic Vulnerability Module

The seismic vulnerability module aims to define a set of stochastically sampled damage scenarios of the productive process subject to earthquake occurrence. For this reason, the $j = 1, 2, .. n$ process components potentially vulnerable to seismic actions must be identified. In conventional productive processes, tanks (Gonzalez et al. 2013), machineries (Swan et al. 1977), pipes and pumps (Fujita et al. 2012; Lanzano et al. 2012) can be usually seismic vulnerable components. For each of them of a set of $k = 1, 2, .. p$ fragility curves should be defined, for quantifying component's vulnerability, based on suitable damage indexes. Hence, productive process damage scenarios are randomly generated through Monte Carlo damage sampling for each j^{th} component, starting from the m vectors of IM values provided by the seismic hazard module.

Thus, a set of r damage scenarios is stochastically generated for each $IM_{h,i}$ value. In this way, a total number of $y = 1, 2, .. z$ (where $z = q * r$) damage scenarios are associated to each i^{th} return period R_P, combining uncertainties associated to damage estimate and hazard definition. Finally a visual survey is needed to define the layout of the productive process, i.e., to identify the logic flow model of the productive chain, and to locate within its rings the previously characterized seismically vulnerable components. This step gives information on the effect of each component on the overall functionality restoration of the system, for later quantification of losses due to business interruption.

1.2.3 Loss Estimation Module: Non-Structural Losses

Loss assessment is carried out taking into account randomness in the economic quantification of repair costs and restoration times, associated to structural damage suffered by each process component. Concerning NS losses, for each y^{th} damage scenario, the estimate is performed for every j^{th} process component, on the basis of its sampled specific damage state.

Uncertainty in the economic quantification of damage is accounted through the identification of a set of p probability density functions of the repair cost ratio RCR_j (i.e., the ratio between the cost to repair vs the total replacement cost RC_j) for the j^{th} process component. A RCR_j value is sampled for each j^{th} process component subject to a generic y^{th} damage scenario, and its *NS* loss $L_{NS,j,y}$ value is thus derived as:

$$L_{NS,j,y} = RCR_{j,y} \cdot RC_j \tag{1.3}$$

whereas productive process *NS* loss $L_{NS,y}$ is thus estimated through the aggregation of each component loss value.

1.2.4 Loss Estimation Module: Business-Interruption Losses

The estimation of *BI* losses is instead rather more complex, since requires additional financial data of the company and a description of the restoration process, clearly influenced by the entity of structural damages. First, a set of p recovery curves is defined for each j^{th} process component: recovery curves are usually described with cumulative probability density functions (HAZUS-MR4 2003). However, when dealing with single process components, continuous functions seem to be quite more conceptual than realistically representative of the effective functionality restoration actions.

For this reason, in this work one-step functions (e.g., Ayyub 2015) are adopted for the characterization of process component recovery, subject to a specific damage state. A one-step recovery function is defined with two parameters: the residual functionality value $RF_{j,k}$ (i.e., the functionality level immediately after the event occurrence) and the recovery time $t_{j,x}$ corresponding to the time instant in which the full recovery of the pre-event functionality is reached, both conditional to the component damage state.

Uncertainty in the quantification of the real recovery time $t_{j,x}$ is taken into account by adopting a *pdf* of $t_{j,x}$, herein assumed Gaussian. Starting from a y^{th} damage scenario, a one-step recovery curve is defined for each j^{th}

process component, by randomly sampling a recovery time value $t_{j,x}$ from the *pdf* associated to its damage state. Hence, the system recovery curve SRC_y is calculated according to graph theory (Zio 2006), since productive processes are mostly characterized by well-defined one-way flow layouts. In such terms, the business interruption time BIT_y caused by the occurrence of the y^{th} damage scenario can be estimated as:

$$BIT_y = \int_{t_0}^{t_{SR}} \left[1 - SRC_y(t)\right] dt \qquad 1.4$$

where t_0 and t_{SR} are respectively the time instant of earthquake occurrence and of the achievement of complete functionality restoration. The business interruption time BIT_y is then used for the economic quantification of losses. For the appraisal of business interruption losses, it is necessary to know the financial profile of the enterprise and thus realize the entity of its revenues and expenses. One other important concept is the distinction between fixed expenses and costs ceasing in case of disruption of the productive chain. Particularly, it is necessary to consider as revenues the sales of goods (*GSR*) manufactured by the production chain, and the closing inventory (*CIR*) thought as future sales. Concerning the expenses, opening stocks (*OSC*), purchase costs for raw materials (*RMC*) to be processed, costs for energy services (*ESC*), costs for salaries of the employees (*SEC*) and other different kinds of expenses (*OC*) must be derived from the income statement of the company. In case of earthquake occurrence, the company loses a fraction of annual revenues proportional to the BIT_y value and at the same time ceasing costs, whereas it still must pay fixed expenses. Some costs like energy services can be considered partially ceasing: for this reason a cessation index α_C (with $0 \leq \alpha_C \leq 1$) representing the percent degree of cessation of a service can be defined. In such way, for a generic y^{th} damage scenario, *BI* losses $L_{BI,y}$ can be calculated as:

$$L_{BI,y} = \frac{BIT_y}{365}\left[\alpha_{C1} GSR + \alpha_{C2} CIR - \alpha_{C3} OSC - \alpha_{C4} RMC - \alpha_{C5} ESC - \alpha_{C6} SEC - \alpha_{C7} OC\right] \qquad 1.5$$

1.2.5 Loss Estimation Module: Total Losses

Total losses $L_{T,y}$ for a generic y^{th} damage scenario can be estimated by the aggregation of direct and indirect contributions as:

$$L_{T,y} = L_{NS,y} + L_{BI,y} \tag{1.6}$$

The loss estimation module thus provides z values of $L_{NS,y}$, $L_{BI,y}$ and $L_{T,y}$, useful for a stochastic description of the impact of earthquakes, with different return periods R_P. Hence, considering a representative value of the loss *pdf* (e.g., 50th percentile), a set of m couples of data can be used for the definition of a loss exceedance curve.

Subsequently, the expected annual non-structural loss EAL_{NS} is derived by integrating the whole NS loss values over the entire range of probabilities, as follows:

$$EAL_{NS} = \int_0^{\infty} L_{NS,y} \left| dP\left(L_{NS,y}\right) \right| \tag{1.7}$$

whereas, similarly, the expected annual loss due to business interruption EAL_{BI} and the expected annual total loss EAL_T can be calculated as:

$$EAL_{BI} = \int_0^{\infty} L_{BI,y} \left| dP\left(L_{BI,y}\right) \right| \tag{1.8}$$

$$EAL_{T} = \int_0^{\infty} L_{T,y} \left| dP\left(L_{T,y}\right) \right| \tag{1.9}$$

EAL_{NS}, EAL_{BI} and EAL_T values are synthetic economic indicators of the impact of seismic events on a productive chain, representative of the weighed sum of losses induced by a wide range of earthquakes with different exceedance probability values.

1.3 Application to a case study

1.3.1 Input data

The proposed framework for the seismic loss assessment for a productive process has been applied to a cheese-producing facility located in the Municipality of Gemona del Friuli, a high seismic area in North-East Italy. First, a probabilistic seismic hazard analysis has been performed, assuming suitable source zone model and ground motion prediction equations (Meletti and Montaldo 2007, Meletti et al. 2008). Peak ground acceleration at bedrock has been amplified by considering a soil-type B and a topographic coefficient T1, in accordance to the Italian Ministry of Infrastructures (2008). Nine return periods R_P have been considered (30, 50, 72, 101, 140, 201, 475, 975 and 2475 years), respectively corresponding to 81%, 63%, 50%, 39%, 30%, 22%, 10%, 5% and 2% exceedance probabilities in a time span T = 50 years (Italian Ministry of Infrastructures 2008). Figure 1.2 shows resulting 16th, 50th and 84th percentile seismic hazard curves for the site of Gemona del Friuli, while Table 1.1 reports the numerical values. A vector of q =150 PGA values has been randomly sampled for each i^{th} return period R_P, accounting for the variability associated with the definition of the seismic action.

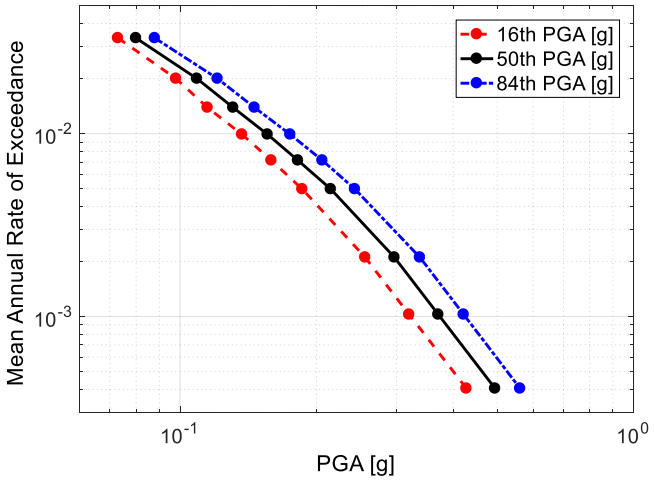

Figure 1.2: Seismic hazard curve of the production site.

Table 1.1: Seismic hazard data of the production site.

$P(IM>im,50)$	81%	63%	50%	39%	30%	22%	10%	5%	2%
Return period R_P	30	50	72	101	140	201	475	975	2475
16^{th} PGA [g]	0.073	0.098	0.115	0.137	0.159	0.186	0.256	0.320	0.428
50^{th} PGA [g]	0.080	0.109	0.131	0.156	0.182	0.215	0.297	0.371	0.495
84^{th} PGA [g]	0.088	0.121	0.146	0.175	0.206	0.243	0.338	0.422	0.562

With reference to the vulnerability module, the first step was to identify the *n* seismically vulnerable components in the production chain: this step is essentially based on knowledge of the productive process itself. Figure 1.3 shows the production scheme of the cheese-producing facility, which is composed by 13 seismically vulnerable elements. The productive process can be briefly described as follows: milk is initially stored in a steel tank (*Tank 1*) from which it is piped (*Pipe 1* and *2*) to two specific tanks (*Tank 2* and *3*) for the pasteurization and subsequent skimming of the cream. Hence, piping systems (*Pipe 3* and *4*) deliver milk to bell boilers (*Machine 1*, *2*, *3* and *4*) and leads to the production of cheese curds. Once properly drained, curds are placed in cheese hoops and then brined in basins containing a saturated salt solution (*Machine 5*). Finally, resulting cheese forms are matured for several months in special shelves (*Shelving*).

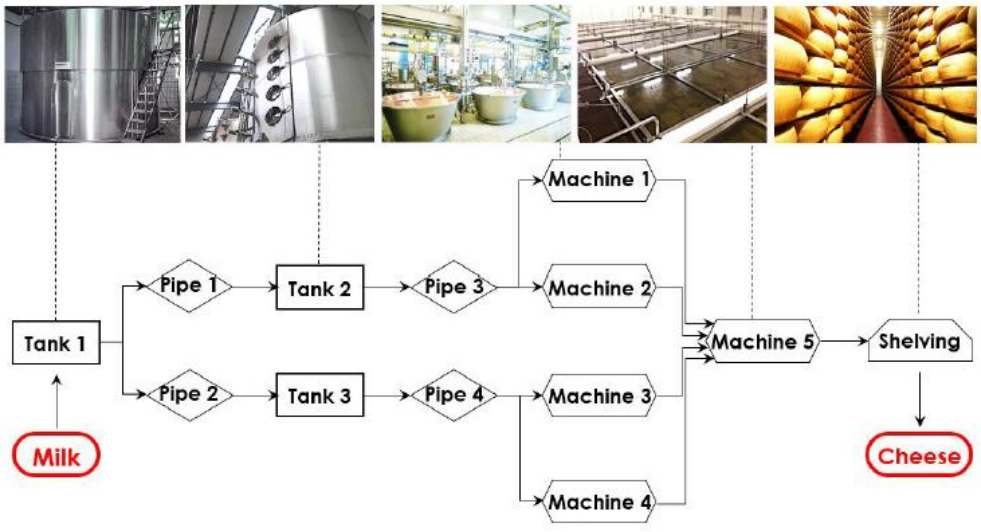

Figure 1.3: Logical scheme of the production process.

A set of fragility curves has been associated to each process component, as listed in Table 1.2. Main parameters have been derived from HAZUS-MR4 (2003): in particular, tanks have been modelled with the water system "on-ground anchored steel tank" type, pipes with the "elevated pipe" type, and for the remaining process components the acceleration-sensitive "manufacturing and process machinery" class has been considered. Specific structural models aimed to calibrate detailed component fragility functions may improve the accuracy of the results, but such analysis was beyond the scope of this work. Randomness in the damage assessment of each element has been considered through sampling r = 150 damage states for each h^{th} PGA value, leading to a total number of z = 22500 damage scenarios for each i^{th} return period R_P.

Table 1.2: Main parameters of fragility curves used for each process component.

Production step	Production process component	Damage State DS_k [PGA(g)]							
		μ_{DS1}	β_{DS1}	μ_{DS2}	β_{DS2}	μ_{DS3}	β_{DS3}	μ_{DS4}	β_{DS4}
Delivery of milk	Tank 1	0.3	0.6	0.7	0.6	1.25	0.65	1.6	0.6
-	Pipe 1	-	-	-	-	0.53	0.6	1.0	0.6
-	Pipe 2	-	-	-	-	0.53	0.6	1.0	0.6
Pasteurization/ Skimming	Tank 2	0.3	0.6	0.7	0.6	1.25	0.65	1.6	0.6
Pasteurization/ Skimming	Tank 3	0.3	0.6	0.7	0.6	1.25	0.65	1.6	0.6
-	Pipe 3	-	-	-	-	0.53	0.6	1.0	0.6
-	Pipe 4	-	-	-	-	0.53	0.6	1.0	0.6
Heating/ Curd production	Machine 1	0.2	0.68	0.4	0.65	0.8	0.65	1.6	0.65
Heating/ Curd production	Machine 2	0.2	0.68	0.4	0.65	0.8	0.65	1.6	0.65
Heating/ Curd production	Machine 3	0.2	0.68	0.4	0.65	0.8	0.65	1.6	0.65
Heating/ Curd production	Machine 4	0.2	0.68	0.4	0.65	0.8	0.65	1.6	0.65
Salt saturation	Machine 5	0.2	0.68	0.4	0.65	0.8	0.65	1.6	0.65
Cheese maturing	Shelving	0.2	0.68	0.4	0.65	0.8	0.65	1.6	0.65

1.3.2 *NS*, *BI* and *T* loss estimation

As regards *NS* loss estimates, a repair cost ratio $RCR_{j,y}$ has been randomly sampled for each j^{th} component from the Gaussian distribution of its specific damage state and for each i^{th} damage scenario. Table 1.3 lists main parameters of $RCR_{j,y}$ Gaussian distributions and replacement cost RC_j adopted for each j^{th} element, each assumed on the basis of an expert judgment.

Table 1.3: Main parameters of rapair cost ratio pdfs and replacement cost of each component.

Production process component	Replacement Cost RC_j [€]	Repair cost ratio $RCR_{j,y}$ [%]							
		$\mu_{RCR\|DS1}$	$\sigma_{RCR\|DS1}$	$\mu_{RCR\|DS2}$	$\sigma_{RCR\|DS2}$	$\mu_{RCR\|DS3}$	$\sigma_{RCR\|DS3}$	$\mu_{RCR\|DS4}$	$\sigma_{RCR\|DS4}$
Tank 1	32000	20	1	50	5	80	4	100	0
Pipe 1	36000	-	-	-	-	80	4	100	0
Pipe 2	36000	-	-	-	-	80	4	100	0
Tank 2	128000	20	1	50	5	80	4	100	0
Tank 3	128000	20	1	50	5	80	4	100	0
Pipe 3	36000	-	-	-	-	80	4	100	0
Pipe 4	36000	-	-	-	-	80	4	100	0
Machine 1	110000	20	1	50	5	80	4	100	0
Machine 2	110000	20	1	50	5	80	4	100	0
Machine 3	110000	20	1	50	5	80	4	100	0
Machine 4	110000	20	1	50	5	80	4	100	0
Machine 5	208000	20	1	50	5	80	4	100	0
Shelving	320000	20	1	50	5	80	4	100	0

Hence, $L_{NS,y}$ values have been stochastically assessed according to Eq. 1.3. Concerning *BI* losses, for each j^{th} process component of a generic y^{th} damage scenario, a one-step fragility curve has been randomly defined through sampling a recovery time value $t_{j,x}$ from the Gaussian *pdf* of its specific damage state. Table 1.4 lists residual functionality values $RF_{j,k}$ and main parameters of recovery time $t_{j,x}$ *pdf*, provided by the technical offices of each component manufacturers; Figure 1.4 shows the recovery functions for the process elements.

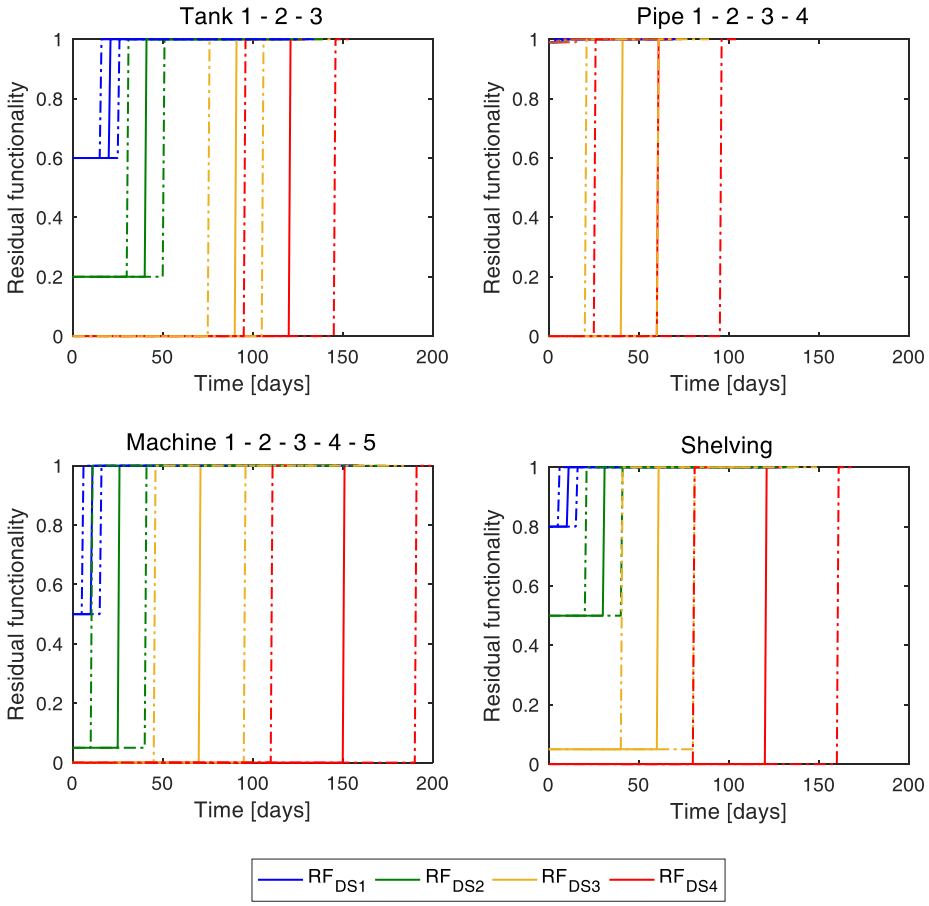

Figure 1.4: Recovery functions for the process elements (dashed lines represent +/- sigma).

Table 1.4: Main parameters of one-step recovery functions of each component.

Production process component	Residual functionality [%]				Recovery time $t_j \mid DS_k$ [days]							
	RF_{DS1}	RF_{DS2}	RF_{DS3}	RF_{DS4}	$\mu_{T\mid DS1}$	$\sigma_{T\mid DS1}$	$\mu_{T\mid DS2}$	$\sigma_{T\mid DS2}$	$\mu_{T\mid DS3}$	$\sigma_{T\mid DS3}$	$\mu_{T\mid DS4}$	$\sigma_{T\mid DS4}$
Tank 1	60	20	0	0	20	5	40	10	90	15	120	25
Pipe 1	-	-	0	0	-	-	-	-	40	20	60	35
Pipe 2	-	-	0	0	-	-	-	-	40	20	60	35
Tank 2	60	20	0	0	20	5	40	10	90	15	120	25
Tank 3	60	20	0	0	20	5	40	10	90	15	120	25
Pipe 3	-	-	0	0	-	-	-	-	40	20	60	35
Pipe 4	-	-	0	0	-	-	-	-	40	20	60	35
Machine 1	50	5	0	0	10	5	25	15	70	25	150	40
Machine 2	50	5	0	0	10	5	25	15	70	25	150	40
Machine 3	50	5	0	0	10	5	25	15	70	25	150	40
Machine 4	50	5	0	0	10	5	25	15	70	25	150	40
Machine 5	50	5	0	0	10	5	25	15	70	25	150	40
Shelving	80	50	5	0	10	5	30	10	60	20	120	40

Hence, SRC_y of the process has been built according to the process logical scheme and the recovery curve, sampled for each component, conditional to its damage state in a generic y^{th} scenario. Figure 1.5 shows, the set of 22500 SRC_y curves obtained for the nine considered R_P, evidencing 25th, 50th and 75th percentile curves (red line 25th percentile, green line 50th percentile, blue line 75th percentile).

R_P = 30 years

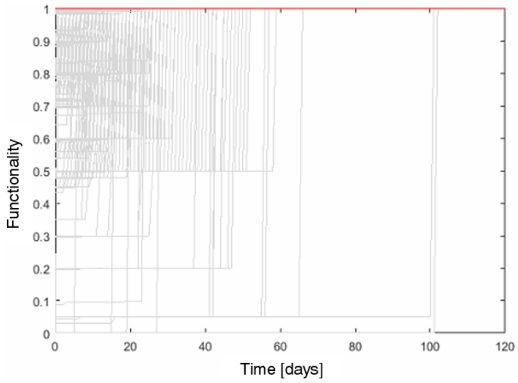

R_P = 50 years

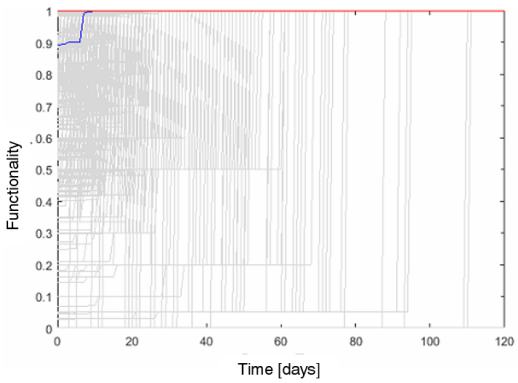

R_P = 72 years

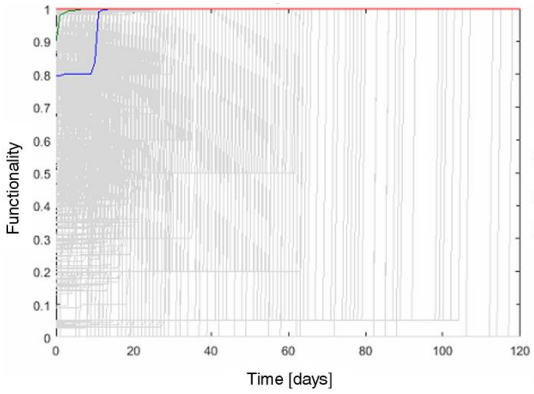

R_P = 101 years

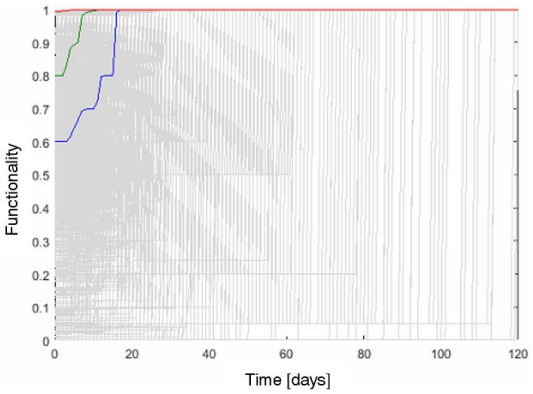

R_P = 140 years

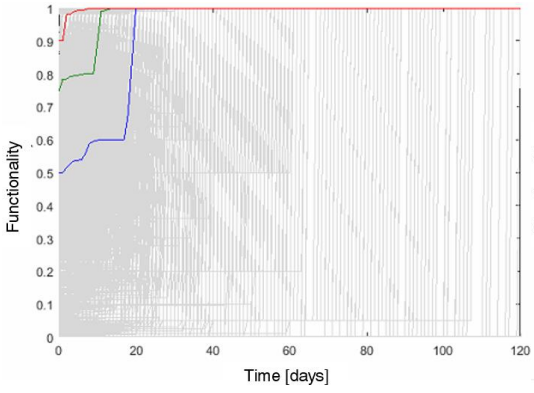

R_P = 200 years

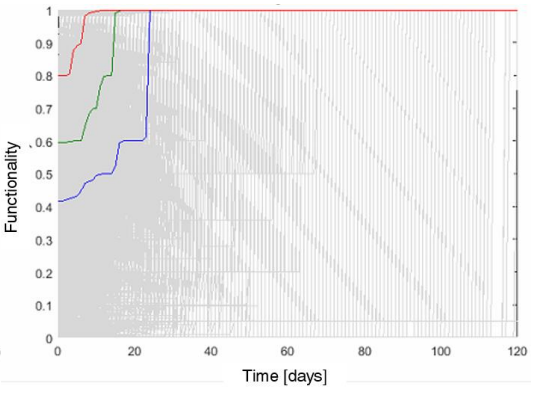

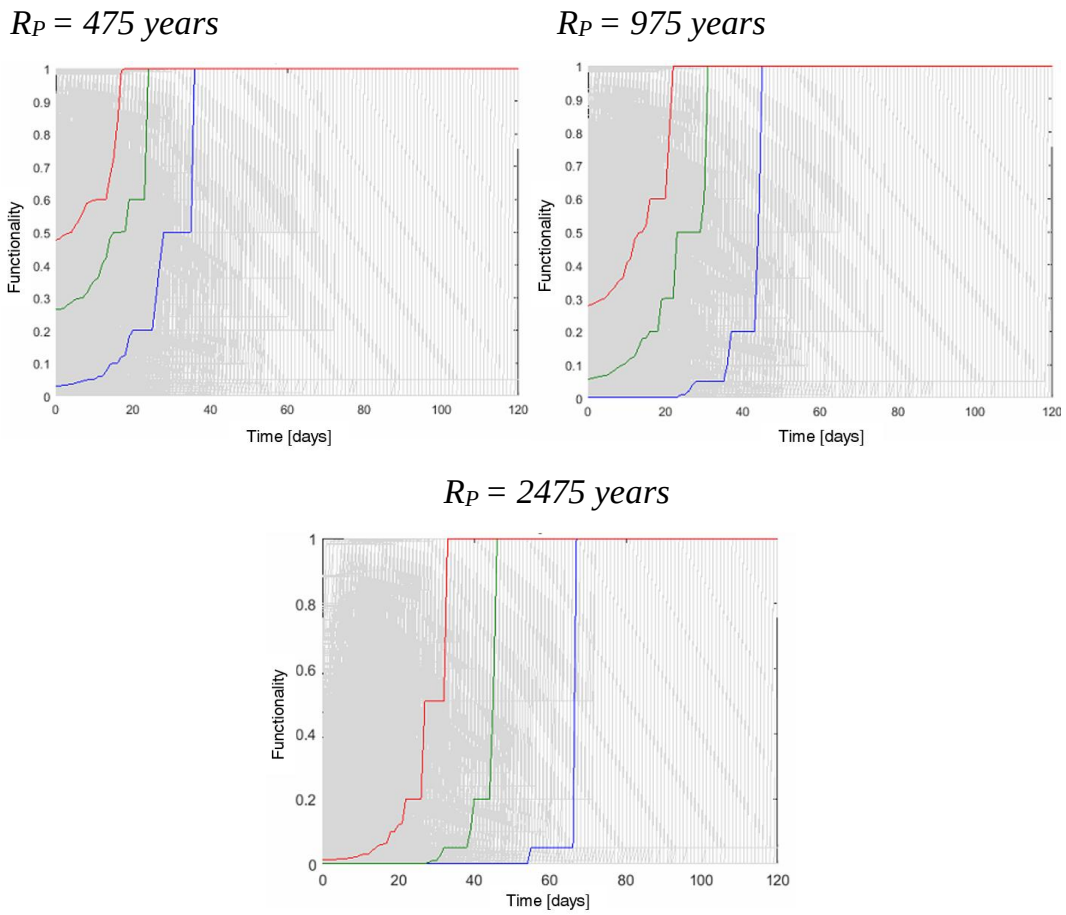

Figure 1.5: SRC_y sets for various return periods in years (red line 25th percentile, green line 50th percentile, blue line 75th percentile).

Business interruption time BIT_y has been calculated for each SRC_y curve, according to Eq. 1.4: Figure 1.6 shows BIT_y distributions for each R_P considered. Lastly, *BI* losses $L_{BI,y}$ have been calculated with Eq. 1.5, using balance sheet data of the cheese-producing facility and cessation coefficients α_C reported in Table 1.5. In such a way, a total number of 202500 *NS*, *BI* and total loss estimates have been stochastically derived for the analyzed nine return periods. Figure 1.7 shows *NS*, *BI* and total loss distribution for every return period.

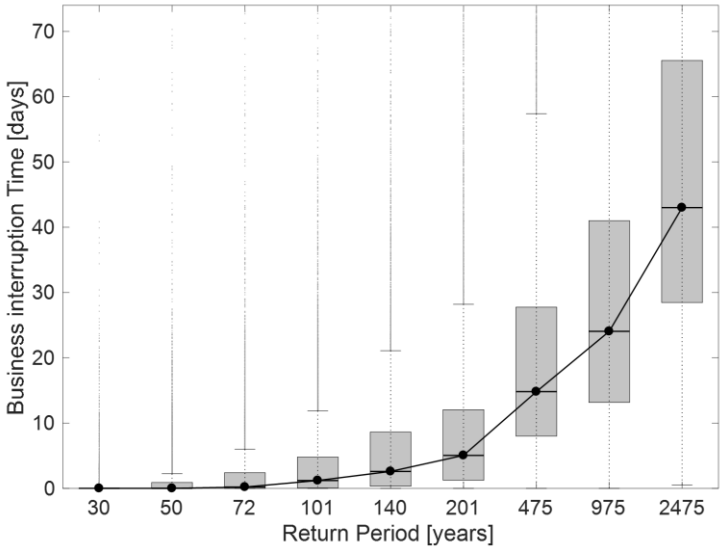

Figure 1.6: BIT_y distributions for each R_P.

Table 1.5: Balance sheet of the cheese-producing facility.

Income statement item	Value [€]	α_c
Revenues from sales of goods (*GSR*)	23,000,000	1
Closing inventory revenues (*CIR*)	50,000	1
Costs of opening stocks (*OSC*)	150,000	1
Costs of raw materials (*RMC*)	18,000,000	1
Energy costs (*ESC*)	2,000,000	0.7
Staff salaries (*SEC*)	1,750,000	0
Other costs (*OC*)	150,000	0.3

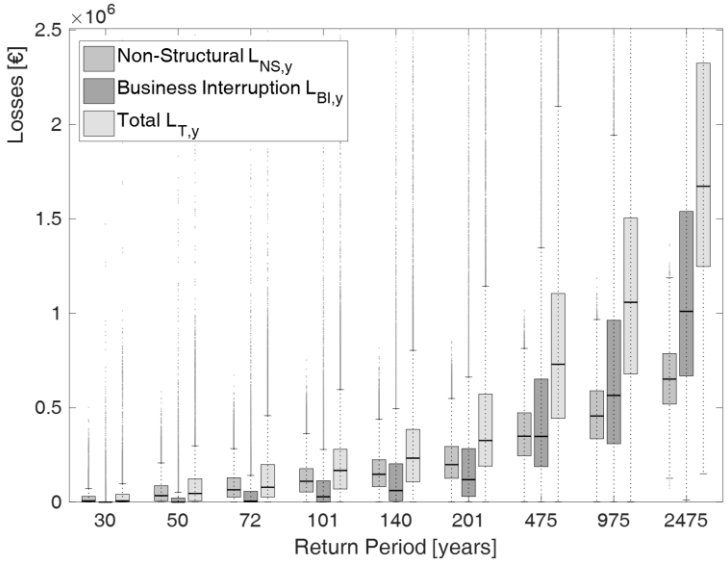

Figure 1.7: $L_{NS,y}$, $L_{BI,y}$ and $L_{T,y}$ for each R_P.

Simulation convergence has been verified observing coefficient of variation (C.O.V.) values lower than 5% for each analysed return period. Figure 1.8 shows total loss simulation convergence results, evidencing how for the specific case study, the sample size of 22500 runs for each return period was a suitable solution for balancing computational efforts and reliability of results.

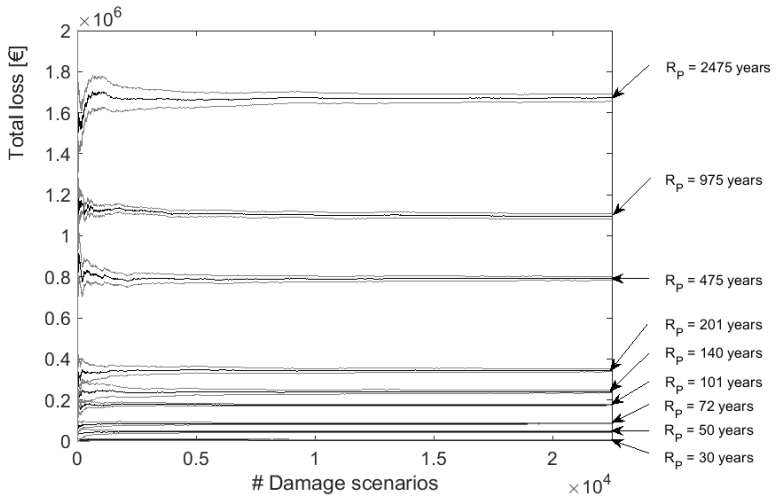

Figure 1.8: Simulation convergence results for total losses.

Hence, 25th, 50th and 75th percentile of *NS*, *BI* and total loss values of each i^{th} R_P have been correlated to the corresponding annual exceedance probability (Eq. 1.1), defining respective loss exceedance curves (Calvi 2013), Figure 1.9. Table 1.6 lists 25th, 50th and 75th percentile values of EAL_{NS}, EAL_{BI} and EAL_T, calculated according to Eqs. 1.7-1.9.

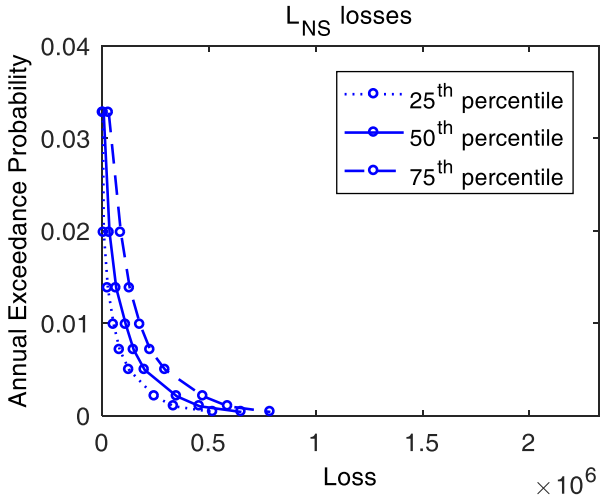

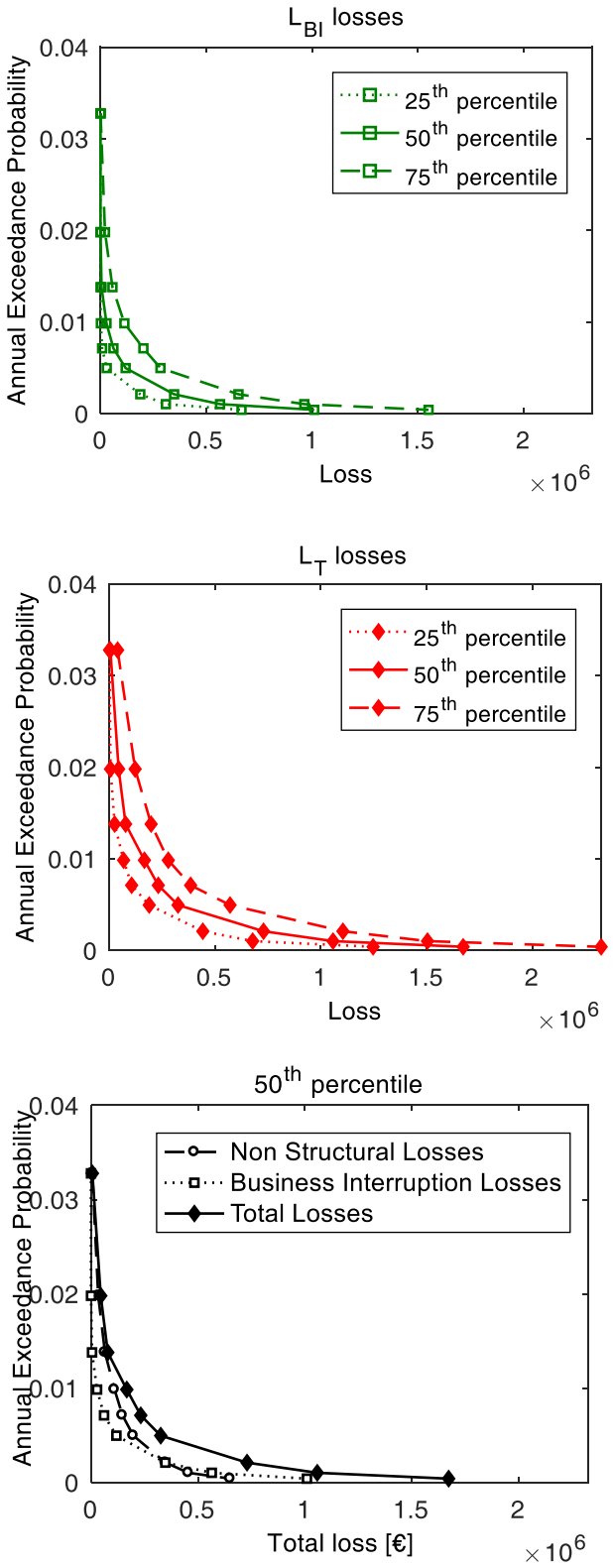

Figure 1.9: 25th, 50th and 75th percentile NS, BI and total loss exceedance curves.

Table 1.6: 25th, 50th and 75th percentile values of EAL_{NS}, EAL_{BI}, EAL_T.

	EAL_{NS} [€]	EAL_{BI} [€]	EAL_T [€]
25th	2119	1209	3606
50th	3660	2455	6552
75th	6540	5277	12211

1.4 Conclusion

In this chapter, a new modular framework based on stochastic seismic hazard, vulnerability, exposure and resilience analysis is presented to assess the probabilistic seismic risk of enterprises. The framework can provide estimations for any kind of production chain, both *NS* losses related to structural damage and *BI* consequences through evaluation of the recovery function of the productive system. Uncertainties in input parameters were characterized in the various modules and calculated with the Monte Carlo sampling technique.

The following economic indicators were defined:

- Expected Annual Non-Structural Loss (EAL_{NS}), related to economic quantification of seismic structural damage to components of a production chain;
- Expected Annual Business Interruption Loss (EAL_{BI}), representing *BI* losses based on probabilistic resilience analysis of the productive process;
- Expected Annual Total Loss (EAL_T), i.e., total losses (sum of *NS* and *BI* for each y^{th} damage scenario).

These indicators can quantify expected annual losses over a wide range of potential scenarios, each characterized by a specific exceedance probability. The proposed framework was then applied to a case study in a typical Italian cheese-producing facility.

Results showed the significant contribution of *BI* in the estimation of total losses. Loss estimation including only structural damage may lead to significant underestimation of total effective losses computed, when *BI* consequences are also taken into account. Results are particularly useful for a rational definition of the optimal seismic retrofit strategy to be implemented. In particular, the proposed hazard-vulnerability-loss module system is a powerful method for assessing the exposure to seismic risk of an industrial productive process (in the so called *as-built* condition) taking into account also business interruption consequences, and an essential tool for evaluating benefits associated with the implementation of alternative seismic retrofit strategies.

2 Profitability Analysis for Assessing the Optimal Seismic Retrofit Strategy of Industrial Productive Processes

In the previous Chapter, a method for assessing the seismic risk for an industrial productive process is proposed. This model allows us to have a quantitative knowledge of the process and it is a fundamental tool for evaluating the best seismic risk mitigation strategy.

This Chapter proposes a financially-based framework for the identification of the optimal seismic risk mitigation strategy for seismic risk reduction. In particular a Profitability Index is defined as suitable economic indicator: this index identifies the best seismic retrofit scheme able to maximize the effectiveness of the investment, given a reference time window. Finally, the proposed financial procedure is applied to the case study described in the previous Chapter.

2.1 Basics of financial analysis

Cost-benefit analysis is a diffused tool for the comparison of alternative investments and can be used in scenario driven application. Various applications to structural engineering problems were recently presented in literature, mainly focused on the identification of the best retrofit intervention (Calvi 2013, Cardone and Flora 2014) and optimal design levels for buildings (Gardoni et al. 2016).

However, no studies are available on the optimal seismic mitigation strategy for a productive process. The financial analysis module herein proposed aims to identify the best mitigation strategy for a productive process, through the identification of the subset of components to be retrofitted and the optimal level of initial investment, conditional to a

reference time window. A brief overview of the economic indicators is reported below.

2.1.1 Economic indicators

Among the economic indicators defined in literature, the Net Present Value (*NPV*) quantifies the present value of all future cash flows (*CF*) in a time span of *t* years. Both negative (expenses) and positive (revenues) flows are considered, using appropriate discounting rate *r* and inflation rate *f*.

Particularly, the former allows comparing benefits that occur in the future to present investments cost, while the latter considers the effect of inflation. The *NPV* is estimated as:

$$NPV(t) = \frac{(1+f)}{(1+r)} CF_1 + \frac{(1+f)^2}{(1+r)^2} CF_1 + ... + \frac{(1+f)^t}{(1+r)^t} CF_t - I_0 \qquad 2.1$$

where the initial investment cost I_0 is subtracted to obtain the actual profit. A project characterized by a positive *NPV* is profitable, i.e., incomes generated by the initial investment exceed the anticipated costs. If all the yearly future cash flows are positive and constant (i.e., benefits *B*), Eq. 2.1 can be rewritten as:

$$NPV(t) = B \cdot \sum_{s=1}^{t} \frac{(1+f)^s}{(1+r)^s} - I_0 \qquad 2.2$$

One other indicator strictly related to the *NPV* is the Break-Even Time (*BET*), representative of the period needed to cover the initial investment. This indicator can be simply obtained by imposing Eqs. 2.1-2.2 equal to 0, and deriving the number of years needed to equalize the initial investment cost I_0 (Mian 2002, Cardone and Flora 2014). Lastly, a Profitability Index *(PI)* is proposed as dimensionless indicator, calculated as the ratio between *NPV* and the initial investment I_0 (Eq. 2.3).

$$PI(t) = \frac{NPV(t)}{I_0} \qquad 2.3$$

Such indicator is useful when comparing different solutions with same or similar positive *NPV* values, since it indicates the most profitable retrofit strategy able to maximize the profit associated with a specific initial investment cost.

2.2 Proposed financial analysis module

The inputs of the proposed financial analysis module are the results of seismic risk analysis of the productive process, particularly the exceedance loss curves and the indicators EAL_{NS}, EAL_{BI} and EAL_T. The first step is the knowledge of seismic risk level in the actual condition (i.e., *as-built*) of the productive process.

Hence, a probabilistic seismic loss estimation procedure must be run, calculating the expected annual loss values $EAL_{As\text{-}Built}$ (i.e., equal to EAL_{NS} if looking to non - structural losses, EAL_{BI} for business interruption or EAL_T for total losses) related to the *as-built* condition. The same procedure has to be run *n* times for calculating EAL_j, i.e., the expected annual losses of the productive chain, in which only the single j^{th} component has been retrofitted. From these data, it is immediate to calculate associated benefit B_j, i.e., the difference between the expected annual loss related to the *as-built* condition and the expected annual loss associated to the process in which the j^{th} component is retrofitted, as follow:

$$B_j = EAL_{As-Built} - EAL_j \tag{2.4}$$

whereas the initial investment $I_{0,j}$ needed for retrofitting the j^{th} element has to be estimated. Then, the definition of a target time window *t* is required. Seismic upgrading of the entire productive chain may involve significant initial investment indeed, that may be not economically profitable if a limited time horizon is considered.

Additionally, if an analyst takes into account *NPV* as economic indicator, a variation of the target time window *t* can misrepresent the rank of the best possible retrofit strategies.

To univocally define the rank of most profitable interventions for the process in a seismic risk mitigation analysis, despite the target time window *t*, the use of *PI* as economic indicator represents a convenient choice.

2.2.1 Actualized Future Cash Flows vs. Initial Investment curve

Hence, considering a specific target time window *t*, PI_j absolute values should be calculated for each j^{th} process component singularly retrofitted, given its intervention benefit B_j, as:

$$PI(t)_j = \frac{NPV(t)_j}{I_{0,j}} = \frac{B_j \sum_{s=1}^{t} \frac{(1+f)^s}{(1+r)^s} - I_{0,j}}{I_{0,j}} \quad 2.5$$

The *n* PI_j values should be ranked in descending order to obtain the list of the most profitable intervention on single process components: *#w* indicates the ranking position of an element in the PI_j list (e.g., if the j^{th} process component is characterized by the highest PI_j value, its ranking position is *#1*, whereas for the one with the lowest PI_j value the ranking position is *#n*).

Once defined the PI_j rank for the process considering only one component to be retrofitted, the probabilistic seismic loss estimation procedure is run again *n-1* times, iteratively retrofitting one more component, in accordance to the PI_j list.

In such a way, the expected annual loss of the productive process for which the first *w* elements of the PI_j list are seismically retrofitted is $EAL_{\#1,\#2,\ldots,\#w}$, whereas the related benefit $B_{\#1,\#2,\ldots,\#w}$ is defined as:

$$B_{\#1,\#2,\ldots\#w} = EAL_{As-Built} - EAL_{\#1,\#2,\ldots\#w} \quad 2.6$$

The associated retrofit cost is simply derived as the sum of the single component costs:

$$I_{0,\#1,\#2,\ldots\#w} = I_{0,\#1} + I_{0,\#2} + \ldots + I_{0,\#w} \quad 2.7$$

Net present value associated to the retrofit of *w* components $NPV(t)_{\#1,\#2,\ldots,\#w}$ and conditional to a target time window *t* can be instead calculated as:

$$NPV(t)_{\#1,\#2,\ldots\#w} = B_{\#1,\#2,\ldots\#w} \cdot \sum_{s=1}^{t} \frac{(1+f)^s}{(1+r)^s} - I_{0,\#1,\#2,\ldots\#w} \qquad 2.8$$

Hence, a total set of n couples of $I_{0,\#1,\#2,\ldots,\#w}$, $NPV(t)_{\#1,\#2,\ldots,\#w}$ is derived, allowing to define the Actualized Future Cash Flows vs Initial Investment curve (*AFCF-II curve*) conditional to a specific target time window *t*. From the *AFCF-II curve*, it is possible to identify the optimal seismic retrofit strategy to be implemented, given a finite amount of economic resources and a specific target time window *t*, in order to maximize the future cash flows for the company.

2.3 Case study

The proposed financial method for finding the optimal retrofit strategy, is applied to the case study described in the previous chapter. In particular, the *as-built* condition has been considered as characterized by the 50^{th} percentile total loss exceedance curve, with an EAL_T value of 6552 €. Then, the probabilistic seismic risk analysis procedure has been used for assessing the impact of each component on the entire process. With this aim, 13 median total loss exceedance curves have been calculated, each one corresponding to the retrofit of one single element of the productive process. The retrofit solution considered for steel tanks and machines consisted in the seismic isolation: the use of isolator devices was in fact proven to be an effective way for significantly reducing damage in such type of components (Phan et al. 2016). Regarding pipes, the insertion of a set of flexible joints represented the most suitable retrofit solution: in particular, unrestrained (e.g., simple bellows / packed slip type joints) and restrained (e.g., tied bellows / hinge / gimbal / packed flexible ball joints) expansion joints were considered for respectively accommodating axial and

angular displacements. The adopted retrofit solutions are specifically designed to avoid seismic damage on retrofitted components, thus leading to failure probabilities values close to zero (e.g., Saha et al. 2016). For this reason, retrofitted components were considered not-susceptible to seismic actions, i.e., a complete reduction of the seismic vulnerability has been considered as reasonable assumption. It is worth noting that specific numerical models for retrofitted components can be developed to improve the reliability of fragility estimate, but this issue is beyond the scope of this work. Figure 2.1 shows the 13 median total loss exceedance curves associated with the retrofit of each component, and the one related to the *as-built* condition.

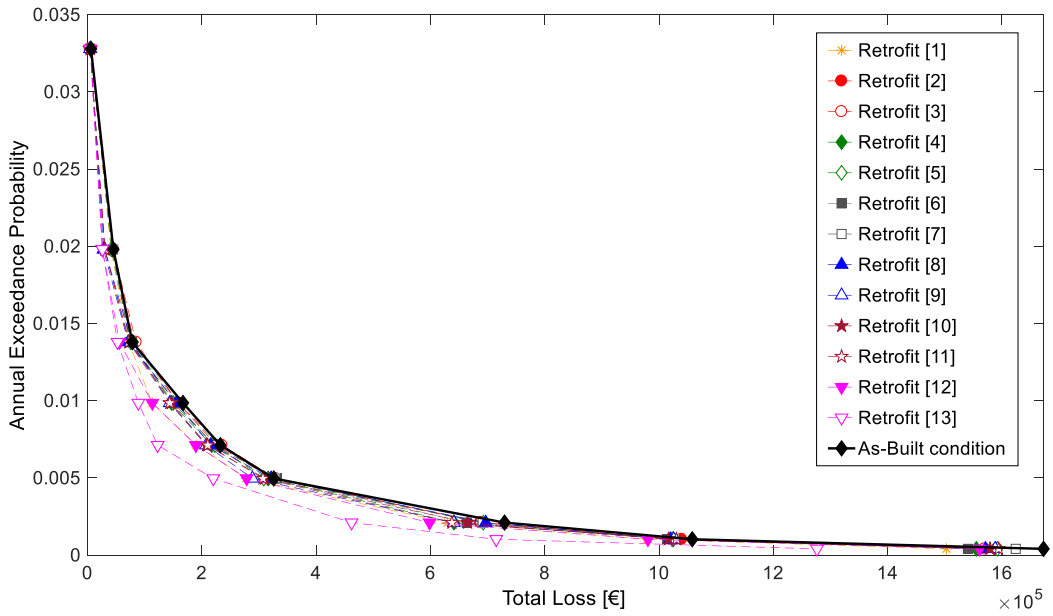

Figure 2.1: 50th percentile total loss exceedance curves related to singularly retrofitted components.

For each j^{th} total loss exceedance curve, EAL_j values have been calculated according to Eq. 1.9 and then the related benefit B_j has been computed, according to Eq. 2.4. Table 2.1 lists EAL_j and B_j values: in particular, benefits can be graphically seen (in Figure 2.1) as the area between the as-built and j^{th} retrofitted condition (Calvi 2013). Retrofit costs $I_{0,j}$ have been adopted on the basis of an expert judgement (Table 2.1).

Discount rate r and inflation rate f have been assumed in accordance with Italian estimates respectively equal to 0.04 (Italian Anticorruption Authority 2017) and 0.02 (OECD 2014). A set of increasing target time windows t (10, 20, 30, 40 and 50 years) have been considered to highlight the influence of the time-dimension on selecting the optimal mitigation strategy to be implemented.

Table 2.1: Benefit in terms of total loss provided by each singularly retrofitted component and associated cost.

Retrofit j^{th} component	EAL_j [€]	B_j [€]	$I_{0,j}$ [€]
1	5674	878	6000
2	6313	239	4000
3	6325	227	4000
4	6105	447	15000
5	6205	348	15000
6	6198	354	4000
7	6253	299	4000
8	6043	509	5000
9	5847	705	5000
10	5931	621	5000
11	5886	666	5000
12	5400	1152	8000
13	4295	2257	30000

Hence, PI_j and NPV_j values have been defined for each j^{th} retrofitted component and target time window t: Figure 2.2 highlights how PI_j rank does not depend on the time, while NPV_j does. Table 2.2 lists PI_j and NPV_j single component ranks: in this specific case study, NPV_j list becomes constant for target time windows t larger than 25 years (i.e., 30, 40 and 50 years). Once defined the PI_j and NPV_j rankings for the set of target time windows t considered, the probabilistic seismic loss estimation procedure has been performed again 12 times for each rank listed in Table 2.2. In such a way, 12 loss exceedance curves have been derived, each associated to an iteratively increasing number of retrofitted elements (from 2 to 13 components).

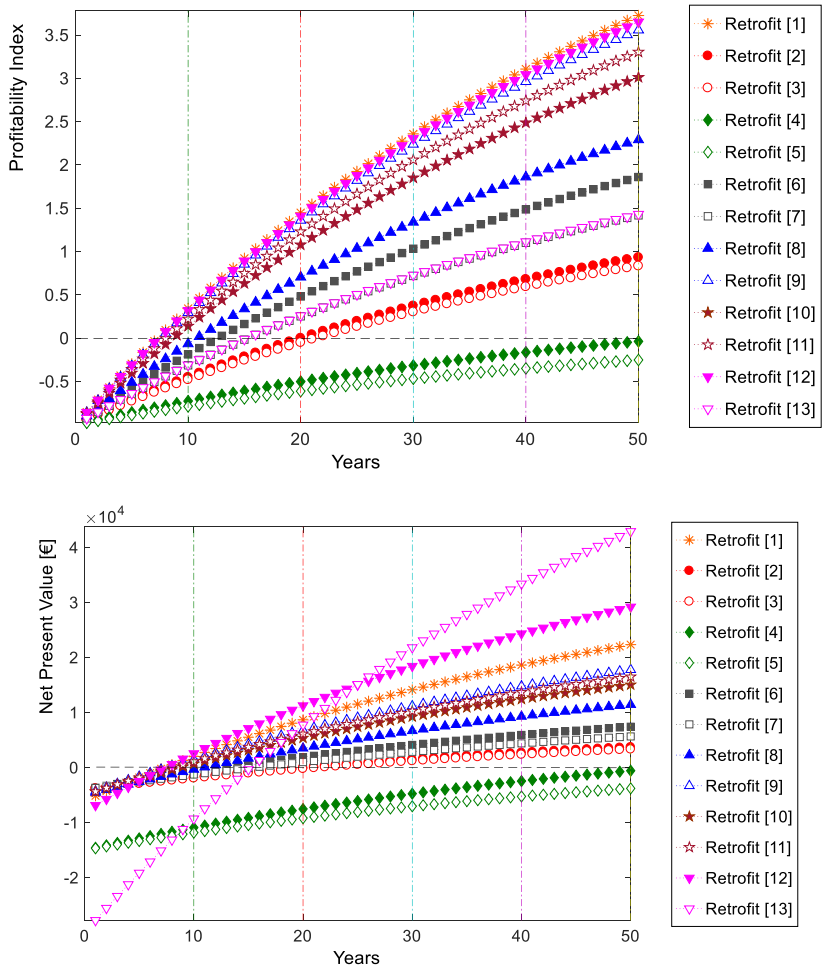

Figure 2.2: $PI_j(t)$ and $NPV_j(t)$ of each component for increasing target time windows.

Table 2.2: Orders of component retrofit interventions based on $PI_j(t)$ and $NPV_j(t)$.

Order #*w*	$PI_j(t)$	$NPV_j(t)$				
		t = 10 years	t = 20 years	t = 30 years	t = 40 years	t = 50 years
#1	Comp. 1	Comp. 12	Comp. 12	Comp. 13	Comp. 13	Comp. 13
#2	Comp. 12	Comp. 1	Comp. 13	Comp. 12	Comp. 12	Comp. 12
#3	Comp. 9	Comp. 9	Comp. 1	Comp. 1	Comp. 1	Comp. 1
#4	Comp. 11	Comp. 11	Comp. 9	Comp. 9	Comp. 9	Comp. 9
#5	Comp. 10	Comp. 10	Comp. 11	Comp. 11	Comp. 11	Comp. 11
#6	Comp. 8	Comp. 8	Comp. 10	Comp. 10	Comp. 10	Comp. 10
#7	Comp. 6	Comp. 6	Comp. 8	Comp. 8	Comp. 8	Comp. 8
#8	Comp. 13	Comp. 7	Comp. 6	Comp. 6	Comp. 6	Comp. 6
#9	Comp. 7	Comp. 2	Comp. 7	Comp. 7	Comp. 7	Comp. 7
#10	Comp. 2	Comp. 3	Comp. 2	Comp. 2	Comp. 2	Comp. 2
#11	Comp. 3	Comp. 13	Comp. 3	Comp. 3	Comp. 3	Comp. 3
#12	Comp. 4	Comp.4	Comp. 4	Comp. 4	Comp. 4	Comp. 4
#13	Comp. 5	Comp. 5	Comp. 5	Comp. 5	Comp. 5	Comp. 5

Figure 2.3 shows the total set of 13 loss exceedance curves compared with the as-built reference condition, according to the list of PI_j and NPV_j. $EAL_{T,\#1,\ \#2,\ldots,\#w}$ values have been subsequently assessed with Eq. 1.9, while related benefits $B_{T,\#1,\#2,\ldots,\#w}$ due to the contemporary retrofitting of w process components have been derived using Eq. 2.6. These values are listed in Table 2.3. According to the simplified assumption adopted for characterizing fragility functions of the retrofitted components, the loss exceedance curve associated to the retrofit of all the 13 process components, is equal to zero (Figure 2.3).

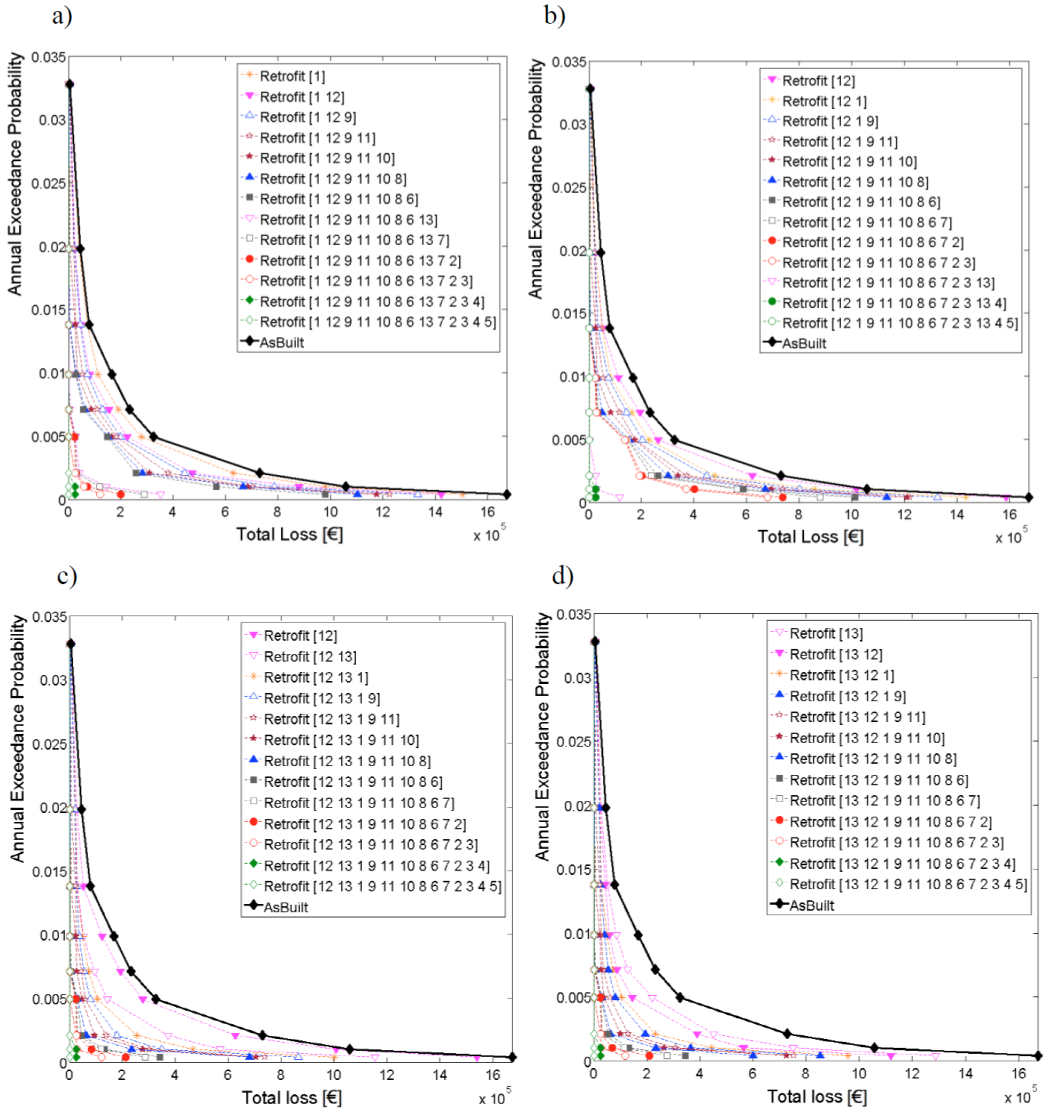

Figure 2.3: 50th percentile loss exceedance curves for contemporary retrofits: PI_j list (a) and NPV_j lists with target time windows of 10 (b), 20 (c) and 30-40-50 (d) years.

Table 2.3: Benefits [€] associated with w retrofitted components.

		$NPV_j(t)$		
	$PI_j(t)$	t = 10 years	t = 20 years	t = 30, 40, 50 years
$B_{T,\#1}$	878	1098	1071	2250
$B_{T,\#1,\#2}$	1966	1919	3196	3108
$B_{T,\#1,\#2,\#3}$	2364	2363	3795	3895
…	2926	2917	4346	4303
…	3462	3380	4851	4870
…	3822	3792	5176	5185
…	4126	4131	5488	5542
$B_{T,\#1,\#2,\ldots,\#w}$	5860	4352	5905	5886
…	6032	4757	6040	6048
…	6216	4882	6196	6209
…	6364	6394	6389	6392
…	6512	6512	6512	6512
$B_{T,\#1,\#2,\ldots,\#13}$	6552	6552	6552	6552

Thus, related benefit equalizes the $EAL_{As\text{-}Built}$ value, as reported in Table 2.3. Lastly, Table 2.4 lists incremental investment costs $I_{0,\#1,\#2,\ldots,\#w}$ derived with Eq. 2.7, in accordance to the ranks defined in Table 2.2.

Table 2.4: Initial investment cost [€] associated with w retrofitted components.

		$NPV_j(t)$		
	$PI_j(t)$	t = 10 years	t = 20 years	t = 30, 40, 50 years
$I_{0,\#1}$	6000	8000	8000	30000
$I_{0,\#1} + I_{0,\#2}$	14000	14000	38000	38000
$I_{0,\#1} + I_{0,\#2} + I_{0,\#3}$	19000	19000	44000	44000
…	24000	24000	49000	49000
…	29000	29000	54000	54000
…	34000	34000	59000	59000
…	38000	38000	64000	64000
$I_{0,\#1} + I_{0,\#2} + \ldots + I_{0,\#w}$	68000	42000	68000	68000
…	72000	46000	72000	72000
…	76000	50000	76000	76000
…	80000	80000	80000	80000
…	95000	95000	95000	95000
$I_{0,\#1} + I_{0,\#2} + \ldots + I_{0,\#13}$	110000	110000	110000	110000

2.4 Results and discussion

AFCF-II curves have been subsequently derived for each target time window *t* (Figure 2.4): results evidence how the use of the profitability index PI_j list provides *AFCF-II* curves higher than those derived following NPV_j list.

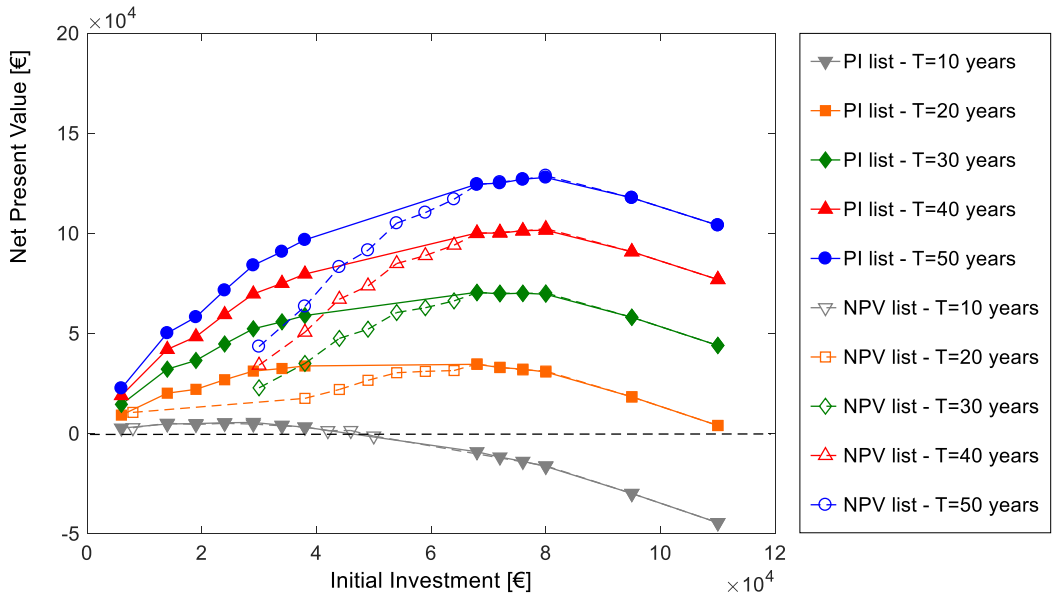

Figure 2.4: Comparison between AFCF-II curves obtained with PI_j and NPV_j lists.

In other terms, considering a fixed initial investment cost, future cash flows are larger if the PI_j list is adopted. Considering for instance a target time window of 30 years and an available budget of 40000 € for seismic mitigation actions, the strategy of retrofitting components 1, 12, 9, 11, 10, 8, 6 in accordance to PI_j list is more profitable than that of retrofitting components 13 and 12, as indicated by the NPV_j rank. *AFCF-II* curves can be viewed as useful financial tool for planning an optimal seismic risk mitigation strategy, when dealing with limited or unlimited economic resources. In the first case, as previously described, given a fixed initial investment, the curve defines the best set of components to be retrofitted. When no restrictions on budget are present, it is possible to define the initial investment needed for peaking the *AFCF-II* curve, as reported in Table 2.5

for the analysed case study. It can be observed how the retrofit of the entire productive process, also if unlimited resources are available, might not be the optimal strategy from the financial point of view, especially for short-to-medium target time windows. Only when long-term horizons are considered, higher initial investment costs can be justified, since a wider time window is available for deriving profit from the implementation of the selected retrofitting strategy.

Table 2.5: Optimal seismic retrofit strategy and related costs for different t values.

Target time window *t* [years]	Retrofitted components	Initial investment [€]
10	1, 12, 9, 11, 10	29000
20	1, 12, 9, 11, 10, 8, 6, 13	68000
30	1, 12, 9, 11, 10, 8, 6, 13	68000
40	1, 12, 9, 11, 10, 8, 6, 13, 7, 2, 3	80000
50	1, 12, 9, 11, 10, 8, 6, 13, 7, 2, 3	80000

A further comparison has been performed, with the aim of highlight the importance of calculate benefit associated to contemporary retrofitting *w* components, as defined in Eq. 2.6. A risk analyst could in fact erroneously derive such benefit as the sum of benefits derived with Eq. 2.41.7, associated to the single retrofit of each component. This approach leads to wrong results, neglecting in such a way the functional relationships between process components (i.e., the logical scheme of production). A significant overestimate can be observed, for instance, if all components are retrofitted: the sum of benefits listed in Table 2.1 (8702 €) is 1.33 times higher than the effective benefit reported in Table 2.3 (6552 €). "Wrong" AFCF-II curves have been also derived in accordance with PI_j list, summing the benefits associated to single component retrofit, with the aim to demonstrate the correctness of the proposed framework. Figure 2.5 shows the comparisons for each target time window *t* considered, evidencing significant overestimates with the *AFCF-II* curves, that might

suggest larger initial investments based on unreal benefits, than those effectively needed.

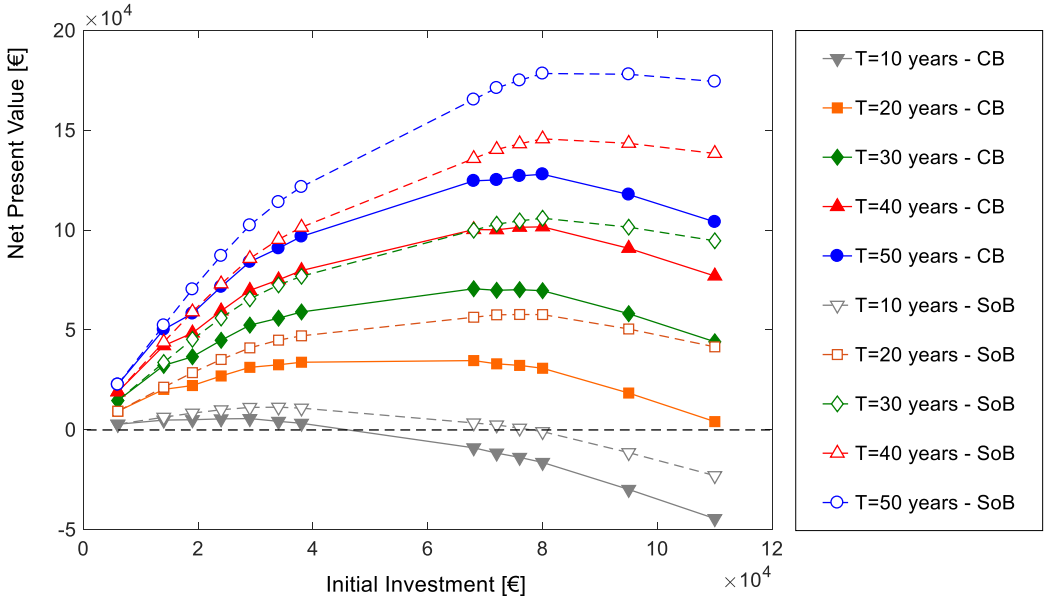

Figure 2.5: Comparison between AFCF-II curves obtained with PIj list: contemporary benefits CB) vs. sum of benefits (SoB).

Lastly, the reliability of the proposed framework has been validated with the use of computationally costly alternative procedure. Starting from the first process component of the PI_j list of Table 2.2 (Component 1), all the 12 possible retrofit strategies with w = 2 (i.e., 1-2, 1-3, 1-4, 1-5, 1-6, 1-7, 1-8, 1-9, 1-10, 1-11, 1-12, 1-13) have been investigated, deriving related PI_j values, and identifying the best one (Components 1-12).

Hence, the process has been iteratively repeated investigating all the 11 retrofit strategies with w = 3 (i.e., 1-12-2, 1-12-3, 1-12-4, 1-12-5, 1-12-6, 1-12-7, 1-12-8, 1-12-9, 1-12-10, 1-12-11, 1-12-13), deriving again the highest PI_j value and iteratively repeat the cycle for a total of 91 probabilistic seismic risk analyses. The order of retrofit interventions derived in such way is coincident with the PI_j list resulting from the application of the proposed financially-based framework, thus highlighting its robustness and reliability.

2.5 Conclusion

In this chapter, a risk-based financial framework was proposed, to support decision making on the identification of the optimal seismic retrofit strategy to be implemented for productive processes located in areas prone to seismic hazard. The approach considers all main variables acting in the complex goal of reducing the potential losses induced by earthquake occurrences. Particularly, the probabilistic seismic loss estimation procedure integrates probabilistic hazard models, fragility of *as-built* and retrofit conditions, recovery curves and financial balance sheet data of the company. The proposed framework uses as input data the results of the probabilistic seismic risk analysis (explained in the previous chapter), retrofit costs of each process component, available investment funds and the target time window of the company. Results are particularly useful for a rational definition of the optimal seismic retrofit strategy to be implemented. Final remarks can be summarized as follows:

- the proposed financial analysis module allows evaluating the profitability of different seismic retrofit strategies: in particular, the Profitability Index has to be used, the proposed financial analysis module allows evaluating the profitability of different seismic retrofit strategies: in particular, the Profitability Index should be used, since it has the clear advantage to provide a unique ranking of the most convenient retrofit strategy, independently from the time window of interest *t*. On the contrary, the *NPV* rank is conditional to *t*. In this regard, it has been demonstrated how the *AFCF-II* curve obtained from the *PI* list is higher than that obtained with the *NPV* rank, and this is precisely due to the dimensionless nature of the *PI*, able to purely capture the profitability level associated with the implementation of a specific strategy characterized by a defined initial investment;

- it is essential to take into account the "non-linear response" associated with the productive process logic scheme: indeed, benefit of contemporary retrofitted components have to be computed through the calculation of $EAL_{T,\#1,\ \#2,\ldots,\#w}$ and not summing single benefits;

• *AFCF-II* curves are able to individuate the best mitigation strategy and the optimal amount of initial investment, considering a specific target time window of interest.

3 Regional Seismic Risk in Italy

3.1 Introduction

Assessing seismic risk at regional level is a multidisciplinary task that requires the knowledge of seismic activity of the region of interest, the susceptibility of built environment to seismic damage, and the level of exposure. Frequency of significant losses due to earthquakes has increased over the last decades in Italy, ending to weight on the public financial funds. For this reason, the Italian Parlament has recently approved specific incentives for householders interested in seismically retrofitting their properties (DM 65, 2017).

The reduction of seismic vulnerability has a beneficial effect on seismic risk, and it is the easiest way for mitigating consequences induced by earthquakes. Previous seismic risk reduction programs (e.g., OPCM3274, 2003; OPCM3362, 2004; OPCM3376, 2004) were tailored on the basis of the seismicity level (i.e., function of the seismic hazard) and the results of standardized seismic assessment procedures. However, when dealing with the definition of seismic mitigation programs, the allocation of economic resources should be done considering risk-targeted indicators, and for this reason, a risk map is required.

Another important feature is the metric that should be used for assessing risk: economic loss (i.e., costs to be sustained to repair seismic damage after an earthquake) has been proved a clearly understandable way to communicate seismic risk also to a non-technical audience (e.g., communities, public authorities, banks, insurers). The development of a seismic risk map is therefore a starting point for the definition of a rational seismic mitigation program, since it allows the competent authorities to understand needs and priorities, and compare resulting benefits with costs associated to the implementation of specific financial measures.

This chapter describes how the seismic risk map is developed, based on the historical seismicity of the country. In particular, the main phases of the work are: the selection of input data used for characterizing the seismicity of the country; the identification of the exposed value (i.e., number and type of residential buildings in each Italian municipality) and its subdivision in different seismic vulnerability classes. Earthquake-induced loss curves are computed, subsequently assessing the expected annual loss for each municipality. Finally, results are shown and widely discussed (Zanini et al. 2017).

3.2 Seismic hazard

When dealing with seismic risk assessment at regional scale, it is required to take into account recorded or simulated earthquake scenarios as input models. Italy is particularly prone to seismic hazard, with a large number of events recorded in the past, quite homogeneously along the national borders.

For the purpose of this work, a set of historical earthquakes stored in the Italian historical earthquake database (Rovida et al. 2016) has been considered for the subsequent calculation of loss values. In particular, events with magnitude M_w higher than 4.5 have been taken into account for a total number of 1433 events, as shown in Figure 3.1. The most significant events occurred along the longitudinal axes of Italy, in correspondence of Apennine.

Along the two coastlines, fewer events, with a smaller magnitude, are present. In northern Italy, the most relevant earthquakes occurred in Friuli Venezia Giulia, in the north-east of the country. North-western Italy is the area less exposed to seismic events, both in terms of events frequency and magnitude. The events were recorded in a time interval of about 10 centuries (1000-2014): Figure 3.2 shows the events' set over time,

highlighting the so-called problem of catalogue completeness, i.e., the difference of the number of records between recent years and past centuries, due to lack of instrumental measurements and reliable perception of the quakes by local communities during the Middle-Ages.

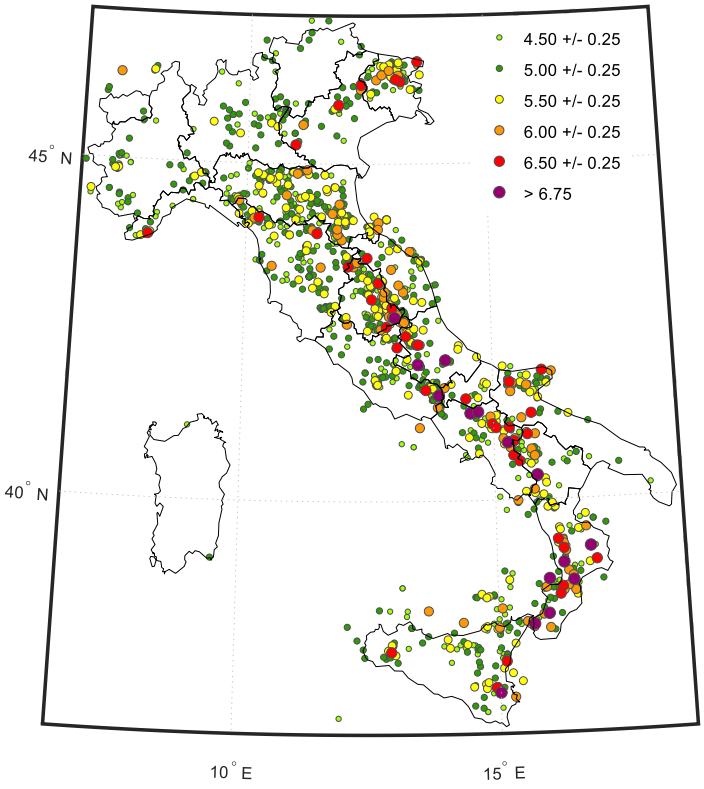

Figure 3.1: Historical Italian earthquakes with M_w higher than 4.5 according to CPTI2015 (Rovida et al. 2016).

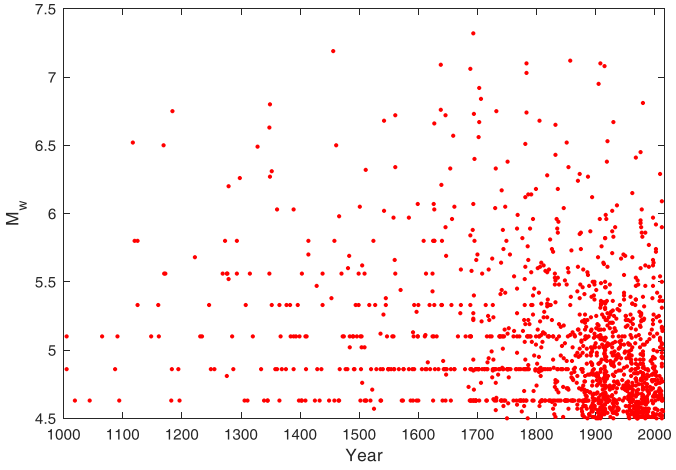

Figure 3.2: Historical Italian earthquakes with M_w higher than 4.5 over time (Rovida et al. 2016).

Earthquake scenarios have thus been simulated for each event of the considered set, via the implementation of a suitable ground motion prediction equation (GMPE). For the Italian context, the GMPE proposed by Bindi et al. (2011) has been adopted herein.

$$\log_{10} Y = e_1 + F_D(R,M) + F_M(M) + F_S + F_{sof} \qquad 3.1$$

where e_1 is the costant term, $F_D(R,M)$, F_S and F_{sof} represent the distance function, the magnitude scaling, the site amplification and the style of faulting correction, respectively. M is the moment magnitude, R is the Joyner-Boore distance, or the epicentral distance (in *km*), when the fault geometry is unknown. Y is the peak ground acceleration, espressed in cm/s^2. Further details and definition of functions in Eq. 3.1, can be found in Bindi et al. (2011).

For each event, the ground motion field has been computed considering peak ground acceleration (PGA) for the bedrock as reference intensity measure. PGA estimates have been subsequently amplified with the topographic-stratigraphic coefficient (Norme Tecniche per le Costruzioni 2008) in order to take into account soil amplification phenomena, adopting the V_{S30} site classification illustrated in Figure 3.3. Ground motion estimates have been calculated for centroids representative of each municipality over the Italian territory. Due to the substantial lack of events, Sardinia has been excluded by the following analyses.

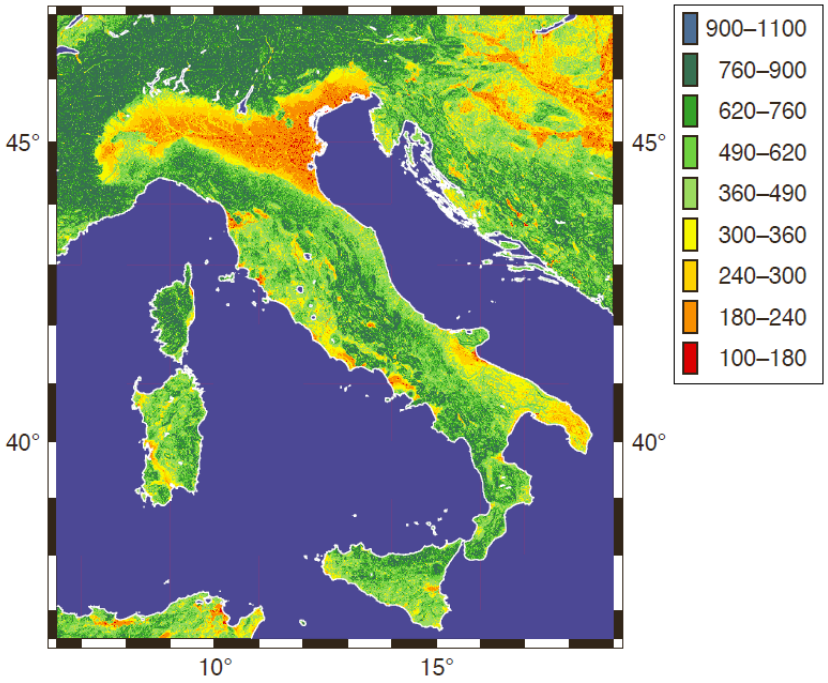

Figure 3.3: V_{S30} site classification on the basis of the topography (https://www.earthquake.usgs.gov).

3.3 Italian buildings and fragility

The Italian building stock has been modelled in this work according to the 15th census database of the National Institute of Statistics (Istituto Nazionale di Statistica 2011). This database provides the number of residential buildings for each municipality, their different construction material (i.e., masonry, reinforced concrete and "other") and the age of construction (i.e., pre 1919, 1919-1945, 1946-1960, 1961-1970, 1971-1980, 1981-1990, 1991-2000, 2001-2005, post 2005). Figure 3.4 shows the number of residential buildings for each municipality, evidencing a higher distribution in the Po plan and around the metropolitan area of the main cities (Florence, Rome, Naples, Bari, Palermo). Built area for each municipality has been derived multiplying built area at provincial level by the ratio between the number of buildings of a generic municipality and those of the entire province (Figure 3.5).

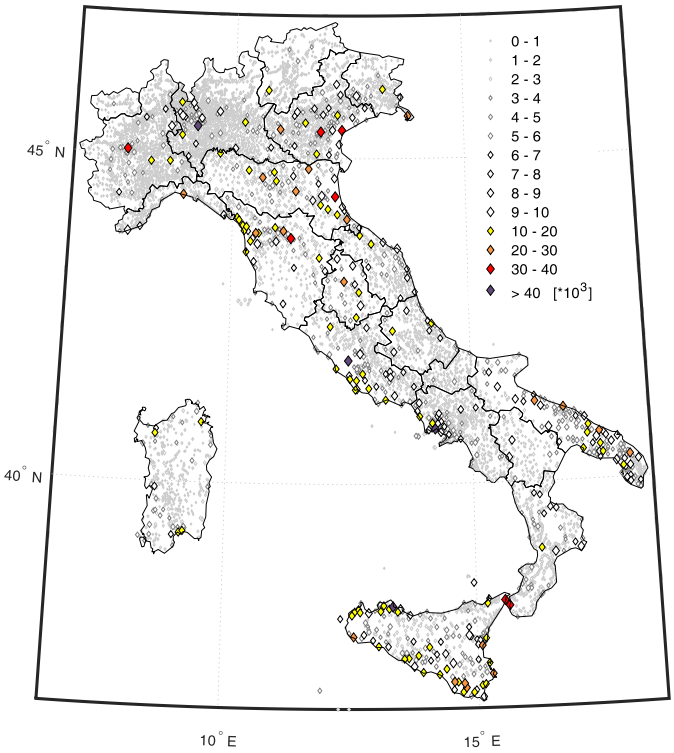

Figure 3.4: Number of residential building for each Italian municipality (Istituto Nazionale di Statistica 2011).

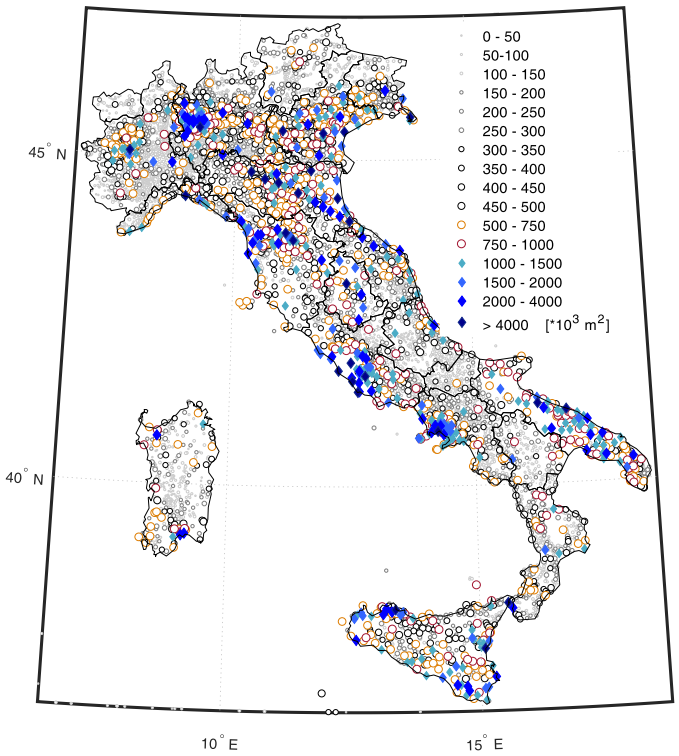

Figure 3.5: Built-area [m^2] for each Italian municipality.

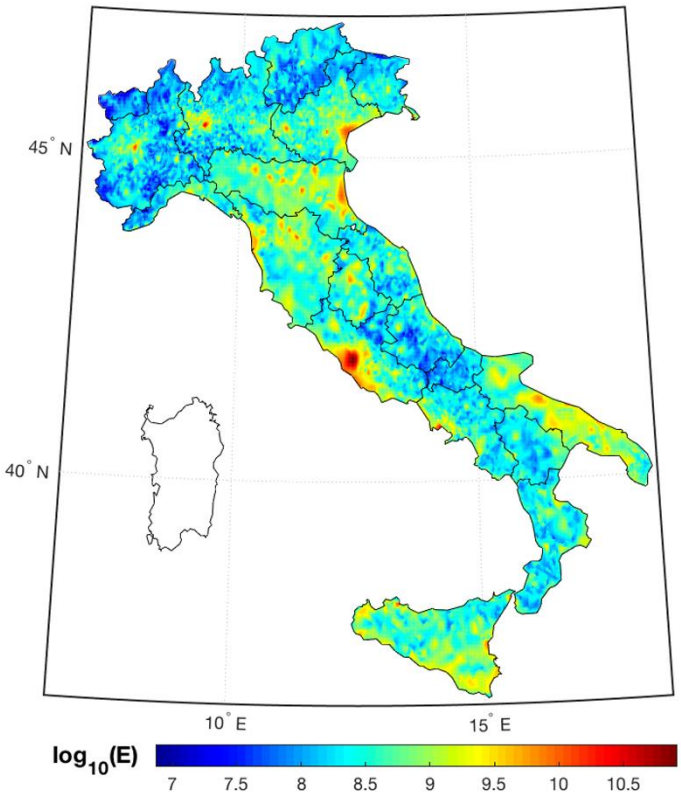

Figure 3.6: Exposed value for the residential asset [€].

Finally, Figure 3.6 illustrates the exposed value, i.e., the economic quantification of the residential asset of each municipality, as the product between the municipal built area and the unit replacement cost RC_{ave}, assumed equal to 1500 €/m^2, according to CRESME (Centre for Sociological, Economics and Market Research, 2011). This value can reasonably considered constant within all the Italian territory.

Table 3.1 shows the number of buildings belonging each categories for the whole Italian stock. It can be noted, that most of buildings are masonry structure built before 1919; secondly, masonry buildings are more numerous than RC structures up to 1981, after which RC buildings spread more. As in Asprone et al. (2013) and Bozza et al. (2015), "other" category has been approximated to be composed of combined RC-masonry structures, since in Italy this typology constitutes the large majority of structures other than masonry and RC structures.

Table 3.1: Number of residential buildings per construction period and structural typology in Italy (Istituto Nazionale di Statistica 2011).

Construction period	*Structural typology*			
	Masonry	RC	Other	**Total**
Pre 1919	1,725,486	--	107,018	**1,832,504**
1919-1945	1,149,082	77,122	100,803	**1,327,007**
1946-1960	1,212,279	303,903	184,654	**1,700,836**
1961-1970	1,087,428	676,242	28,163	**1,791,833**
1971-1980	863,668	907,046	34,937	**1,805,651**
1981-1990	467,821	737,632	25,314	**1,230,767**
1991-2000	251,721	455,906	16,390	**724,017**
2001-2005	125,719	247,516	9,869	**383,104**
post 2005	92,773	189,328	77,878	**359,979**
Total	**6,975,977**	**3,594,695**	**585,026**	**11,155,698**

Fragility models available in literature and classified per structural category have been used for representing the structural vulnerability of the Italian residential building stock. An extended literature survey has been performed for identifying the most suitable fragility function to be used in the loss-calculation model. According to Kostov et al. 2004, two categories of masonry buildings have been considered: masonry buildings built before and after 1919.

Regarding reinforced concrete (RC) and combined RC-masonry structures, the distinction between gravity-load and seismic-load designed structures has been done comparing the age of construction with the temporal evolution of Italian seismic codes, to know whether or not each municipality was classified as a seismic risk-prone area (Legge 64, 1974; DM 1984). Hence, for each municipality, structures built before that year, have been considered gravity-load designed, whereas those built after that year as seismic-load designed.

A further subdivision has been also performed both for RC-gravity and RC-seismic buildings, considering the number of storeys and thus defining two additional subclasses (1-2 story, more than 3 stories). For obtaining the built area for each building category in each municipality, the provincial

built area has been disaggregated on the base of the number of buildings of each category that are located in each municipality. Therefore, based on the above-described analysis, eight structural categories were identified for representing in detail the taxonomy of each Italian municipality:

1. Masonry structures built before 1919;
2. Masonry structures built after 1919;
3. RC structures, gravity-design, 1-2 storey,
4. RC structures, gravity-design, 3+ storeys,
5. RC structures, seismic-design, 1-2 storey,
6. RC structures, seismic-design, 3+ storeys,
7. Other structures, gravity-design,
8. Other structures, seismic-design.

Table 3.2 reports the mean μ and standard deviation σ (characterizing analytical lognormal fragility functions) of the damage states of each structural category.

Table 3.2: Set of fragility curves used for the analysis.

Structural type	*Limit State*								*Authors*
	Light LS1		*Medium LS2*		*Heavy LS3*		*Collapse LS4*		
	μ *[g]*	σ	μ *[g]*	σ	μ *[g]*	σ	μ *[g]*	σ	
#1	0.10	0.79	0.14	0.80	0.17	0.81	0.24	0.80	Kostov et al. 2004
#2	0.12	0.79	0.17	0.81	0.19	0.79	0.33	0.79	Kostov et al. 2004
#3	0.09	0.33	0.12	0.44	0.25	0.37	0.33	0.36	Ahmad et al. 2009
#4	0.08	0.32	0.11	0.43	0.17	0.40	0.22	0.38	Ahmad et al. 2009
#5	0.09	0.33	0.12	0.44	0.24	0.37	0.48	0.36	Ahmad et al. 2009
#6	0.08	0.32	0.11	0.41	0.17	0.39	0.31	0.36	Ahmad et al. 2009
#7	0.11	0.79	0.16	0.78	0.27	0.78	0.35	0.79	Kostov et al. 2004
#8	0.12	0.79	0.19	0.79	0.30	0.79	0.41	0.79	Kostov et al. 2004

3.4 Seismic loss analysis

A loss analysis has been carried out for each earthquake considered in the set of events. Direct losses, i.e., costs to be sustained for repairing seismic damage due to the occurrence of an earthquake scenario, have been computed for each municipality and subsequently aggregated to derive the total loss value induced by each of the 1433 events.

Loss values have been calculated for the municipalities within a radius of 200 *km* from the epicenter, due to constraints in the applicability of the GMPE, and the negligible effects in terms of seismic damage at such source-to-site distances. For a given z^{th} earthquake scenario, the loss value for a generic i^{th} municipality has been estimated according to Bai et al. (2009):

$$L_{f,i} = \sum_{y=1}^{8} \sum_{k=1}^{5} \left[P\left(DS_{k,y} \mid PGA_{z,i} \right) \right] \cdot RCR_k \cdot RC_{ave} \cdot A_{j,y} \qquad 3.2$$

where $PGA_{i,z}$ is the peak ground acceleration in the i^{th} municipality due to the z^{th} earthquake scenario, $DS_{k,y}$ is the k^{th} damage state (with k = 1, 2, 3, 4, 5) of the y^{th} building typology (with y = 1, 2, …, 8).

In Eq. 3.2, $A_{i,y}$ is the built area (in m^2) for the y^{th} building type in a generic i^{th} municipality, and RCR_k is the repair cost ratio for the the k^{th} damage state (i.e., ratio between unit cost to repair a building in the k^{th} damage state and the unit replacement cost RC_{ave}). Repair cost ratios RCR_k have been extrapolated from Dolce and Manfredi (2015), assuming the same deterministic values for each structural type equal to 0, 0.15, 0.4, 0.65, 1, respectively for DS_1, DS_2, DS_3, DS_4 and DS_5.

Each loss value $L_{i,z}$ has been subsequently aggregated to obtain the total loss L_z associated with the z^{th} earthquake scenario. For validating the loss estimation model proposed in this work, a back analysis of the 2002 Molise earthquake, and of the 2009 L'Aquila earthquake, has been performed. For the M_W=5.8 Molise earthquake (31st of October, 2002) a

total loss of 1425.5 M€ was obtained, while for the M_W=6.3 L'Aquila earthquake (6th of April, 2009) the obtained loss was about 5493.2 M€.

Comparisons of such aggregates losses with real data are sometimes difficult, but these values are plausible if compared with available data. In particular, for the Molise earthquake a loss of 1.8 *bn* € was estimated by the Molise region administration (Regione Molise 2010) while for L'Aquila Earthquake of 5.9 *bn* € was allocated for private reconstruction (Commissariato per la Ricostruzione 2012). Since in both cases, data includes structural and non-structural damage and considering that a part of funds was used for retrofitting the buildings beyond their previous capacity, the proposed loss estimation model is able to well describe losses from earthquakes in Italy.

The calculation has been repeated for each of the 1433 simulated events; starting from these results, the annual loss exceedance curve of Italy has been computed, by first assessing the rate of exceedance of each loss value and subsequently deriving the yearly exceedance probability value (Crowley and Silva 2013). Figure 3.7 shows the loss exceedance probability curve of Italy: the area under the curve represents the *EAL*, i.e., the yearly average loss due to the occurrence of seismic events in Italy, estimated in 1.634 *bn* €. *EAL* represents in such a way the amount of resources that should yearly be saved for covering future losses induced by quakes.

The exceedance probability curve is particularly valuable for the national authorities to know the size and distribution of their portfolios' potential losses. In particular, it can be used to determine what proportion of their risk need to be transferred to either a reinsurer and/or the capital market.

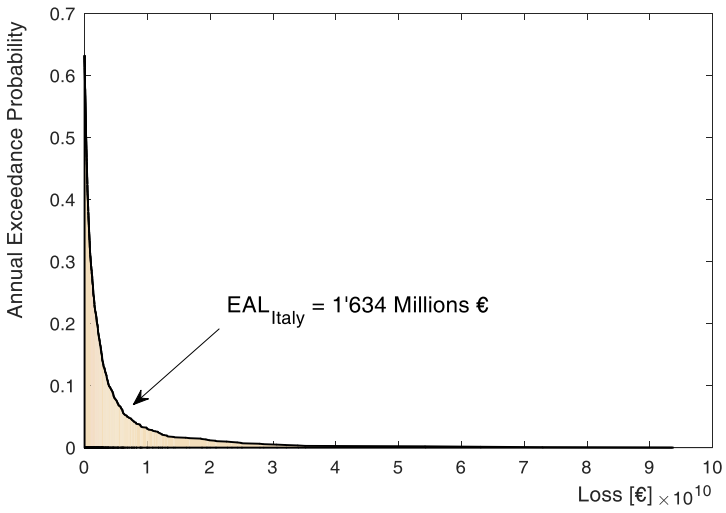

Figure 3.7: Loss Exceedance Probability Curve for Italy

3.5 Seismic risk map of Italy

EAL has also been used as risk-targeted indicator for the development of the seismic risk map of Italy. For each municipality, a *loss exceedance curve* and the *EAL* have been calculated. Figure 3.8 shows the *EAL* map for Italy, evidencing how the exposed value gives a predominant contribution to the final risk rating. The map suggest the yearly amount that should be saved by each Italian municipality to be able to face future repair and reconstruction costs of the residential building stock.

Figure 3.8 shows how extended areas between Emilia-Romagna and Tuscany, the Gargano peninsula, as also the metropolitan areas of Verona, Rome, Naples, Syracuse, are high risk area. Less risky-area of Italy, is the area between Torino and Milano, due both to the very low level of seismicity and to the limited exposure. To better compare risk-levels, *EAL* values have been subdivided by the built area of each municipality deriving the Italian seismic risk map per unit area (Figure 3.9).

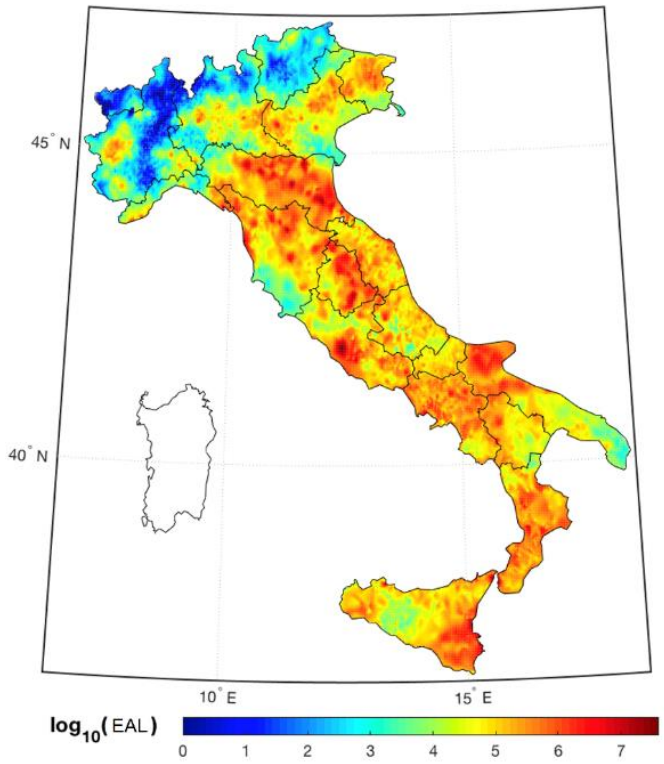

Figure 3.8: Seismic risk map of Italy in terms of EAL [€].

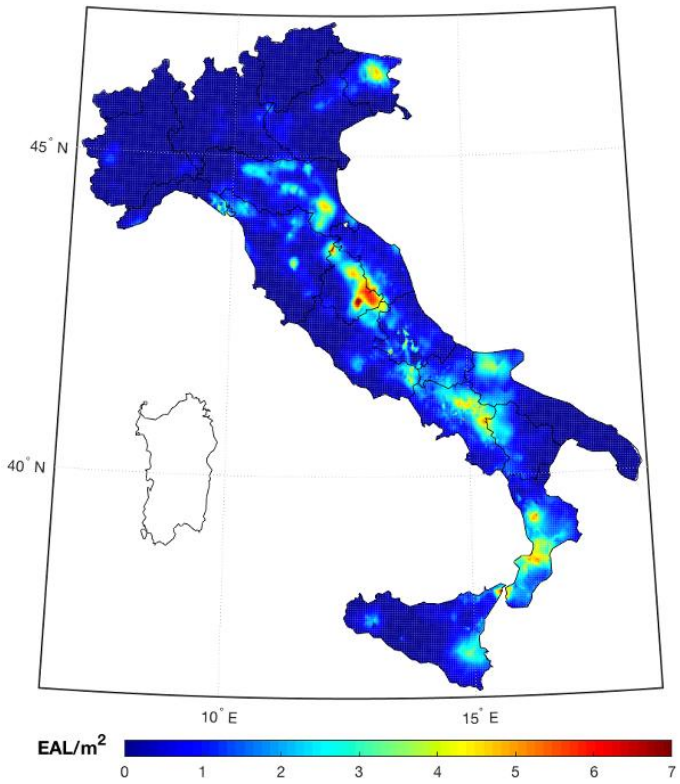

Figure 3.9: Seismic risk map of Italy in terms of EAL/m^2 [€/m^2].

Figure 3.9 shows the resulting map, that can be used as a tool for assessing seismic-induced yearly losses per unit area: in such way, it is possible to take into account seismic risk in relative terms, i.e., considering also the built area of the residential asset in each municipality. The maximum value of EAL/m^2 is of about 7 €/m^2, and such value has been computed for few municipalities over the entire national area, like those in Southern Umbria, recently affected by the 2016 Amatrice seismic sequence, in Irpinia, and for some municipalities close to the cities of Messina and Cosenza. Also Emilia Romagna and Friuli are exposed to a significant level of risk, varying from 3-5 €/m^2.

A further comparison has been carried out between the seismic risk map per unit area and the seismic hazard map of Italy (Figure 3.10), with reference to PGA estimates characterized by a 10% exceedance probability during the service life of a common residential building (i.e., 50 years) (OPCM 3519, 2006). Data of both maps have been subdivided by the respective maximum values, obtaining |*EAL*/m^2| and |PGA| dimensionless values, ranging between 0 and 1. Hence, the residual between |*EAL*/m^2| and |PGA| has been computed for each municipality: this quantity can be seen as a measure directly proportional on how the perception of seismic risk can be over- or under-estimated, with respect to the case in which only seismic hazard is considered as a prioritization criterion. In particular, if the residuals are higher than 0, it means that considering only hazard estimates leads to an underestimation of seismic risk, whereas on the contrary, for values lower than 0, taking into account only hazard estimates implies an overestimation of seismic risk. Figure 3.11 illustrates the map of the residuals between |*EAL*/m^2| and |PGA| dimensionless values, evidencing how in most of highly-prone seismic hazard areas, the risk is overestimated, and this can be attributed to improved quality of building portfolios in terms of structural response and/or a reduced exposure level.

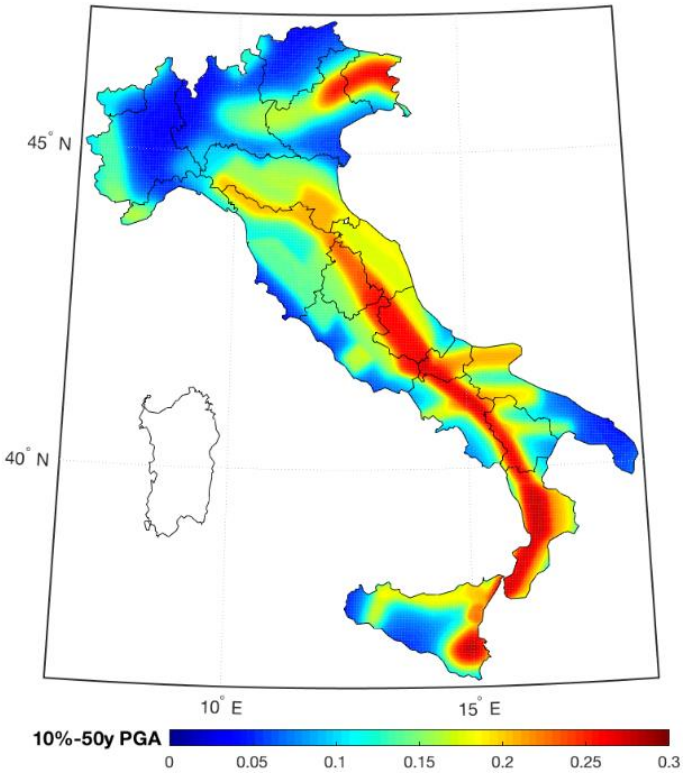

Figure 3.10: Seismic hazard map of Italy (OPCM 3519, 2006).

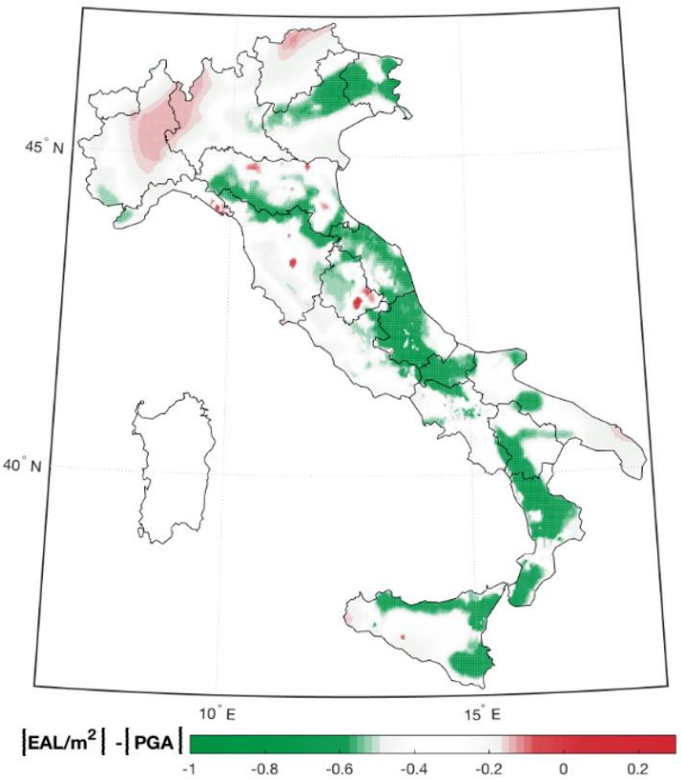

Figure 3.11: Map of the residuals between |EAL/m^2| and |PGA| values.

The comparison evidences how the most critical areas of the country are those characterized by medium levels of seismic hazard, like many cities in the Emilia-Romagna region, and municipalities close to the boundaries of Liguria and Tuscany, and the areas recently affected by the 2016 Amatrice sequence. There are areas with comparable level of seismic hazard, which have a totally different level of seismic risk. In particular, Northern Emilia Romagna and the area around the Garda Lake have almost the same value of PGA (10% in 50 years) of 0.15g (light green), but they are quite different in terms of EAL/m^2. Umbria region, has a medium seismicity level, mainly from 0.2 to 0.25g, while it has the highest level of seismic risk, due to a combination of relatively high exposure and buildings fragility. Other regions of Italy, as Abruzzo and northern Calabria have a very high *PGA* with a return period of 475, but low level of seismic risk, mainly due to the limited exposure.

3.6 Comparison with loss data of historical earthquakes

In section 3.4 we computed the *Expected Annual Loss* for Italy, that represents the amount of money that has to be saved yearly to face seismic risk in Italy. This section analyses historical loss data and shows how a catastrophe fund, could have faced Italian historical earthquakes, by yearly accumulating 1.634 *bn* €. Historical seismicity has been considered starting from 1945, especially due to the absence of reliable monetary data for earlier years. In particular, only earthquakes with magnitude bigger that 5.5 are considered, since smaller earthquakes caused negligible losses. Table 3.3 reports the considered earthquakes with the associated loss and magnitude; in particular, all loss data has been discounted to 2016 to make them comparable. Loss discount has been performed by using official discount rate provided by ISTAT (National Institute of Statistics, http://rivaluta.istat.it/Rivaluta/). Losses of the Amatrice seismic sequence

(2016) were not included in this this study due to the absence of reliable data. Competent authorities are still evaluating the total amount of losses, since little time is passed from the last shake.

Table 3.3: Considered earthquakes from 1945.

#	Location	Year	M_w	Loss [*bn €*]	Reference
1	Calabria Centrale	1947	5.70	0.031	Guidoboni et al. 1997
2	Gargano	1948	5.55	0.011	Guidoboni et al. 1997
3	Gran Sasso	1950	5.69	0.009	Catenacci V. 1992
4	Irpinia	1962	6.15	0.950	Corriere della sera 2017
5	Belice	1968	6.41	8.096	Catenacci V. 1992
6	Friuli	1976	6.45	19.618	Catenacci V. 1992
7	Golfo di Patti	1978	6.03	0.427	Catenacci V. 1992
8	Valnerina	1979	5.83	2.264	Catenacci V. 1992
9	Irpinia	1980	6.81	61.572	Catenacci V. 1992
10	Monti della Meta	1984	5.86	1.178	Catenacci V. 1992
11	Umbria	1984	5.62	0.254	Catenacci V. 1992
12	Carlentini (SR)	1990	5.61	0.151	Guidoboni et al. 1997
13	Potentino	1990	5.77	0.070	Regione Basilicata 2011
14	Umbria – Marche	1997	5.97	5.106	COMFOLIGNO 1998
15	Molise	2002	5.92	1.973	Regione Molise 2010
17	L'Aquila	2009	6.29	5.900	Commissariato per la Ricostruzione 2012
18	Emilia	2012	6.09	5.565	Regione Emilia Romagna 2012

Figure 3.12 reports the aggregate earthquake losses (red line) from 1945 to today, showing an overall loss of 115 *bn* € in only 70 years, while Figure 3.13 shows where these events occurred. Earthquakes occurred in Irpinia (1980) and Friuli (1976), were the two most costly earthquakes from 1945; they caused a loss, respectively of 61.57 *bn* € and 19.62 *bn* €. Figure 3.12 also shows the increasing in time of a potential catastrophe fund (blue line) in which every year, starting from 1945, 1.634 *bn* € are accumulated. When the blue line is above the red one, means that there are accumulated money, available for paying possible losses. On the contrary, when the red line is over the blue line, the fund is recovering from past significant losses.

If Italy had yearly accumulated 1.634 *bn* € (i.e., *EAL*), all the earthquake losses up to 1980 would be covered entirely by this fund.

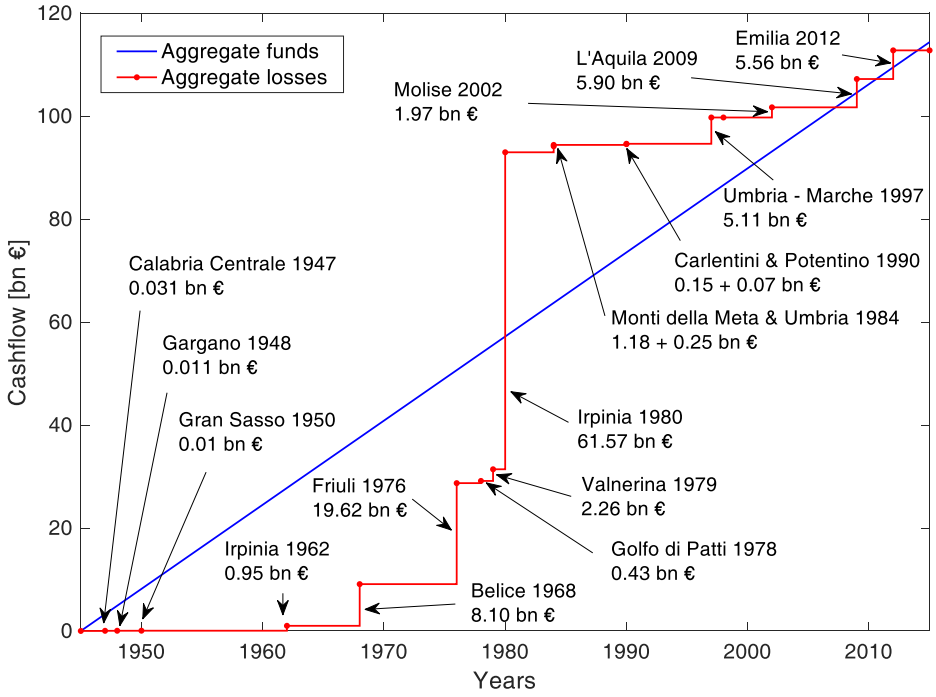

Figure 3.12: Earthquake losses in Italy from 1945.

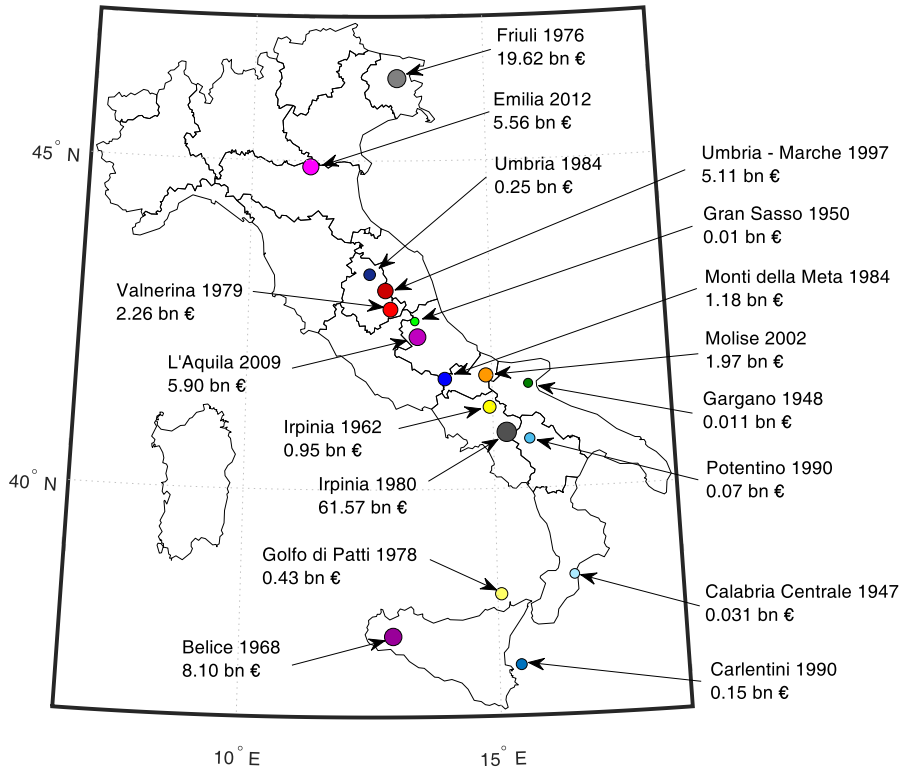

Figure 3.13: Main earthquakes in Italy (1945-2016, $M_w \geq 5.5$).

In particular, accumulated money up to 1980 would have been enough for pay, in relatively little time, the entire losses due to Belice and Friuli earthquakes, respectively 1968 and 1976, and half of the significant loss caused by the earthquake occurred in Irpinia in 1980. About 25 years are needed for recovery from the Irpinia earthquake. Finally, half of the losses caused by L'Aquila and Emilia earthquake would have been covered by accumulated losses. The advantage of this potential solution for managing risk, is the possibility of having a fund working as a reservoir, with relatively small steady income, that accumulated can face some possible big losses. On the contrary, the cons of this strategy are the amount of the sum and the required annual commitment.

3.7 Conclusion

The present chapter illustrated the procedure adopted by the authors to build the seismic risk map of Italy. This goal was achieved simulating a wide set of earthquake scenarios based on the historical seismicity of the Italian peninsula, and the consequent loss assessment performed on the basis of census data of the residential building stock provided by the Italian Institute of Statistic. Loss values were computed at each municipality and then aggregated to derive total losses for each simulated historical event: these data were preliminary used to derive the loss exceedance curve for the entire country, highlighting an *EAL* equal to 1.634 *bn* €, based on the historical seismicity. Hence, loss exceedance curves were built for each municipality leading to the development of the seismic risk map of Italy, in terms of municipal *EAL* values: this tool can be useful for public authorities dealing with the delineation of seismic risk mitigation/transfer policies. Loss estimates were subsequently related to built areas in order to provide the Italian seismic risk map per unit area, useful for the calculation of yearly losses of a building with a certain areal extension placed in a specific

municipality. The importance of adopting a risk-based map was highlighted via a comparison between the proposed seismic risk and the actual seismic hazard maps and supported with specific contextual examples. Finally a comparison with data of the most damaging Italian earthquakes has been done, for the evidencing the behavior of a potential national catastrophe fund, where the yearly sum to be saved is assumed equal to the *Expected Annual Loss of Italy.*

4 Reliability-based CAT bond pricing considering parameter uncertainties

This Chapter analyses Catastrophe bonds (CAT bond) as financial methos for risk-transferring. In particular, CAT bond are risk-linked securities used by the insurance industry to transfer risks associated with the occurrence of natural disasters to the capital markets. Current formulations for pricing analysis do not account for the uncertainties in model parameters. Neglecting such uncertainties might lead to assuming risks that are higher than intended. In this chapter we develop a reliability-based bond pricing considering the uncertainties in the model parameters. The proposed formulation allows for the definition of CAT bond pricing based on a fixed accepted level of risk. The proposed theory is illustrated at the end of the Chapter with a numerical example, and it is widly discussed (Hofer et al. 2018b).

4.1 Introduction

Natural disasters are a source of major concerns worldwide since they can have devastating effects on the communities, in terms of costs for repairing damaged structures, human losses, interruption of business operations and environmental consequences. Rainfalls, windstorms, tornadoes, floods, and earthquakes cause billion dollars losses every year (Gardoni et al. 2016; Gardoni and LaFave 2016).

In 2011, Munich Re (2011) estimated the highest losses induced by natural catastrophes, with more than 380 billion dollars of insurance claims. Private insurance can partially reduce the exposure, especially when dealing with large-scale events like earthquakes and hurricanes, often able to affect the entire economy of a region, leading to high losses. In such cases, financial losses can severely drain the capital capacity of private insurance

companies. This is one of the causes of the reduced diffusion of earthquake insurance policies, in particular in areas highly prone to such type of hazard. In some countries, catastrophe losses are managed by governments and public authorities. In this "welfarist" context, householders are not encouraged to subscribe private insurance contracts, and, biased by a low perception of risk, they are often not willing to invest in retrofit interventions. Such situations can be particularly difficult for governments, but also for private reinsurance companies with large portfolios.

For this reason, capital capacity needs to be secured for covering high-level losses via the development of more sophisticated Alternative Risk Transfer (ALR) products. One ALR solution is represented by the insurance-linked securitization, an alternative way for transfer catastrophe risk into securities (i.e., CAT bonds) and selling them to financial entities able to absorb such high levels of losses (i.e., financial markets). CAT bonds offer a significant supply for reinsurance surpassing the capacity of traditional providers and are therefore well suited to provide coverage for substantial losses (Kunreuther 2001).

CAT bonds are usually structured as coupon-paying bonds with a default linked to the occurrence of a trigger event. One of the main concerns in issuing an earthquake CAT bond is the definition of the trigger event. A commonly used trigger event is the overcoming of a loss threshold (Kunreuther and Pauly 2010). For some specific natural catastrophes, like for earthquakes, physically-based parametric triggers can be alternatively used to avoid the manipulation of the payment mechanism and moral hazard issues (Cummins 2008).

Some studies provide examples of national scale application. Hardle and Cabrera (2010) developed the calibration of a real parametric catastrophe bond for earthquakes. The authors proposed the creation of 160 million dollars 3 years CAT bond sold by the CAT-Mex Ldt class B insurer special purpose vehicle, defining a trigger magnitude value for each of the 9

seismic regions considered. Franco (2010) presented a process to minimize the trigger error with an example of an earthquake CAT bond for Costa Rica. Goda (2013) investigated the effectiveness of two trigger mechanisms for parametric earthquake catastrophe bonds using alternatively scenario-based and station intensity-based approaches to a case study of 2,000 wood-frame houses in southwestern British Columbia.

Recently, Takahashi (2017) developed new financial derivatives for encouraging earthquake protection, in which the building owner has to pay for the earthquake protection only when the specified earthquake occurs.

However, further work is needed to improve the pricing of CAT bonds and reduce errors associated with the definition of the trigger event that might leads to the CAT bond default. In particular, no research has been done regarding the computation of the default probability of a CAT bond and the propagation of parameters uncertainties on the probability of failure itself and the pricing. Assessing the uncertainties underlying the CAT bonds issuance is a crucial step for their accurate pricing and economic sustainability.

In this chapter we propose proposes a mathematical framework able to compute in a semi-analytical form the probability of failure P_f (i.e., the probability that the losses exceed a certain threshold D before the bond expiration time T) and its uncertainty associated with the stochastic process underlying bond pricing. This piece of information is used for the reliability assessment of the CAT bond pricing through the computation of the pricing probability distribution. A compound doubly stochastic Poisson process is used in this work (Burnecki and Kukla 2003). However the approach is general and can also consider to non-Poissonian processes.

This Chapter starts with a brief overview of the current pricing methodology. Then following sections present the proposed mathematical formulation for the computation of P_f and for a reliability-based CAT bond pricing. Finally, an application to a benchmark case study is reported.

4.2 CAT bond issuing practices

Despite their growing importance, different and relatively few researches on CAT bond pricing can be found in the literature (Braun 2016, Shao 2015). Barishnikov et al. (2001) developed a pricing methodology, subsequently improved by Burnecki and Kukla (2003) and Burnecki et al. (2005), based on the characteristic of the dominant underlying process. Härdle and Cabrera (2010) adopted the same approach to calibrate CAT bond prices for Mexican earthquakes and demonstrated the benefit of using a combination of reinsurance and CAT bond. Galeotti et al. (2013) and Jaeger et al. (2010) compared selected premium calculation models present in literature to see their accuracy and predictive power.

Burnecki and Kukla (2003) and Härdle and Cabrera (2010) modeled the catastrophe process as a compound doubly stochastic Poisson process. The underlying assumption is that potentially catastrophic events follow a Poisson point process, constant or more generally varying intensity function over time. Catastrophes may cause significant economic losses, that can be assumed independent and generated from a common probability distribution (Burnecki et al. 2005). The CAT bond is usually defined in a specific region, considering a certain type of catastrophe, its intensity over time, and referring to a specific insured property class.

In mathematical terms, an aggregate loss process L_t and its probability of overcoming a certain triggering threshold D has to be known for CAT bond pricing. Given a probability space (Ω, F, Ft, ν), and an increasing filtration $F_t \subset F$, $t \in [0, T]$ the following assumptions are introduced:

- A doubly stochastic Poisson process M_s with s ∈ [0, T] is considered (Burnecki and Kukla 2003), whose marks are independent, identically distributed (*iid*) random variables. The process is characterized by a constant intensity function ms in case of homogeneous Poisson process (HPP), or varying $m_s(s)$ in case of

non-homogeneous Poisson process (NHPP). Parameters characterizing the Poisson point process are denoted by $\boldsymbol{\Theta}_P$. The Poisson point process describes the flow of the considered catastrophic natural event in the specific region of the CAT bond contract. The Poisson process is calibrated according to the physics of the considered natural disaster and its behaviour. The time instants t_i of potential loss events are denoted as $0 \le t_1 \le \ldots \le t_i \le \ldots \le T$; in particular, the probability of n shocks in the interval [0, t] for the more general *NHPP*, is given by

$$P\left[N(t)=n\right]=\frac{\left[\int_0^t m_s(s)\,ds\right]^n \cdot e^{-\int_0^t m_s(s)ds}}{n!} \quad n=0,1,... \tag{4.1}$$

In the case of HPP, Eq. 1.1 becomes

$$P\left[N(t)=n\right]=\frac{(m_s t)^n \cdot e^{-m_s t}}{n!} \quad n=0,1,... \tag{4.2}$$

- Financial losses $\{X_i\ ,\ i = 1,2,...n\}$ associated to each event t_i are independent, identically distributed random variables with common cumulative distribution function (CDF) such that $F(x) = P(X_i \le x)$. This distribution function has to correctly fit the observed claims. Parameters describing the loss distribution are referred as $\boldsymbol{\Theta}_L$;
- Accumulated losses at time instant t are represented by a predictable, left-continuous and increasing aggregate loss process L_t, defined as

$$L_t(t)=\sum_{i=1}^{N(t)} X_i \tag{4.3}$$

- A continuous progressive process of the discount interest rate r describes the value at time s of 1 US$ paid at time t (with $s > t$) by

$$e^{-R(s,t)} = e^{-\int_s^t r(\xi)d\xi} \tag{4.4}$$

- the first failure of the system is considered when the accumulated losses exceed the threshold level D; formally the threshold time

event is given by τ = Inf $\{t: L_t \geq D\}$. Barishnikov et al. (2001) introduced a new doubly stochastic Poisson process $N_t = \mathbf{1}_{(Lt \geq D)}$ of the threshold time and showed that the associated intensity is equal to

$$\lambda_s = m_s \{1 - F(D - L_s)\} \mathbf{1}(L_s < D) \quad 4.5$$

Under these assumptions, given the threshold D, the doubly stochastic Poisson process M_s and the distribution function of incurred losses F, the no-arbitrage price of the zero-coupon CAT bond (V_t^1) paying Z at maturity (Burnecki and Kukla 2003) is

$$V_t^1 = E\left[Z\, e^{-\int_t^T r(\xi)d\xi} (1 - N_T) \mid F_t \right] = E\left[Z\, e^{-\int_t^T r(\xi)d\xi} \left\{ 1 - \int_t^T m_s \left[1 - F(D - L_s) \right] \mathbf{1}_{(L_s < D)} ds \right\} \mid F_t \right] \quad 4.6$$

Similarly, Burnecki and Kukla (2003) provided the following no-arbitrage pricing formula for the only-coupon CAT bond (V_t^2), which has only coupon payments C_s, and terminate at the threshold time τ:

$$\begin{aligned} V_t^2 &= E\left[\int_t^T e^{-\int_t^s r(\xi)d\xi} C_s (1 - N_s) ds \mid F_t \right] = \\ &= E\left[\int_t^T e^{-\int_t^s r(\xi)d\xi} C_s \left\{ 1 - \int_t^s m_\xi \left[1 - F(D - L_\xi) \right] \mathbf{1}_{(L_\xi < D)} d\xi \right\} ds \mid F_t \right] \end{aligned} \quad 4.7$$

Finally, combining Eq. 4.6 with Z equal to par value (PV) and Eq. 4.7, the no-arbitrage price of the coupon CAT bond (V_t^3) paying PV at maturity, and coupon payments C_s, which cease at threshold time τ, can be obtained (Burnecki and Kukla 2003) as

$$V_t^3 = E\left[PV\, e^{-\int_t^T r(\xi)d\xi} (1 - N_T) + \int_t^T e^{-\int_t^s r(\xi)d\xi} C_s (1 - N_s) ds \mid F_t \right] \quad 4.8$$

Eqs. 4.6-4.7 provide the CAT bond pricing surface for each combination of maturity time T and threshold level D (T-D combination), depending on the initial parameters $\mathbf{\Theta} = [\mathbf{\Theta}_P; \mathbf{\Theta}_L]$. However, this approach is unable to show

how the variability in $\boldsymbol{\Theta}$ influences the pricing. To show such dependence on $\boldsymbol{\Theta}$, the notation $V_t^1(T,D;\boldsymbol{\Theta})$, $V_t^2(T,D;\boldsymbol{\Theta})$ and $V_t^3(T,D;\boldsymbol{\Theta})$ is introduced in the following section.

4.3 Proposed probabilistic reliability-based CAT bond design

4.3.1 Failure probability assessment for the compound doubly stochastic Poisson process

The investigation of the influence of $\boldsymbol{\Theta}$ on *CAT* bond pricing requires a deeper knowledge of the stochastic process underlying the pricing. In particular, the first failure probability P_f of the Compound Doubly Stochastic Poisson process has to be assessed for each *T-D* combination, given the initial parameters $\boldsymbol{\Theta}$, as

$$P_f(T,D;\boldsymbol{\Theta}) = P\left[L_s(T;\boldsymbol{\Theta}) \geq D\right] \tag{4.9}$$

Using Eq. 4.3 for the accumulated losses by time *T*, and conditioning on the number of events, Eq. 4.9 becomes

$$P_f(T,D;\boldsymbol{\Theta}) = \sum_{n=1}^{\infty} P\left[\sum_{i=1}^{n} X_i(\boldsymbol{\Theta}_L) \geq D \,\middle|\, N(T;\boldsymbol{\Theta}_P) = n\right] \cdot P\left[N(T;\boldsymbol{\Theta}_P) = n\right] \tag{4.10}$$

Given the independence between the Poisson point process and the incurred losses, Eq. 4.10 furtherly simplifies to

$$\begin{aligned} P_f(T,D;\boldsymbol{\Theta}) &= \sum_{n=1}^{\infty} P\left[\sum_{i=1}^{n} X_i(\boldsymbol{\Theta}_L) \geq D\right] \cdot P\left[N(T;\boldsymbol{\Theta}_P) = n\right] \\ &= \sum_{n=1}^{\infty} \left\{1 - P\left[\sum_{i=1}^{n} X_i(\boldsymbol{\Theta}_L) < D\right]\right\} \cdot P\left[N(T;\boldsymbol{\Theta}_P) = n\right] \\ &= \sum_{n=1}^{\infty} \left[1 - C_X^n(D;\boldsymbol{\Theta}_L)\right] \cdot P\left[N(T;\boldsymbol{\Theta}_P) = n\right] \end{aligned} \tag{4.11}$$

where $C_X^n(D;\boldsymbol{\Theta}_L)$ is the *n*-fold convolution of the loss distribution evaluated in *D*, and represents the *CDF* of ($X_1 + X_2 + \ldots + X_n$). In the most general case, $P[N(T;\boldsymbol{\Theta}_P)=n]$ is given by Eq. (4.1).

Similar approaches have been used to model the failure probability in deteriorating engineering systems (Kumar et al. 2015). This formulation is general and can be applied to every loss distribution type.

4.3.2 Uncertainty of P_f *arising from parameter uncertainties*

Exact evaluation of the distribution of P_f (T,D;$\boldsymbol{\Theta}$) due to the uncertainties in $\boldsymbol{\Theta}$ requires nested reliability calculations (Der Kiureghian 1989; Gardoni et al. 2002). Uncertainty inherent in the calculation due to parameters variability can be assessed through approximate confidence bounds obtained by first-order analysis (Gardoni et al. 2002). The mean reliability index corresponding to the failure probability in Eq. 4.11 is defined as

$$\beta\left(T,D;\boldsymbol{\Theta}\right)=\Phi^{-1}\left[1-P_f\left(T,D;\boldsymbol{\Theta}\right)\right] \tag{4.12}$$

where $\Phi^{-1}(\cdot)$ represents the inverse of the standard normal cumulative probability. The variance of $\sigma_\beta^2\left(T,D;\boldsymbol{\Theta}\right)$ can be approximated using a first-order Taylor series expansion around $\mathbf{M}_{\boldsymbol{\Theta}}$, where $\mathbf{M}_{\boldsymbol{\Theta}}$ is the mean vector of the model parameters $\boldsymbol{\Theta}$

$$\sigma_\beta^2\left(T,D;\boldsymbol{\Theta}\right)\approx\nabla_{\boldsymbol{\Theta}}\,\beta\left(T,D;\boldsymbol{\Theta}\right)^T\boldsymbol{\Sigma}_{\boldsymbol{\Theta}\boldsymbol{\Theta}}\nabla_{\boldsymbol{\Theta}}\,\beta\left(T,D;\boldsymbol{\Theta}\right) \tag{4.13}$$

where $\boldsymbol{\Sigma}_{\boldsymbol{\Theta}\boldsymbol{\Theta}}$ is the covariance matrix of the model parameters and $\nabla_{\boldsymbol{\Theta}}\,\beta\left(T,D;\boldsymbol{\Theta}\right)$ is the gradient column vector of $\beta\left(T,D;\boldsymbol{\Theta}\right)$ at $\mathbf{M}_{\boldsymbol{\Theta}}$, calculated as

$$\nabla_{\boldsymbol{\Theta}}\,\beta\left(T,D;\boldsymbol{\Theta}\right)^T=\left[\frac{\partial\beta}{\partial\Theta_1};\ \frac{\partial\beta}{\partial\Theta_2}\cdots\frac{\partial\beta}{\partial\Theta_n}\right] \tag{4.14}$$

The vector $\mathbf{M}_{\boldsymbol{\Theta}}$ can be estimated either with the maximum likelihood estimation method or, more precisely, with the Bayesian updating technique, as the posterior mean vector. As for $\mathbf{M}_{\boldsymbol{\Theta}}$, the covariance matrix $\boldsymbol{\Sigma}_{\boldsymbol{\Theta}\boldsymbol{\Theta}}$ can be computed in first approximation as the negative of the inverse of the Hessian of the log-likelihood function or, again, more accurately with a Bayesian updating technique (Gardoni et al. 2002).

The gradient of β in Eq. 4.14 is computed applying the chain rule to Eq. 4.12 as

$$\nabla_{\boldsymbol{\Theta}} \beta(T, D; \boldsymbol{\Theta}) = -\frac{1}{\varphi\left[\beta(T, D; \boldsymbol{\Theta})\right]} \nabla_{\boldsymbol{\Theta}} P_f(T, D; \boldsymbol{\Theta}) \qquad 4.15$$

where $\varphi(\cdot)$ represents the standard normal probability density function and $\nabla_{\boldsymbol{\Theta}} P_f(T, D; \boldsymbol{\Theta})$ is the gradient column vector of $P_f(T, D; \boldsymbol{\Theta})$ computed at $\mathbf{M}_{\boldsymbol{\Theta}}$. As a result, $\nabla_{\boldsymbol{\Theta}} P_f(T, D; \boldsymbol{\Theta})$ can be computed using a first order approximation in $\mathbf{M}_{\boldsymbol{\Theta}}$ as

$$\nabla_{\boldsymbol{\Theta}} P_f(T, D; \boldsymbol{\Theta}) = \begin{bmatrix} \dfrac{\partial P_f}{\partial \Theta_1} = \dfrac{P_f(T, D; \Theta_1 + \delta\Theta, \Theta_2, \ldots \Theta_n) - P_f(T, D; \Theta_1, \Theta_2, \ldots \Theta_n)}{\delta\Theta} \\ \vdots \\ \dfrac{\partial P_f}{\partial \Theta_n} = \dfrac{P_f(T, D; \Theta_1, \Theta_2, \ldots \Theta_n + \delta\Theta) - P_f(T, D; \Theta_1, \Theta_2, \ldots \Theta_n)}{\delta\Theta} \end{bmatrix} \qquad 4.16$$

(16)

Bounds on the reliability index β can be computed in terms of a specified number *k* of standard deviations away from the mean μ_β, as $\mu_\beta(T, D; \boldsymbol{\Theta}) + k \cdot \sigma_\beta(T, D; \boldsymbol{\Theta})$. Transforming $\mu_\beta(T, D; \boldsymbol{\Theta}) + k \cdot \sigma_\beta(T, D; \boldsymbol{\Theta})$ back into the probability space, and considering *k = -1* and *k = 1*, one obtains

$$\left\{\Phi\left[-\mu_\beta(T, D; \boldsymbol{\Theta}) - \sigma_\beta(T, D)\right], \Phi\left[-\mu_\beta(T, D; \boldsymbol{\Theta}) + \sigma_\beta(T, D)\right]\right\} \qquad 4.17$$

as the approximate 15% and 85% percentile bounds of P_f, containing approximately 70% of the probability.

4.3.3 Failure Probability in CAT bond pricing formula

The detailed knowledge of the stochastic process underlying *CAT* bond pricing given by the accurate computation of P_f and its confidence bounds is then used in the probabilistic assessment of *CAT* bond pricing.

Starting from Eqs. 4.6-4.8, formulations are rearranged by using the definition of the expected value. For the *zero-coupon CAT* bond (V_t^1) price, this gives

$$
\begin{aligned}
V_t^1(T,D;\Theta) &= E\left[Z\, e^{-\int_t^T r(\xi)d\xi} \left(1-N_T\right) \middle| F_t \right] = \\
&= Z\, e^{-\int_t^T r(\xi)d\xi} E\left[1\text{-}1\left(L_T \geq D\right) \middle| F_t\right] = \\
&= Z\, e^{-\int_t^T r(\xi)d\xi} \left\{1-1\cdot P\left[L_s(T;\Theta) \geq D \middle| F_t\right]\right\} = \\
&= Z\, e^{-\int_t^T r(\xi)d\xi} \left[1-P_f\left(T,D;\Theta \middle| F_t\right)\right]
\end{aligned}
\qquad 4.18
$$

Similar to the previous case, Eq. 4.8 for *only-coupon CAT* bond (V_t^2) price becomes

$$
\begin{aligned}
V_t^2(T,D;\Theta) &= E\left[\int_t^T e^{-\int_t^s r(\xi)d\xi} C_s \left(1-N_s\right) ds \middle| F_t \right] = \\
&= \int_t^T e^{-\int_t^s r(\xi)d\xi} C_s \left\{1-1\cdot P\left[L_s(s,D;\Theta) \geq D \middle| F_t\right]\right\} ds \\
&= \int_t^T e^{-\int_t^s r(\xi)d\xi} C_s \left[1-P_f\left(s,D;\Theta \middle| F_t\right)\right] ds
\end{aligned}
\qquad 4.19
$$

As done for the first two cases, the *coupon CAT* bond (V_t^3) price formula can be written as

$$
\begin{aligned}
V_t^3(T,D;\Theta) = \Bigg\{ & PV\, e^{-\int_t^T r(\xi)d\xi} \left[1-P_f\left(T,D;\Theta \middle| F_t\right)\right] + \\
& + \int_t^T e^{-\int_t^s r(\xi)d\xi} C_s \left[1-P_f\left(s,D;\Theta \middle| F_t\right)\right] ds \Bigg\}
\end{aligned}
\qquad 4.20
$$

4.3.4 Reliability-based CAT bond design

The final objective, and the aim of this Chapter consists in defining a procedure for *CAT* bond pricing, based on a fixed accepted level of risk. In other terms, the issuer defines a quantile $\overline{p}$ on the $P_f(T,D;\Theta)$ distribution and finds the related *CAT* bond pricing surface, characterized by a constant

reliability value for each *T-D* combination. Figure 4.1 shows the P_f curve for a certain money threshold *D*; (1- $\bar{p}$) represents the probability that the real P_f is bigger than the probability $P_{f,d}$ assumed for the pricing design. In the following we also show that the same quantile represents the probability that the bond price is under-priced.

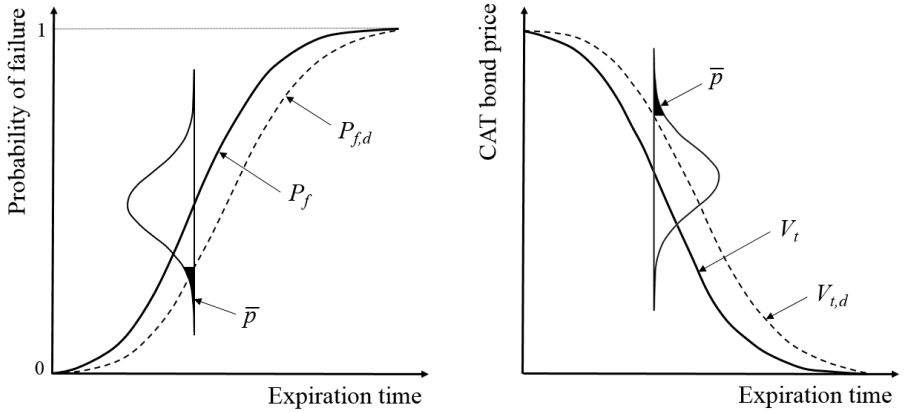

Figure 4.1: Relationship between failure probabilities P_f, $P_{f,d}$ and CAT bond prices V_t, $V_{t,d}$, given a quantile $\bar{p}$.

Formally, this condition can be written in the following way:

$$P\left[P_f\left(T,D;\Theta\right) < P_{f,d}\left(T,D;\Theta\right)\right] = \bar{p} \tag{4.21}$$

Using Eq. 4.12, previous formula can be furtherly simplified in

$$F_\beta\left[\Phi^{-1}\left(1-P_{f,d}\left(T,D;\Theta\right)\right)\right] = 1-\bar{p} \tag{4.22}$$

where F_β is the CDF of β.

Since the reliability index is normally distributed around the mean μ_β with standard deviation σ_β computed according to Eq. 4.13, Eq. 4.22 becomes

$$\begin{aligned}&\Phi\left[\frac{\Phi^{-1}\left(1-\bar{p}\right)-\mu_\beta\left(T,D;\Theta\right)}{\sigma_\beta\left(T,D;\Theta\right)}\right] = \\ &= \Phi\left[\frac{\mu_\beta\left(T,D;\Theta\right)+k\cdot\sigma_\beta\left(T,D;\Theta\right)-\mu_\beta\left(T,D;\Theta\right)}{\sigma_\beta\left(T,D;\Theta\right)}\right] = 1-\bar{p}\end{aligned} \tag{4.23}$$

where $k \cdot \sigma_\beta$ represents the quantile of β reflecting the level of risk that the analyst wants to assume with $\bar{p}$. From Eq. 4.23 *k* and $P_{f,d}$ can be derived as follows:

$$k = \Phi^{-1}\left[1 - \bar{p}\right] \tag{4.24}$$

$$P_{f,d}\left(T, D; \Theta\right) = \Phi\left[-\mu_\beta\left(T, D; \Theta\right) - k \cdot \sigma_\beta\left(T, D; \Theta\right)\right] \tag{4.25}$$

Note that *k* is a constant that is calculated starting from the assumed quantile $\bar{p}$. The design $P_{f,d}$ can now be used for calculating the corresponding *CAT* bond pricing $V_{t,d}^{i}$ surface, respectively for the *zero-coupon*, *only-coupon* and *coupon CAT* bond pricing, where Eqs. 4.18-4.20 have been modified by substituting P_f with $P_{f,d}$ as follows:

$$V_{t,d}^{1}\left(T, D; \Theta\right) = Z\, e^{-\int_t^T r(\xi)d\xi}\left[1 - P_{f,d}\left(T, D; \Theta \mid F_t\right)\right] \tag{4.26}$$

$$V_{t,d}^{2}\left(T, D; \Theta\right) = \int_t^T e^{-\int_t^s r(\xi)d\xi} C_s\left[1 - P_{f,d}\left(s, D; \Theta \mid F_t\right)\right] ds \tag{4.27}$$

$$V_{t,d}^{3}\left(T, D; \Theta\right) = \left\{ PV\, e^{-\int_t^T r(\xi)d\xi}\left[1 - P_{f,d}\left(T, D; \Theta \mid F_t\right)\right] + = + \int_t^T e^{-\int_t^s r(\xi)d\xi} C_s\left[1 - P_{f,d}\left(s, D; \Theta \mid F_t\right)\right] ds \right\} \tag{4.28}$$

In particular, for all these cases, assuming a quantile on P_f implies considering the same probability that the *CAT* bond is under-priced. Formally, this statement is given by the following:

$$P\left[P_f < P_{f,d}\right] = P\left[V_t^i > V_{t,d}{}^i\right] = \bar{p} \qquad for\ i = 1,2,3 \tag{4.29}$$

When $\bar{p}$ = 0.5 the *predictive* value of P_f and V_t^i is computed, according to Eq. (11, 18-20), without any further information related to parameter uncertainties (*k=0*). With this procedure, we can use the information related to the parameter uncertainties and find pricing surfaces

$V_{t,d}^{i}$ where all points are characterized by a constant level of risk, even if they correspond to different values of P_f.

4.3.5 Proof of Eq. 4.29

***Zero-coupon CAT* bond**

We need to prove that using $P_{f,d}$ in Eq. 4.26 leads to $V_{t,d}^{1}$ such that the probability content assumed with $\bar{p}$ on P_f is also maintained in the CAT bond price distribution. Formally it has to be proven that

$$P\left[V_t^1 > V_{t,d}{}^1\right] = \bar{p} \quad \rightarrow \quad P\left[V_t^1 < V_{t,d}{}^1\right] = 1 - \bar{p} \tag{4.30}$$

In the proof, for the sake of clarity, the dependence on T, D and $\boldsymbol{\Theta}$ has been omitted from the notation. Using Eq. 4.18, Eq. 4.30 becomes

$$P\left[P_f > 1 - x\right] = 1 - \bar{p} \quad with \quad x = \frac{V_{t,d}{}^1}{Z\, e^{-\int_t^T r(\xi) d\xi}} \tag{4.31}$$

Using the relation between the failure probability and the reliability index $P_f = \Phi(-\beta)$, Eq. 4.31 simplifies further as

$$P\left[\beta < -\Phi^{-1}(1-x)\right] = F_\beta\left[-\Phi^{-1}(1-x)\right] = 1 - \bar{p} \tag{4.32}$$

Because of the normality of the reliability index with parameters μ_β and σ_β, one obtains

$$\Phi\left[\frac{-\Phi^{-1}(1-x) - \mu_\beta}{\sigma_\beta}\right] = \Phi\left[\frac{\mu_\beta + k \cdot \sigma_\beta - \mu_\beta}{\sigma_\beta}\right] = 1 - \bar{p} \tag{4.33}$$

that leads to $x = 1 - \Phi\left[-\mu_\beta - k \cdot \sigma_\beta\right] = 1 - P_{f,d}$. Replacing x in Eq. 4.33, we obtain the Zero Coupon pricing formula evaluated with $P_{f,d}$.

$$V_{t,d}^{1} = Z\, e^{-\int_t^T r(\xi) d\xi}\left[1 - P_{f,d}\right] \tag{4.34}$$

***Only-coupon CAT* bond**

This is a special case of *Coupon CAT* bond discussed next.

***Coupon CAT* bond**

Also in this case, we can show that the quantile assumption on P_f is maintained in V_t^3 when calculated using $P_{f,d}$ and k. The only difference, in this case, is that the pricing formula for $V_{t,d}^3$ is more complex that the one for $V_{t,d}^1$ because it is the sum of two contributions. Also in this case, the dependence on D and $\boldsymbol{\Theta}$ will be omitted from the notation. Starting from

$$V_{t,d}^3 = PV\, e^{-\int_t^T r(\xi)d\xi}\left[1-P_{f,d}(T)\right] + \int_t^T e^{-\int_t^s r(\xi)d\xi}\, C_s\, \left[1-P_{f,d}(s)\right]ds \qquad 4.35$$

and using the definition of $P_{f,d}$ (Eq. 4.25), Eq. 4.35 can be written as

$$\begin{aligned} V_{t,d}^3 = PV\, e^{-\int_t^T r(\xi)d\xi}\left\{1-\Phi\left[-\mu_\beta(T)-k\cdot\sigma_\beta(T)\right]\right\} + \\ + \int_t^T e^{-\int_t^s r(\xi)d\xi}\, C_s\, \left\{1-\Phi\left[-\mu_\beta(s)-k\cdot\sigma_\beta(s)\right]\right\}ds \end{aligned} \qquad 4.36$$

Eq. 4.36 can be simplified by using a Taylor expansion of $\Phi\left[-\mu_\beta(s)-k\cdot\sigma_\beta(s)\right]$ up to the first order, around $-\mu_\beta(s)$

$$\Phi\left[-\mu_\beta(s)-k\cdot\sigma_\beta(s)\right] = \Phi\left[-\mu_\beta(s)\right] - k\cdot\frac{\partial\Phi}{\partial\beta}\left[-\mu_\beta(s)\right]\cdot\sigma_\beta(s) \qquad 4.37$$

Using Eq. 4.35, Eq. 4.36 becomes

$$\begin{aligned} V_{t,d}^3 &= PV\, e^{-\int_t^T r(\xi)d\xi}\left\{1-\Phi\left[-\mu_\beta(T)\right]\right\} + \int_t^T e^{-\int_t^s r(\xi)d\xi}\, C_s\, \left\{1-\Phi\left[-\mu_\beta(s)\right]\right\}ds + \\ &+ k\cdot\left\{PV\, e^{-\int_t^T r(\xi)d\xi}\cdot\frac{\partial\Phi}{\partial\beta}\left[-\mu_\beta(T)\right]\cdot\sigma_\beta(T) + \int_t^T e^{-\int_t^s r(\xi)d\xi}\, C_s\, \frac{\partial\Phi}{\partial\beta}\left[-\mu_\beta(s)\right]\cdot\sigma_\beta(s)ds\right\} = \\ &= V_t^3 + k\cdot\left\{PV\, e^{-\int_t^T r(\xi)d\xi}\cdot\frac{\partial\Phi}{\partial\beta}\left[-\mu_\beta(T)\right]\cdot\sigma_\beta(T) + \int_t^T e^{-\int_t^s r(\xi)d\xi}\, C_s\, \frac{\partial\Phi}{\partial\beta}\left[-\mu_\beta(s)\right]\cdot\sigma_\beta(s)ds\right\} \end{aligned} \qquad 4.38$$

where $V_{t,d}^3$ can be seen as the sum of the predicted value, function of $\boldsymbol{\Theta}$, and a q fraction of the standard deviation $\sigma_{V_t^3}$ ($V_{t,d}^3 = V_t^3 + q\cdot\sigma_{V_t^3}$). From Eq. 4.38, the following relation can thus be derived:

$$q\cdot\sigma_{V_t^3}=k\cdot\left\{PV\,e^{-\int_t^T r(\xi)d\xi}\cdot\frac{\partial\Phi}{\partial\beta}\left[-\mu_\beta(T)\right]\cdot\sigma_\beta(T)+\right.$$
$$\left.=+\int_t^T e^{-\int_t^s r(\xi)d\xi}\,C_s\,\frac{\partial\Phi}{\partial\beta}\left[-\mu_\beta(s)\right]\cdot\sigma_\beta(s)ds\right\} \qquad 4.39$$

Using a first order approximation of $P_f(s)=\Phi[-\beta(s)]$, the standard deviation of P_f can be written as $\sigma_{P_f}(s)=\frac{\partial\Phi}{\partial\beta}\left[-\mu_\beta(s)\right]\cdot\sigma_\beta(s)$; consequently Eq. 4.39 becomes

$$q\cdot\sigma_{V_t^3}=k\cdot\left[PV\,e^{-\int_t^T r(\xi)d\xi}\cdot\sigma_{P_f}(T)+\int_t^T e^{-\int_t^s r(\xi)d\xi}\,C_s\;\sigma_{P_f}(s)ds\right] \qquad 4.40$$

Now, the variance of V_t^3 can be calculated in analogy to Eq. 4.13 as $\sigma^2_{V_t^3}\approx\nabla_{\boldsymbol{\Theta}}{}^T V_t^3\,\boldsymbol{\Sigma}_{\boldsymbol{\Theta}\boldsymbol{\Theta}}\nabla_{\boldsymbol{\Theta}}V_t^3$. Since the gradient of V_t^3 respect to the distributions' parameters is

$$\nabla_{\boldsymbol{\Theta}}V_t^3=-PV\,e^{-\int_t^T r(\xi)d\xi}\nabla_{\boldsymbol{\Theta}}P_f(T)-\int_t^T e^{-\int_t^s r(\xi)d\xi}\,C_s\,\nabla_{\boldsymbol{\Theta}}P_f(s)ds \qquad 4.41$$

and $\sigma_{P_f}(s_1)\,\sigma_{P_f}(s_2)\approx\nabla_{\boldsymbol{\Theta}}{}^T P_f(s_1)\boldsymbol{\Sigma}_{\boldsymbol{\Theta}\boldsymbol{\Theta}}\nabla_{\boldsymbol{\Theta}}P_f(s_2)$, the variance has the following formulation:

$$\sigma^2_{V_t^3}\approx PV^2\,e^{-2\cdot\int_t^T r(\xi)d\xi}\sigma^2_{P_f}(T)+$$
$$+\int_t^T\int_t^T e^{-\int_t^{s_1} r(\xi)d\xi}\,e^{-\int_t^{s_2} r(\xi)d\xi}\,C_{s_1}C_{s_2}\;\sigma_{P_f}(s_1)\sigma_{P_f}(s_2)ds_1ds_2+ \qquad 4.42$$
$$+2\,PV\cdot e^{-\int_t^T r(\xi)d\xi}\,\sigma_{P_f}(T)\int_t^T e^{-\int_t^s r(\xi)d\xi}\,C_s\,\sigma_{P_f}(s)ds$$

If we square both sides of Eq. 4.40, the formula in the square brackets is $\sigma^2_{V_t^3}$ as derived in Eq. 4.42 and consequently q has to be equal to k. Since $q=k$ is valid for any k, partial quantile descriptors of β, P_f and V_t^3 are the same and consequently also the correspondent probability. Finally, since

V_t^3 is proportional to the complementary probability of P_f, as seen in the previous proof, it can be stated that

$$P\left[P_f < P_{f,d}\right] = P\left[V_t^3 > V_{t,d}^{\ 3}\right] = \overline{p} \qquad 4.43$$

4.4 Case study

The proposed formulation is used to a benchmark case described in Burnecki and Kukla (2003), in which CAT bonds were priced from US market's loss amounts caused by natural perils occurred between 1990 and 1999. In Burnecki and Kukla (2003), loss amounts were characterized by a lognormal distribution with parameters μ = 18.4406 and σ = 1.1348, and a daily intensity of the Poisson process m_s = 0.095. The continuous discount rate r equivalent to LIBOR = 2.5% was assumed constant and equal to $ln(1.025)$. Expiration time and threshold level were considered respectively ranging between [90, 720] days (i.e., 0.25, 2 years) and [1.71, 8.55] *bn* US$. CAT bond pricing was evaluated at time $t = 0$, considering a principal equal to 1 US$. In the first case, for the *zero-coupon* CAT bond, it was priced at 3.5% over LIBOR. If no trigger event occurs, the total yield was 6% and consequently Z = 1.06 US$. With reference to the second and third cases, coupon payments equal to C_s = 0.06 US$ and PV = 1.00 US$ were considered. A covariance matrix is assumed without correlation between loss distribution and the Poisson point process, as follows:

$$\boldsymbol{\Sigma}_{\boldsymbol{\Theta\Theta}} = \begin{bmatrix} \sigma_{\mu}^2 & \rho_{\sigma_\mu\sigma_\sigma}\sigma_\mu\sigma_\sigma & 0 \\ \rho_{\sigma_\mu\sigma_\sigma}\sigma_\mu\sigma_\sigma & \sigma_\sigma^2 & 0 \\ 0 & 0 & \sigma_{m_s}^2 \end{bmatrix} = 10^{-3}\begin{bmatrix} 0.1 & 0.02 & 0 \\ 0.02 & 0.1 & 0 \\ 0 & 0 & 0.1 \end{bmatrix} \qquad 4.44$$

4.4.1 Results and discussion of the proposed formulation

Figure 4.2 shows the P_f surface derived with Eq. (4.11), and cut by two planes with D and T fixed values. For a given threshold level D, P_f

increases from 0 to 1 over time, whereas for a set expiration time *T*, P_f decreases as the threshold level *D* increases.

Three percentile values have been assumed $\bar{p} = \{0.20, 0.10, 0.02\}$ corresponding to $k = \{0.84, 1.28, 2.05\}$. Selecting a small $\bar{p}$ implies considering a low $P_{f,d}$, with a consequent high probability of P_f of being higher than $P_{f,d}$. The distance between the expected P_f and $P_{f,d}$ increases for higher *D* and *T* values, showing the growing dispersion of the underlying stochastic process.

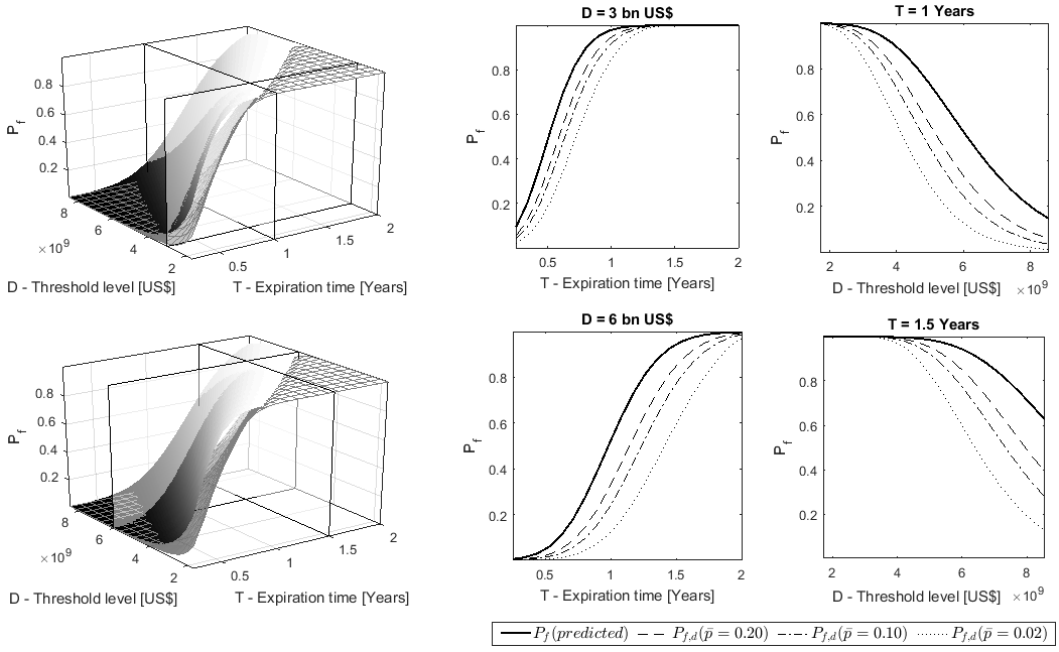

Figure 4.2: Failure probability P_f of the compound doubly stochastic Poisson process and $P_{f,d}$ curves for different quantiles $\bar{p}$.

The reliability-based CAT bond pricing is performed next. Figure 4.3 shows the *zero-coupon* CAT bond pricing surface for each $\bar{p}$ value. In this case, for a given threshold level *D*, the CAT bond value decreases over time, whereas for a set expiration time *T*, the *CAT* bond value increases as the threshold level D increases.

The influence of $\bar{p}$ is clearly evident as assuming a conservative $\bar{p}$ value leads to higher prices. Even in this case, the influence of $\bar{p}$ becomes more important as *D* and *T* increase.

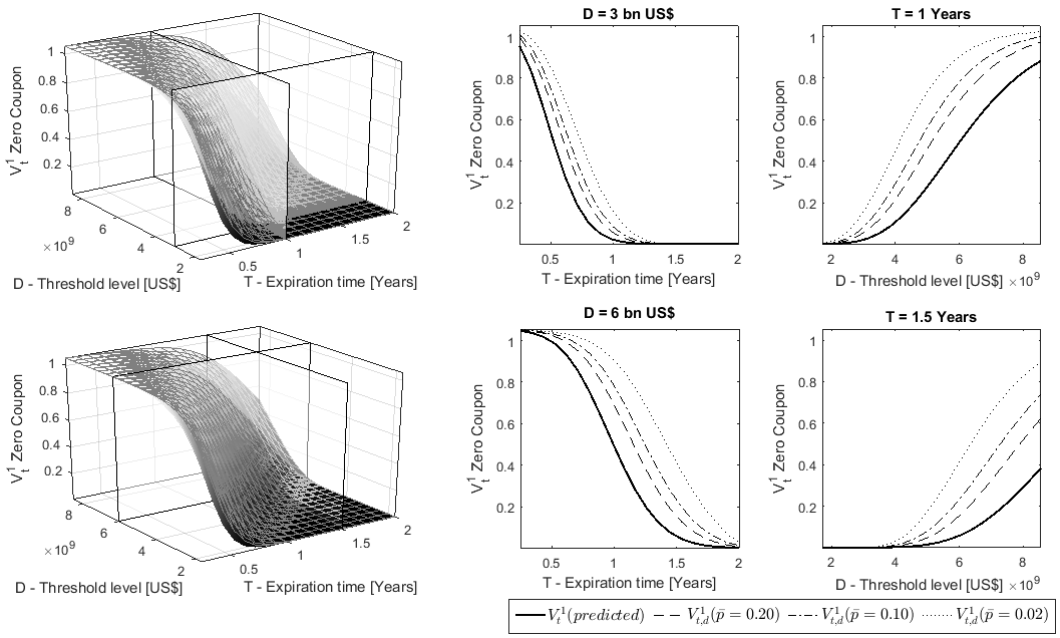

Figure 4.3: Zero-coupon CAT bond price $V_{t,d}^1$ *for different quantiles* $\bar{p}$.

Figure 4.4 shows the *only-coupon CAT* bond pricing surface for the same three possible values of $\bar{p}$. In this case, the price of the *only-coupon* CAT bond increases when the expiration time and threshold level are greater, since the chance of receiving more coupons is higher. Even in this case, the influence of $\bar{p}$ on the price is clear. The more conservative is the assumed $\bar{p}$, the higher is the CAT bond price.

Finally, Figure 4.5 illustrates the case of the *coupon* CAT bond, evidencing how the overall trend is similar to the *zero-coupon* one, even if numerical results are the combination of two contributions. As time passes, the chance of receiving more coupon payments is bigger, but at the same time, the possibility of losing the principal increases.

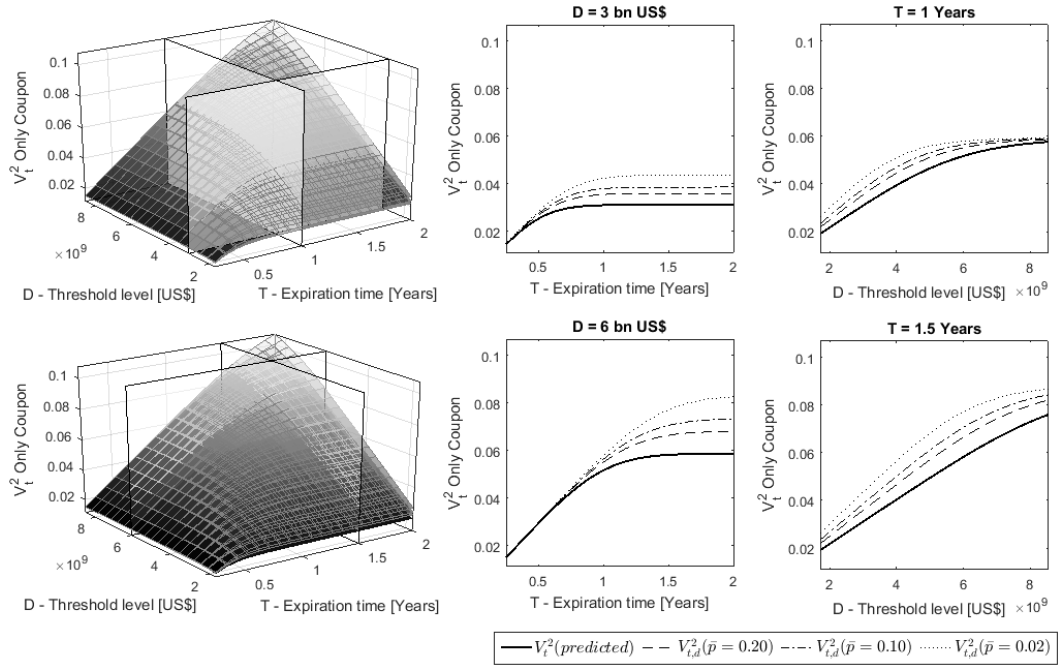

Figure 4.4: Only-coupon CAT bond price $V_{t,d}^2$ for different quantiles $\bar{p}$.

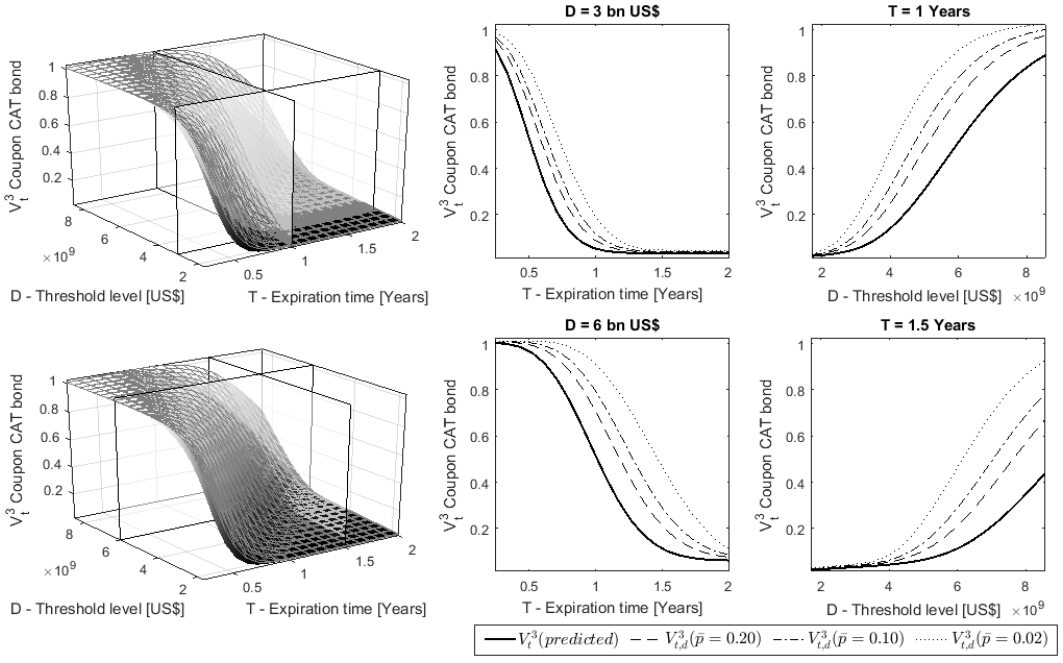

Figure 4.5: Coupon CAT bond price $V_{t,d}^3$ for different quantiles $\bar{p}$.

4.4.2 Influence of covariance matrix on CAT bond pricing

The results show the importance of considering parameter uncertainties in CAT bond pricing. Uncertainty in the model parameters is described with the covariance matrix $\boldsymbol{\Sigma}_{\boldsymbol{\Theta\Theta}}$. High values along the diagonal of the covariance matrix mean high uncertainties in parameters. Consequently, it is crucial to use all of the available knowledge to obtain accurate estimates. To explore the significance of the convariance matrix we consider a second covariance matrix $\boldsymbol{\Sigma}_{\boldsymbol{\Theta\Theta}}$ defined as

$$\boldsymbol{\Sigma}_{\boldsymbol{\Theta\Theta}} = \begin{bmatrix} \sigma_{\mu}^2 & \rho_{\sigma_\mu\sigma_\sigma}\sigma_\mu\sigma_\sigma & 0 \\ \rho_{\sigma_\mu\sigma_\sigma}\sigma_\mu\sigma_\sigma & \sigma_{\sigma}^2 & 0 \\ 0 & 0 & \sigma_{m_s}^2 \end{bmatrix} = 10^{-4}\begin{bmatrix} 0.1 & 0.02 & 0 \\ 0.02 & 0.1 & 0 \\ 0 & 0 & 0.1 \end{bmatrix} \qquad 4.45$$

to represente an hypothetical cases with a more accurate knowledge of the distributions underlying the pricing process (i.e., smaller values) than the one adopted in Eq. 4.44.

Figure 4.6 shows results of the *Zero-coupon* CAT bond calculated with a smaller covariance matrix for the same values of $\bar{p}$. Similarly, Figure 4.7 and Figure 4.8 shows results for the *Only-coupon* and *Coupon* CAT bond calculated the covariance matrix of Eq. 4.45.

Compared to the previous example, Figure 4.6 - Figure 4.8 show $V_{t,d}^i$ curves that are closer to the V_t^i expected one. This behavior is the consequence of a better knowledge about the input parameters that allows the analysis to set lower bond's prices with the same reliability level as before. In other words, smaller uncertainties on the model parameters allow to define lower prices with the same probability that the bond is under-priced.

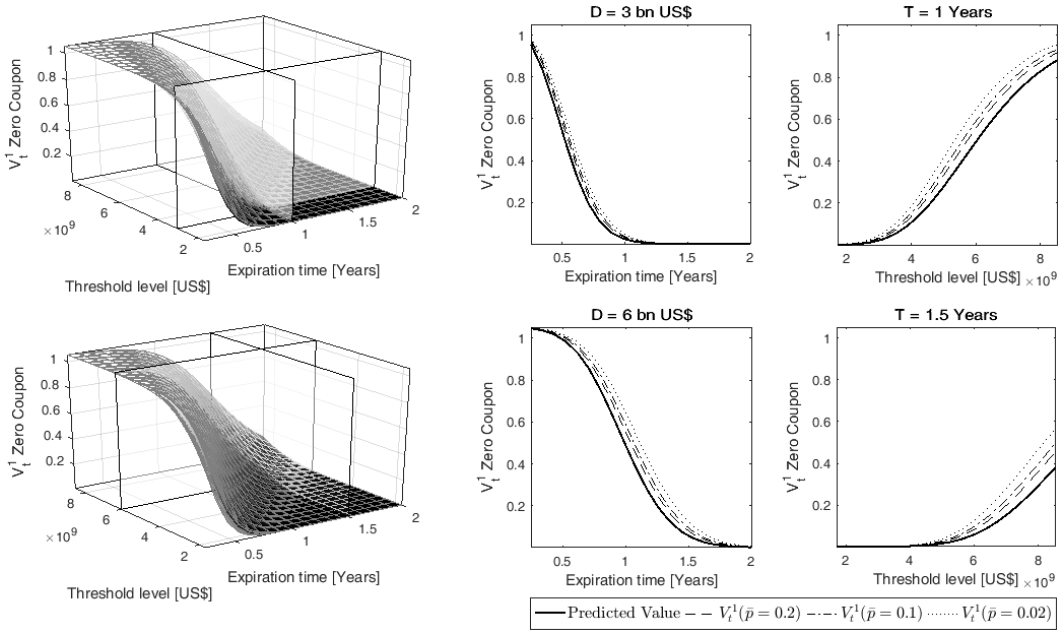

Figure 4.6: Zero-coupon CAT bond price $V_{t,d}^1$ calculated with a smaller covariance matrix.

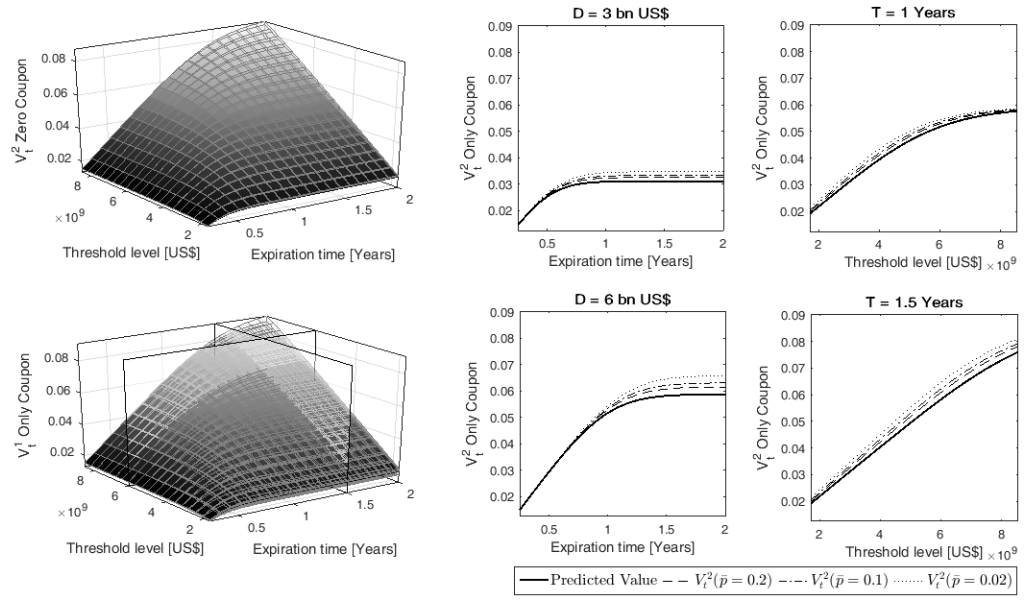

Figure 4.7: Only - coupon CAT bond price $V_{t,d}^2$ calculated with a smaller covariance matrix.

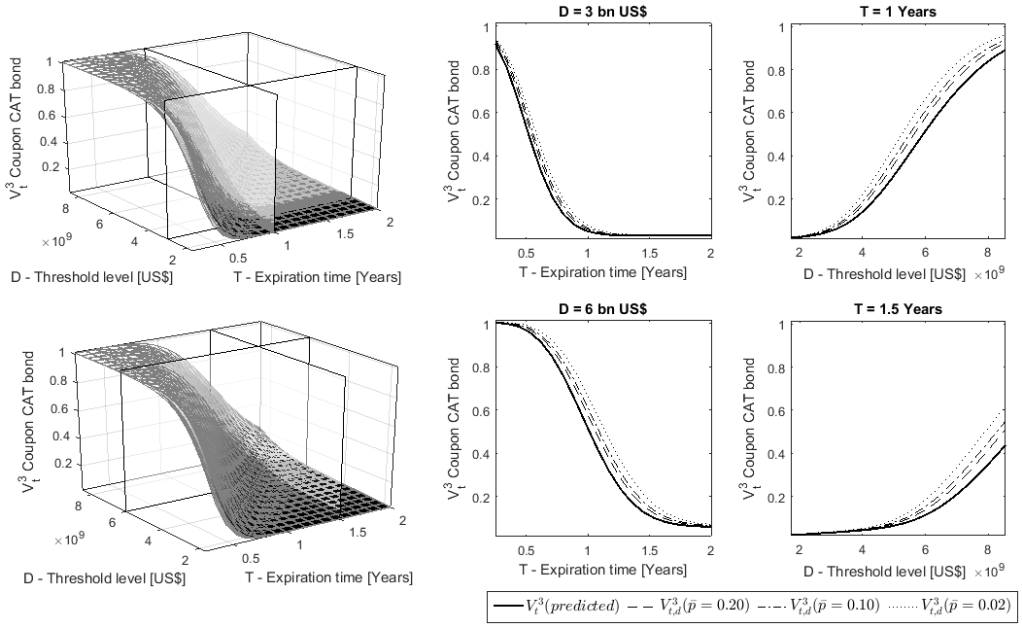

Figure 4.8: Coupon CAT bond price $V_{t,d}^3$ calculated with a smaller covariance matrix.

Finally, Figure 4.9 shows the ratio between $V_{t,d}^3 / V_t^3$ for the two covariance matrixes $\boldsymbol{\Sigma}_{\boldsymbol{\Theta\Theta}}$, with $\bar{p} = 0.02$. For the sake of brevity, this ratio was calculated only for the *coupon* CAT bond. The results show how for some *T-D* combinations, the increment due to $\bar{p}$ assumption is not negligible, whereas in other cases it can be neglected (i.e., when the ratio is close to 1). This observation implies that an accurate knowledge of the parameter uncertainties has a different influence pricing over the *T-D* domain. Although for some *T-D* combination, results obtained with the formulations proposed by Burnecki and Kukla (2003) may be acceptable, such *T-D* combinations are less attractive for investors, since they are either too safe (low *T* - high *D*) or too unsafe (high *T* - low *D*).

On the contrary, low *T* – low *D* or high *T* - high *D* combinations are more profitable, but in these cases, initial uncertainties have to be taken into account with the proposed framework since uncertainties play a fundamental role in CAT bond pricing. In particular, for the analyzed case,

the maxima $V_{t,d}^3 / V_t^3$ ratios are equal to 1.67 and 4.32 for the small (Eq. 4.44) and big (Eq. 4.45) covariance matrixes, respectively.

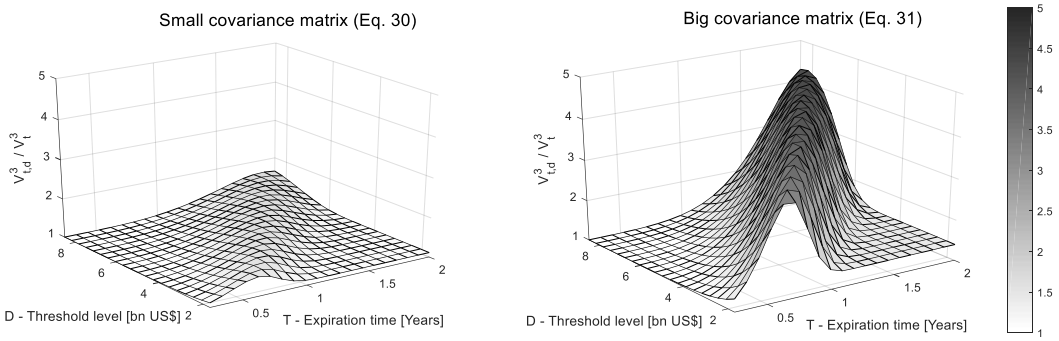

Figure 4.9: $V_{t,d}^3 / V_t^3$ ratio for small (Eq. 4.44) and big (Eq. 4.45) assumed covariance matrixes.

4.5 Conclusions

In this Chapter we presented a mathematical formulation for CAT bond pricing based on a reliability assessment of the P_f underlying the pricing process.

This work aims to overcome the limitations of current formulations that do not properly take into account uncertainties in the model parameters. A procedure for CAT bond pricing based on a fixed accepted level of risk was proposed. The related CAT bond pricing surface is characterized by a constant reliability for each expiration time – threshold level combination. Finally, the application of the procedure to a benchmark case-study allowed to quantify differences between the proposed formulation and results obtained based the existing literature, which is based on the expected values of the model parameters. The case study also shows influence of the covariance matrix of the model parameters on the CAT bond price.

Results allows to outline the following final remarks:

- Uncertainties on model parameters can significantly affect the distribution of the probability of failure of the compound doubly stochastic Poisson process and consequently the CAT bond price.

- The proposed formulation allows to characterize the uncertainty in the P_f of the compound doubly stochastic Poisson process starting from the uncertainties in the model parameters.
- Quantification of the uncertainty in the failure probability allows to derive a distribution of CAT bond price for a generic expiration time T – threshold level D combination.
- The use of the proposed reliability-based formulation allows to characterize a CAT bond pricing surface that corresponds to a fixed accepted level of risk, expressed in terms of a quantile $\overline{p}$ of the $P_f\left(T,D;\Theta\right)$ or $V_t^i\left(T,D;\Theta\right)$ distributions.
- Taking into account uncertainties leads to significantly different pricing estimates for some *T-D* combinations compared to those obtained with current formulations. Such differences are magnified if a poor knowledge of distributions' parameters is available (i.e., the case of large covariance matrix).
- The use of the proposed reliability-based formulation allows to update price estimates when additional information improve the knowledge on the model parameters, thus reducing the influence of their uncertainties on CAT bond prices.

5 CAT bond pricing for Italian Earthquakes

In this Chapter we apply the CAT bond pricing theory, derived and explained in Chapter 4. CAT bond pricing is a fundamental step of a more general framework used for financially covering a region exposed to potential high losses due to natural disasters. In particular, this chapter illustrates a possible CAT bond-based coverage configuration, against earthquake-induced losses, for the Italian territory. First, an overview of the steps needed for covering a region is provided and then their application to the Italian case is widely discussed.

5.1 Introduction and general framework

The study of natural catastrophe models has an important role in the prevention and mitigation of disasters and related significant losses. After the occurrence of a natural disaster, the reconstruction can be financed with catastrophe bonds. Usually insurers, reinsurers or governments can be interested in using CAT bond as hedging instruments that offer multi-year protection without the credit risk when providing a full direct collateral. As starting point, the area of the contract has to be defined. This area can coincide with the spatial distribution of a certain portfolio of insured buildings (or a part of it), or can be, for example, the total national area. This decision mostly depend on the ceding company (private insurance/reinsurance companies, national governments…) who wants to adopt CAT bond as risk-transfer method. Extended areas can be subdivided in order to define different risk-level zones. In such a way, CAT bonds with a different probability to be triggered are priced and offered to the financial market. The higher is the default probability, the higher is the gain provided by the bond to the investors. Since the trigger depends both on the frequency of events, and on the loss associated to each events (Chapter 4),

the area of the contract has to be characterized in terms of hazard, vulnerability and exposure. Once defined the region of interest, the type of loss covered by the bond has to be set. Generally, e.g., in case of seismic hazard, losses can arise from direct damage to residential buildings, or from business interruption of productive processes etc. The loss distribution and the Poisson process representing the occurrence of the events are the inputs of the pricing model explained in Chapter 4. Loss distributions can be fitted from real past claims data, or modelled data. In the former case, the availability of enough data is needed, while in the latter, scenario analysis have to be run to obtain a loss estimate. Once defined the possible combination of expiration time *T* and threshold level *D* (*T-D* domain), type and characteristics of the bond have to be set. In particular, if *coupon* or *zero-coupon* CAT bond and the type/frequency of *coupon* payment. In the following, only the main two equations for CAT bond pricing are reported; all the theory is described in detail in Chapter 4.

- *Zero-coupon* CAT bond

$$V_{t,d}^{1}\left(T,D;\Theta\right)=Z\,e^{-\int_{t}^{T}r(\xi)d\xi}\left[1-P_{f,d}\left(T,D;\Theta\mid F_{t}\right)\right] \tag{5.1}$$

- *Coupon* CAT bond

$$V_{t,d}^{3}\left(T,D;\Theta\right)=\left\{PV\,e^{-\int_{t}^{T}r(\xi)d\xi}\left[1-P_{f,d}\left(T,D;\Theta\mid F_{t}\right)\right]+\right. \tag{5.2}$$

$$\left.=+\int_{t}^{T}e^{-\int_{t}^{s}r(\xi)d\xi}\,C_{s}\,\left[1-P_{f,d}\left(s,D;\Theta\mid F_{t}\right)\right]ds\right\}$$

5.2 Application to the Italian case

The abovementioned procedure is applied in this Chapter for designing a CAT bond-based coverage configuration, against earthquake-induced losses to the residential building asset of Italy. A detailed

description of the seismicity and characteristics of the main residential building types and their distribution over the country is provided, and then used for the definition of the CAT bond-based coverage financial solution.

5.2.1 Zonation of Italy

Historically, numerous seismic events occurred within the Italian territory, most of them along the Apennine Mountains in Central and South-Italy. A total of 1433 seismic events with $M_W \geq 4.5$ occurred in Italy since A.D. 1005. Starting from the map of the historical events, Italy has been divided into three zones. Figure 5.1 shows the three zones in which the Italian territory has been divided. As a consequence, three CAT bonds have been designed and priced for the Italian territory.

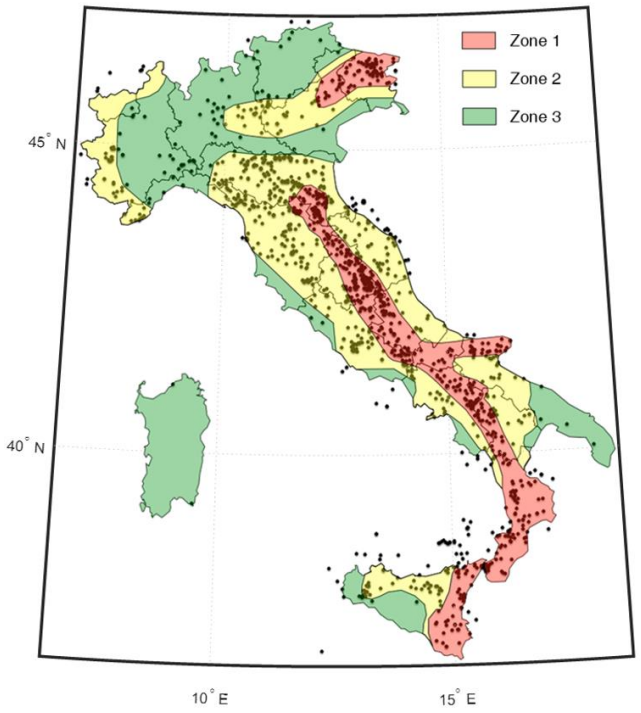

Figure 5.1: Different CAT bond default-risk level zones (MW ≥ 4.5).

In particular, Zone 1 (red-coloured) represents the highest default-risk level zone, while Zone 3 is the lowest default-risk level zone (green-coloured). The yellow zone (Zone 2) has intermediate features, in terms of both events frequency and magnitude, than the other two. Figure 5.2 shows earthquakes occurred in each zone: most number of earthquakes, and the

ones of higher magnitude occurred in the red zone. CAT bond having Zone 1 as contract area, is the most risky bond, for which the gain is maximum, but where the default-probability is higher with respect to Zones 2 and 3. On the contrary, CAT bond characterizing Zone 3 is the one exposed to the lowest default risk, and consequently it provides the lowest gain.

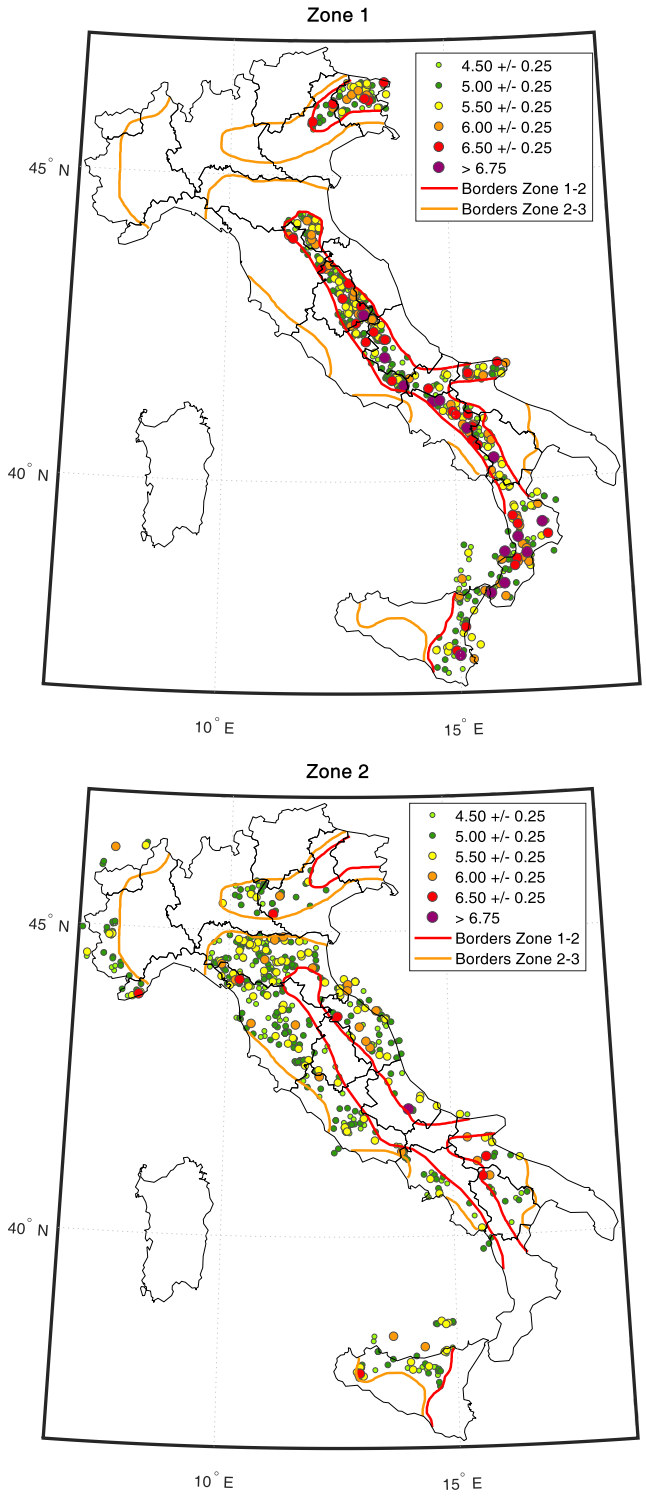

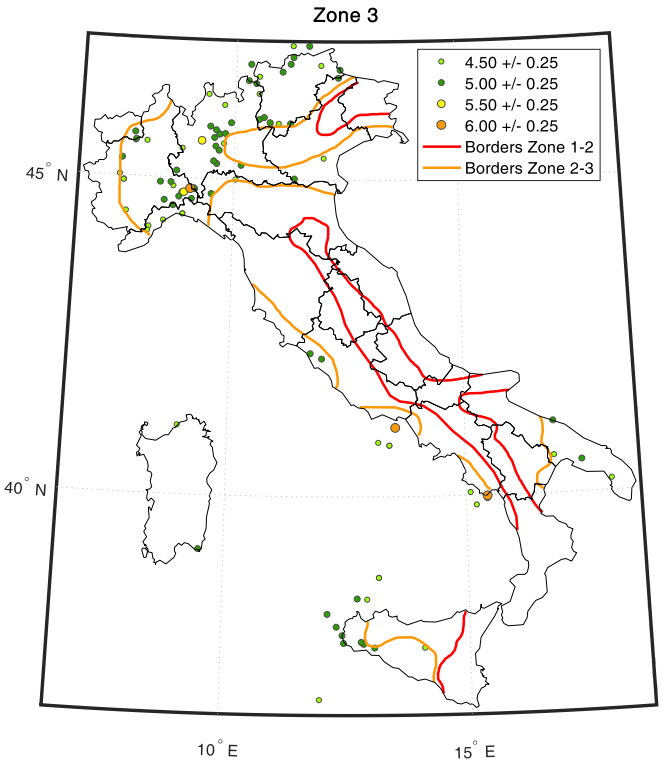

Figure 5.2: Earthquakes occurred in each zone since 1005 with Mw ≥ 4.5 (Rovida et a. 2016).

5.2.2 Derivation of model parameters

Once individuated the three different default-risk level zones, model input parameters have to be determined for each zone. In particular, loss distribution parameters and the Poisson process parameters characterize the stochastic process of the accumulated losses of each Zone. Covariance matrixes are then needed for the reliability based pricing.

5.2.2.1 Homogeneous Poisson process

For obtaining the Poisson process intensity describing the catastrophic flow of each zone, the historical catalogue of Italian earthquakes has to be analysed. Figure 5.3 shows all the events occurred in the three zones since A.D. 1005: it can be noted how the majority of earthquakes are concentrated in the last century, highlighting the so-called problem of catalogue-completeness, i.e., the lack of data related to low-to-medium events during the Middle Ages.

According to these data, events occurred starting from 1890 have been taken into account for the estimation of the Poisson process intensity, for all the three Zones. In particular, since 1890, 383 earthquakes occurred in Zone 1, 295 in Zone 2, and 61 in Zone 3, showing a descendent occurring frequency and magnitude, within the three zones. From selected earthquakes of each zone, Poisson process parameters have to be calibrated.

Figure 5.4 shows the aggregate number of earthquakes over years occurred in the three areas. In all cases, the assumption of homogeneous Poisson process, characterized by a constant intensity (i.e., slope of the curve), is well justified by the observed data.

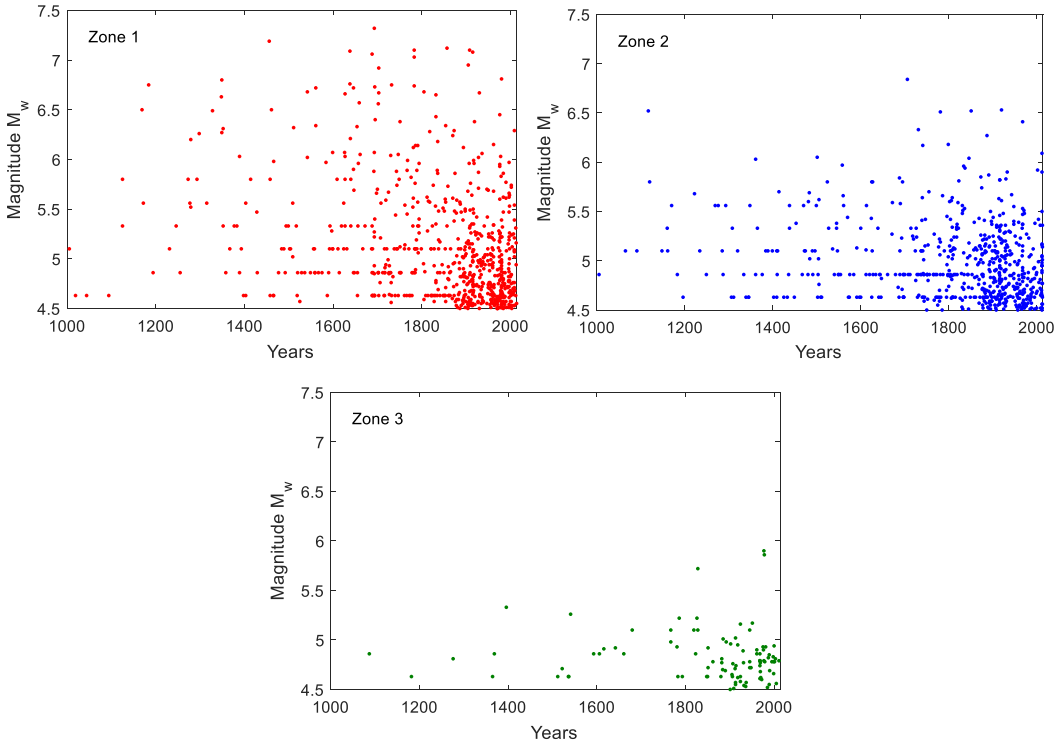

Figure 5.3: Earthquakes Zone 1, Zone 2 and Zone 3 since 1005.

For each i^{th} zone (i=1,2,3), the posterior mean $\mathrm{M}_{\boldsymbol{\Theta}_P,i}$, containing the mean intensity of the Poisson process m_s^i, and the posterior covariance matrix $\boldsymbol{\Sigma}_{\boldsymbol{\Theta}_P\boldsymbol{\Theta}_P,i}$, containing the variance $\sigma^2_{m_{si}}$ of the intensity, were calculated with the Bayesian updating technique as explained in Gardoni et al. (2002); Table 5.1 lists results for each Zone: it can be noted how the intensity of the

third Zone (m_s^3) is significantly smaller than the first two (m_s^1, m_s^2) due to the lower number of events occurred in the reference time window (1890-2015).

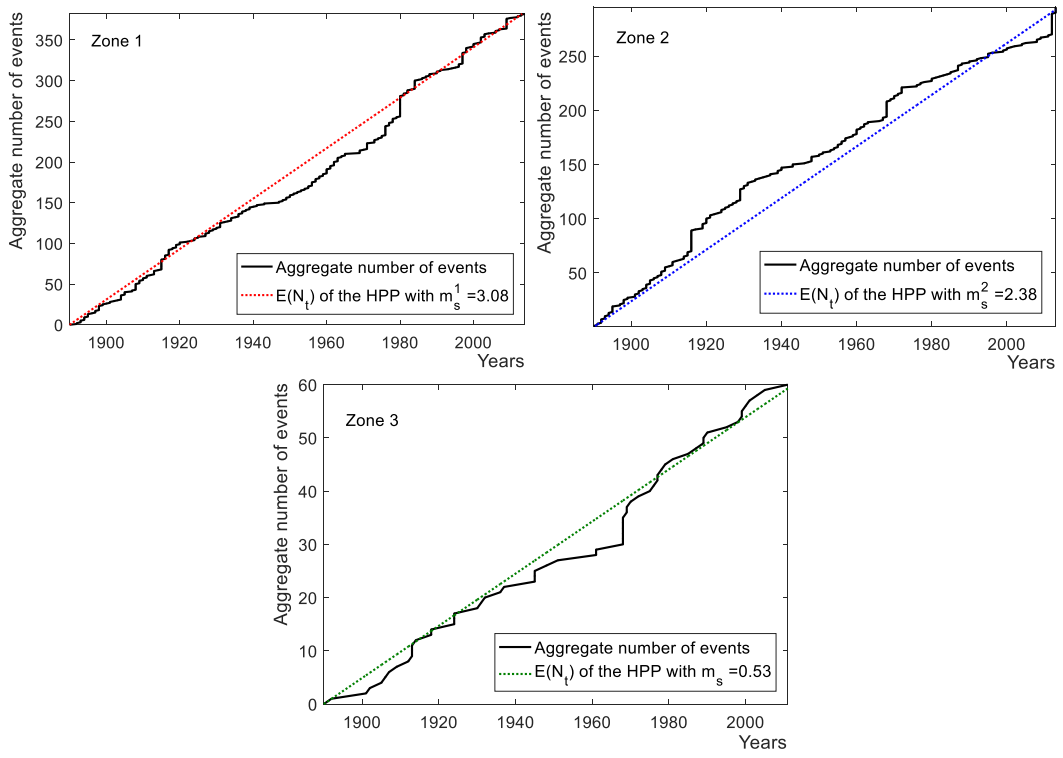

Figure 5.4: Aggregate number of earthquakes in the three different zones.

Table 5.1: Mean value and variance of the intensity of the Poisson process for the three zones.

	$\mathbf{M}_{\Theta_p,i}=[m_{si}]$	$\mathbf{\Sigma}_{\Theta_p\Theta_p,i}=\left[\sigma^2_{m_{si}}\right]$
Zone 1	3.08	0.025
Zone 2	2.38	0.019
Zone 3	0.53	0.005

5.2.2.2 Loss distribution

For each i^{th} Zone (i=1,2,3), loss distribution associated to earthquakes occurred inside the zone has to be defined. In this study, direct losses residential building (i.e., costs to be sustained for repairing seismic damage) have been computed, since these are the most relevant costs that usually the

Italian government has to face during seismic recovery processes. Due to the lack of real loss data, earthquake-scenario analyses have been performed for assessing loss amounts induced by each event of those considered in Section 5.2.2.1. In particular, the loss value L_{ij} caused by the j^{th} seismic events occurred in the i^{th} zone has to be computed (j = 383 in Zone 1, j = 295 in Zone 2, j = 61 in Zone 3). Uncertainty in scenario predictions has been taken into account via the simulation of ten cross-correlated ground motion fields, according to the theory explained in Goda et Hong (2008) Goda et Atkinson (2009) and Goda et Atkinson (2010), and considering peak ground acceleration (PGA) as reference intensity measure.

As a consequence, for each considered earthquake, eleven shake fields have been calculated, one deterministic and ten cross-correlated, leading to eleven loss values for each event of the dataset. The number of shake-fields associated to each zone is f = 4213 (383*11) in Zone 1, f = 3245 (295*11) in Zone 2, and f = 671 (383*11) in Zone 3. Similarly to Chapter 3, direct economic loss $L_{f,i}$ due to the f^{th} shake-field, caused by a seismic event occurred in the i^{th} zone, is calculated according to Bai et al. 2009 as

$$L_{f,i} = \sum_{z=1}^{n.municipality<200km} \left\{ \sum_{y=1}^{8} \sum_{k=1}^{5} \left[P\left(DS_{k,y} \mid PGA_{z,f,i} \right) \right] \cdot RCR_k \cdot RC_{ave} \cdot A_{y,z} \right\} \qquad 5.3$$

where $PGA_{z,f,i}$ is the peak ground acceleration in the z^{th} municipality due to the f^{th} shake-field, caused by a seismic event occurred in the i^{th} zone. $DS_{k,y}$ is the k^{th} damage state (with k = 1, 2, 3, 4, 5) of the y^{th} building typology (with y = 1, 2, …, 8). In Eq. 5.3 $A_{y,z}$ is the built area (in m^2) in the z^{th} municipality associated to the y^{th} building typology. Finally, RCR_k is the repair cost ratio for the the k^{th} damage state (i.e., ratio between unit cost to repair a building in the k^{th} damage state and the unit replacement cost RC_{ave}).

As done in Chapter 3, repair cost ratios RCR_k have been extrapolated from Dolce and Manfredi (2015), assuming the same deterministic values

for each structural type equal to 0, 0.15, 0.4, 0.65, 1, respectively for DS_1, DS_2, DS_3, DS_4 and DS_5; the unit replacement cost RC_{ave}, also in this case has been assumed equal to 1500 €/m^2, according to CRESME (Centre for Sociological, Economics and Market Research, 2011). For each zone, a loss distribution was fitted from losses associated to events occurred that zone.

Distribution parameters were derived via the Bayesian updating technique, as reported in Gardoni et al. (2002). Figure 5.5 shows the empirical CDF of the generated losses and the fitted LogNormal distributions. For each zone, input model data are the posterior mean vector (Eq. 5.4) containing the mean values of distributions' parameters and the covariance matrix (Eq. 5.5).

Distributions' mean values decrease from Zone 1 to Zone 3, meaning that the biggest losses happen in Zone 1. Mean values of Zones 1 and 2 are quite similar, and this evidence can be generally attributed to the fact that medium intense earthquakes in Zone 2 strike areas with a high exposure, whereas strong earthquakes of Zone 1 hit a low-exposure area. Mean value of Zone 3 is indeed significantly smaller than those of Zones 1 and 2, mainly due to the low-intensity of earthquake occurrences.The sigma of the three distribution are comparable, while the covariance matrix reflect the lower number of earthquakes occurred in Zone 3 for which, as a consequence, less information is available.

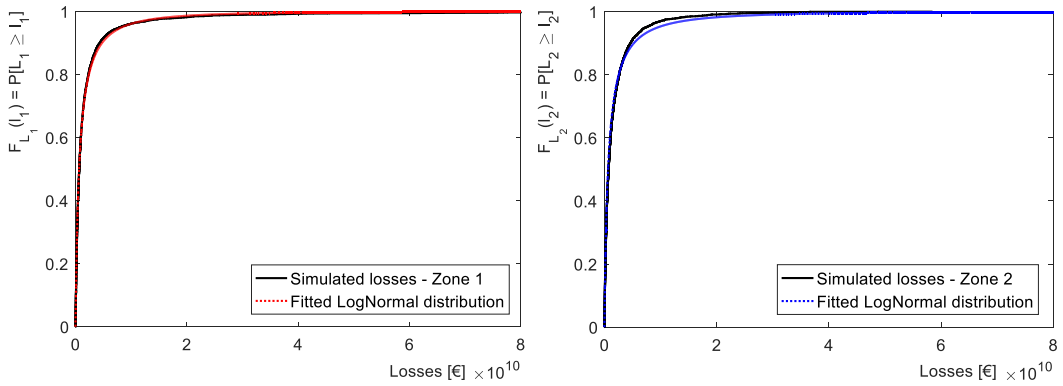

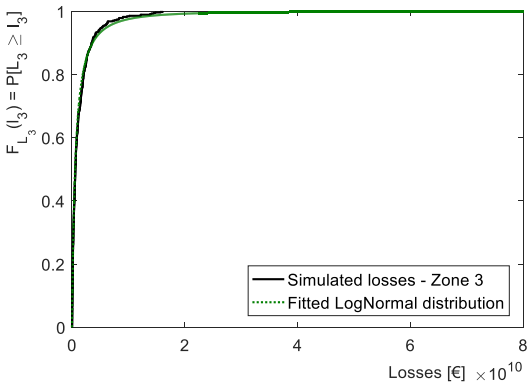

Figure 5.5: Fitting of loss data with LogNormal distribution.

According to the hypothesis of no correlation between loss distribution and the Poisson point process for a doubly stochastic Poisson process, input data for the three zones become the following:

$$\mathbf{M}_{\Theta,1} = \begin{bmatrix} \mu_1 \\ \sigma_1 \\ m_{s1} \end{bmatrix} = \begin{bmatrix} 20.303 \\ 1.548 \\ 3.08 \end{bmatrix}$$

$$\mathbf{M}_{\Theta,2} = \begin{bmatrix} \mu_2 \\ \sigma_2 \\ m_{s2} \end{bmatrix} = \begin{bmatrix} 20.279 \\ 1.640 \\ 2.38 \end{bmatrix} \qquad 5.4$$

$$\mathbf{M}_{\Theta,3} = \begin{bmatrix} \mu_3 \\ \sigma_3 \\ m_{s3} \end{bmatrix} = \begin{bmatrix} 20.133 \\ 1.469 \\ 0.53 \end{bmatrix}$$

$$\mathbf{\Sigma}_{\Theta\Theta,1} = \begin{bmatrix} \sigma^2_{\mu_1} & \rho_{\sigma_{\mu_1}\sigma_{\sigma_1}}\sigma_{\mu_1}\sigma_{\sigma_1} & 0 \\ \rho_{\sigma_{\mu_1}\sigma_{\sigma_1}}\sigma_{\mu_1}\sigma_{\sigma_1} & \sigma^2_{\sigma_1} & 0 \\ 0 & 0 & \sigma^2_{m_{s1}} \end{bmatrix} = \begin{bmatrix} 0.000617 & 0 & 0 \\ 0 & 0.000308 & 0 \\ 0 & 0 & 0.025 \end{bmatrix}$$

$$\mathbf{\Sigma}_{\Theta\Theta,2} = \begin{bmatrix} \sigma^2_{\mu_2} & \rho_{\sigma_{\mu_2}\sigma_{\sigma_2}}\sigma_{\mu_2}\sigma_{\sigma_2} & 0 \\ \rho_{\sigma_{\mu_2}\sigma_{\sigma_2}}\sigma_{\mu_2}\sigma_{\sigma_2} & \sigma^2_{\sigma_2} & 0 \\ 0 & 0 & \sigma^2_{m_{s2}} \end{bmatrix} = \begin{bmatrix} 0.00092 & 0 & 0 \\ 0 & 0.00046 & 0 \\ 0 & 0 & 0.019 \end{bmatrix} \qquad 5.5$$

$$\mathbf{\Sigma}_{\Theta\Theta,3} = \begin{bmatrix} \sigma^2_{\mu_3} & \rho_{\sigma_{\mu_3}\sigma_{\sigma_3}}\sigma_{\mu_3}\sigma_{\sigma_3} & 0 \\ \rho_{\sigma_{\mu_3}\sigma_{\sigma_3}}\sigma_{\mu_3}\sigma_{\sigma_3} & \sigma^2_{\sigma_3} & 0 \\ 0 & 0 & \sigma^2_{m_{s3}} \end{bmatrix} = \begin{bmatrix} 0.0038 & 0 & 0 \\ 0 & 0.0019 & 0 \\ 0 & 0 & 0.005 \end{bmatrix}$$

5.2.3 Results and discussion

Figure 5.6 shows P_f the surfaces for all the three Zones, calculated according to Eq. 4.11; four cuts of the surface are also reported, corresponding to planes with T = 1 and 3 years, and D = 10 and 20 *bn* €. As general behaviour, common for all the three Zones, for a given threshold level D, P_f increases from 0 to 1 over time, whereas for a set of expiration time T, P_f decreases as the threshold level D increases. The distance between the expected P_f and $P_{f,d}$ ($\overline{p} = 0.20$) increases for higher D and T values, due to the growing dispersion of the underlying stochastic process.

As expected, the P_f of Zone 1 is always bigger than the other two, since more events with associated bigger losses occur in this zone. Zone 1 is the most risky zone, since the probability of trigger the CAT bond is the highest, and the gain is maximum if the bond is not triggered. The most significant differences are between Zone 3 and the first two Zones: as sake of example, considering a threshold level of D = 10 *bn* €, it can be noted how after 4 years the mean P_f value for Zones 1 and 2 is respectively equal to 0.85 and 0.65, whereas for Zone 3 is about 0.10.

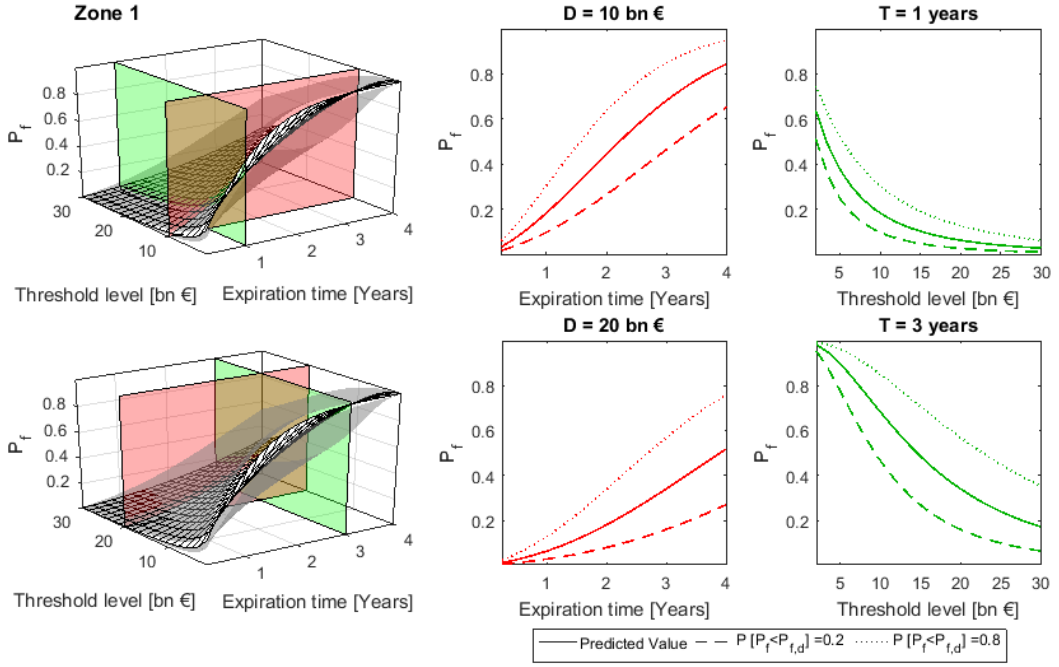

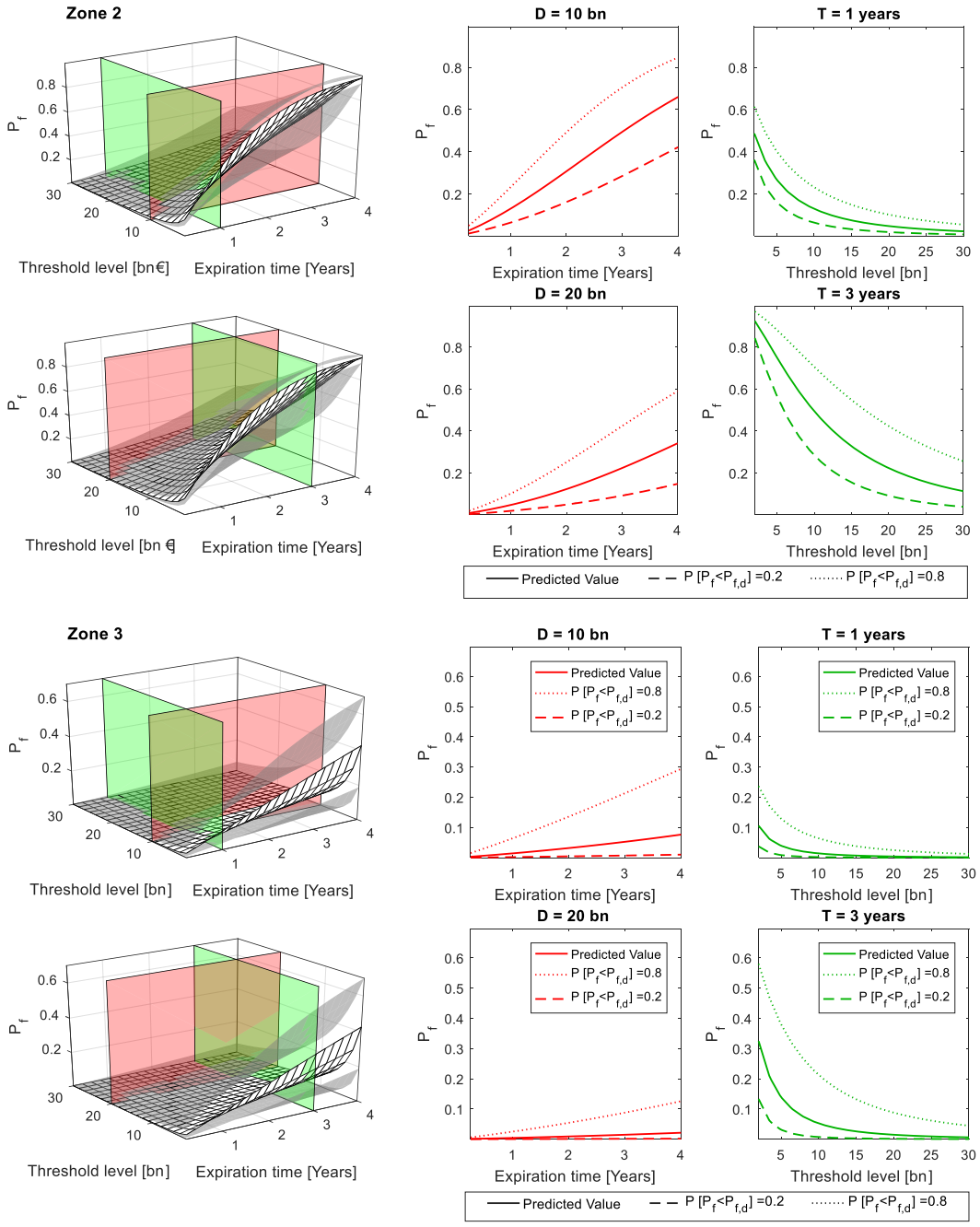

Figure 5.6: Failure probability Pf surface for the three zones

Figure 5.7 shows the *zero-coupon* CAT bond pricing surfaces paying $Z = 1.06$ € at maturity, for the three considered zones, calculated according to Eq. 5.1. CAT bond price is proportional to the survival probability: consequently for a given threshold level D, the CAT bond price decreases over time, whereas for a set expiration time T, the CAT bond value increases as the threshold level D increases. Figure 5.7 shows also the *iso-*

value lines corresponding to the *predicted value* V_t^1 and to $V_{t,d}^1$ with $\bar{p}=0.2$ and 0.8, that are useful for the CAT-bond price design. In particular, Zone 1 has the lowest CAT bond values, while Zone 3 has the highest, reflecting the default-risk associated to each zone; Table 5.2 lists, as example, *zero-coupon* CAT bond prices approached in the three zones when T = 2 years and D = 20 *bn €*.

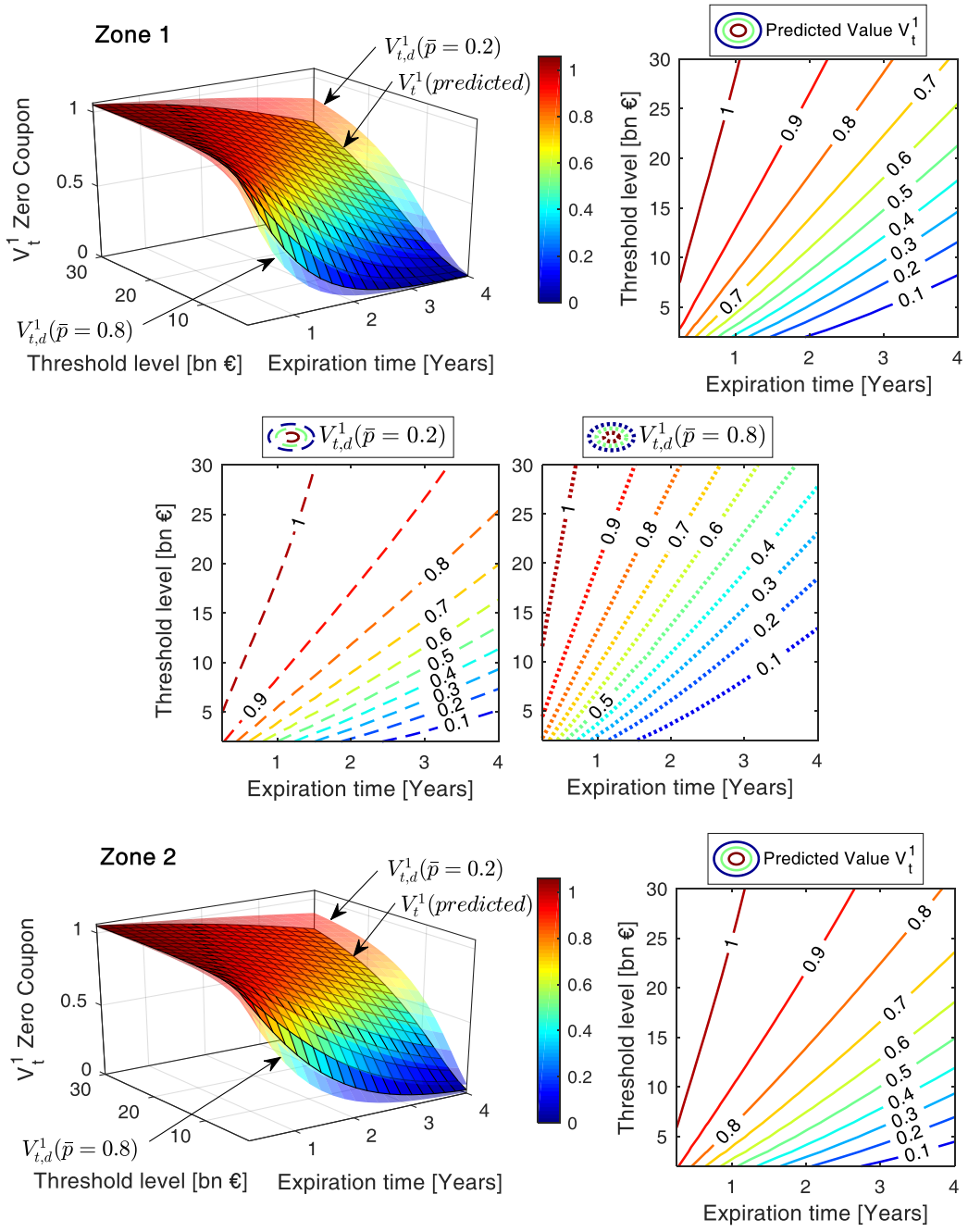

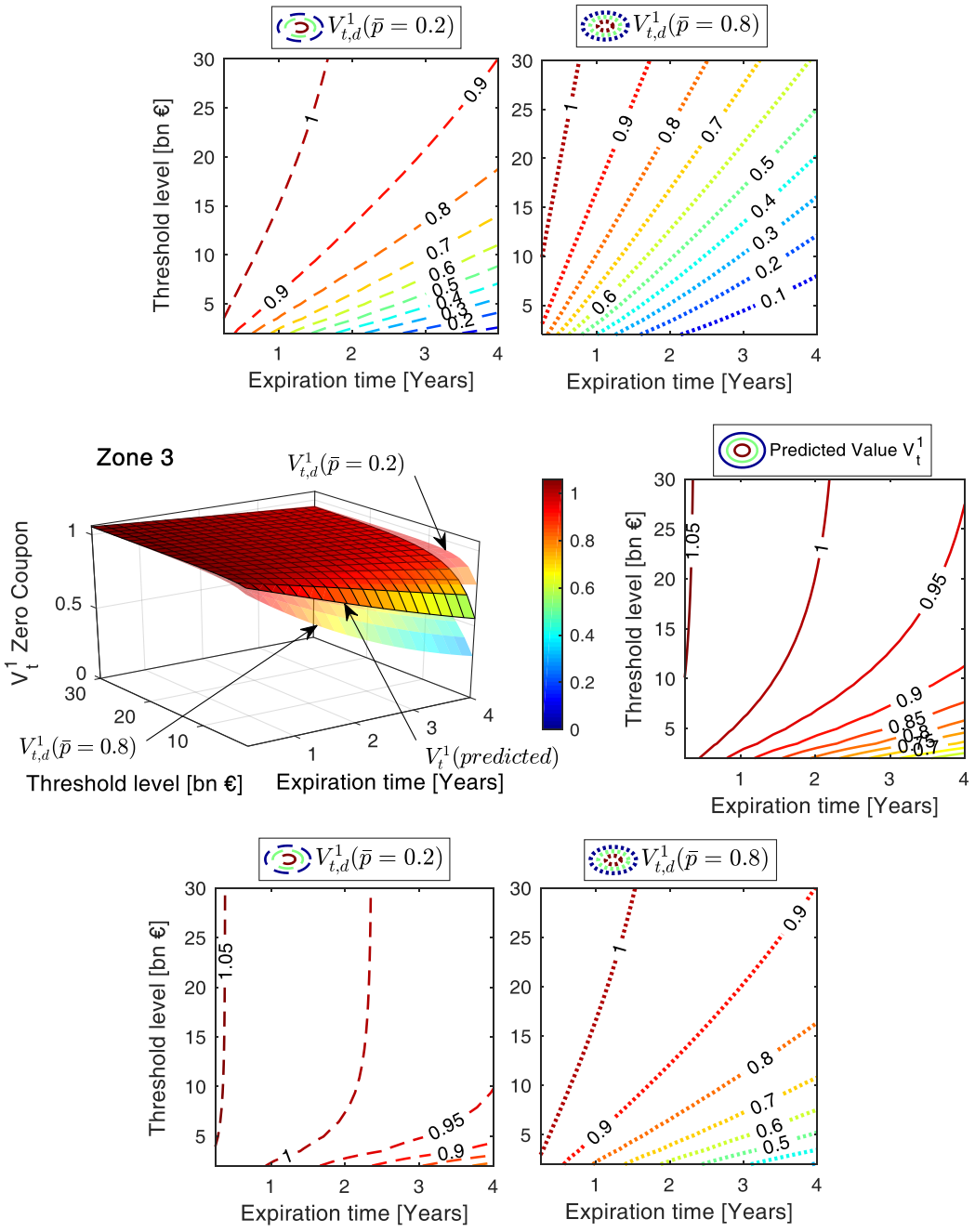

Figure 5.7: Zero coupon CAT bond price for the three zones.

Table 5.2: Zero Coupon CAT bond price [€] for T = 2 years and D = 20 bn €.

Zone	*Zero Coupon CAT bond price [€]*		
	$V^1_{t,d}\left(\bar{p}=0.20\right)$	V^1_t	$V^1_{t,d}\left(\bar{p}=0.80\right)$
1	0.925	0.825	0.65
2	0.95	0.875	0.75
3	1.01	1.00	0.95

Figure 5.8 shows the *only-coupon* CAT bond pricing surface for the three zones, calculated according to 4.27 with C_s=0.06. In this case, the price of the *only-coupon* CAT bond increases when the expiration time and threshold level are greater, since the chance of receiving more coupons is higher. For a given *T-D* combination, P_f of Zone 3 is lower than those of Zones 1 and 2, and the chance of receiving coupons is therefore higher. For this reason, pricing surface of Zone 3 is higher than the previous two.

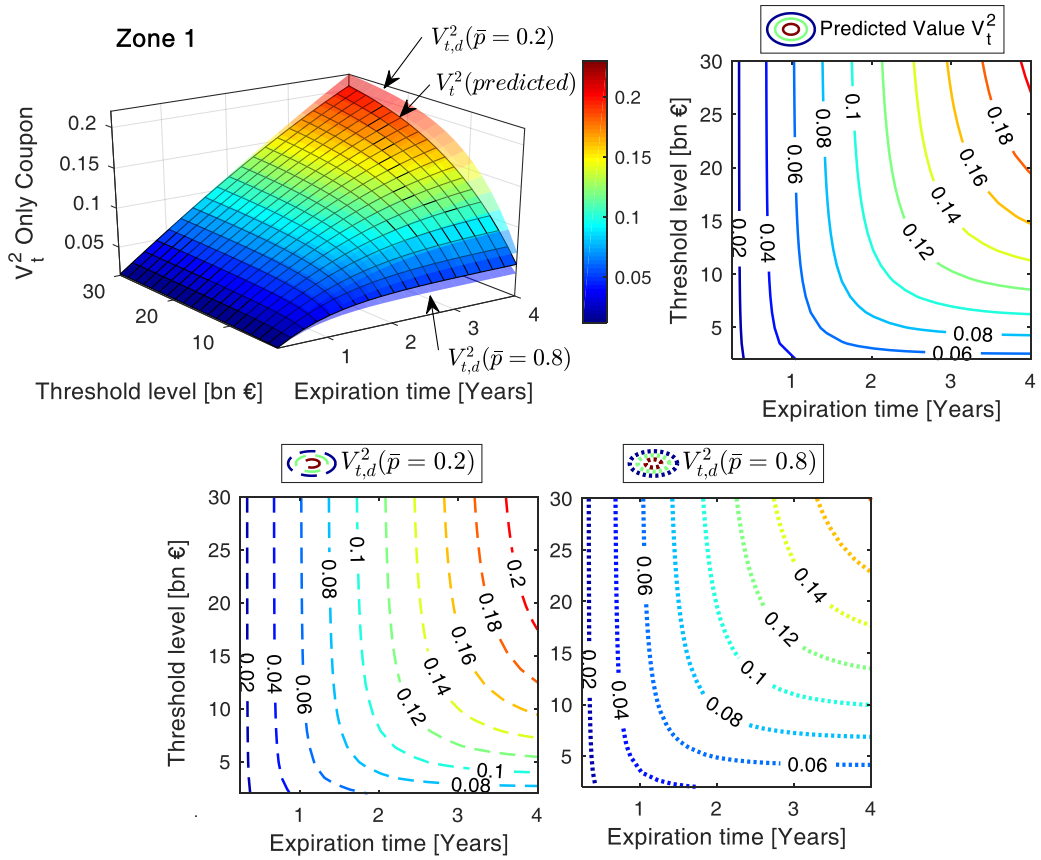

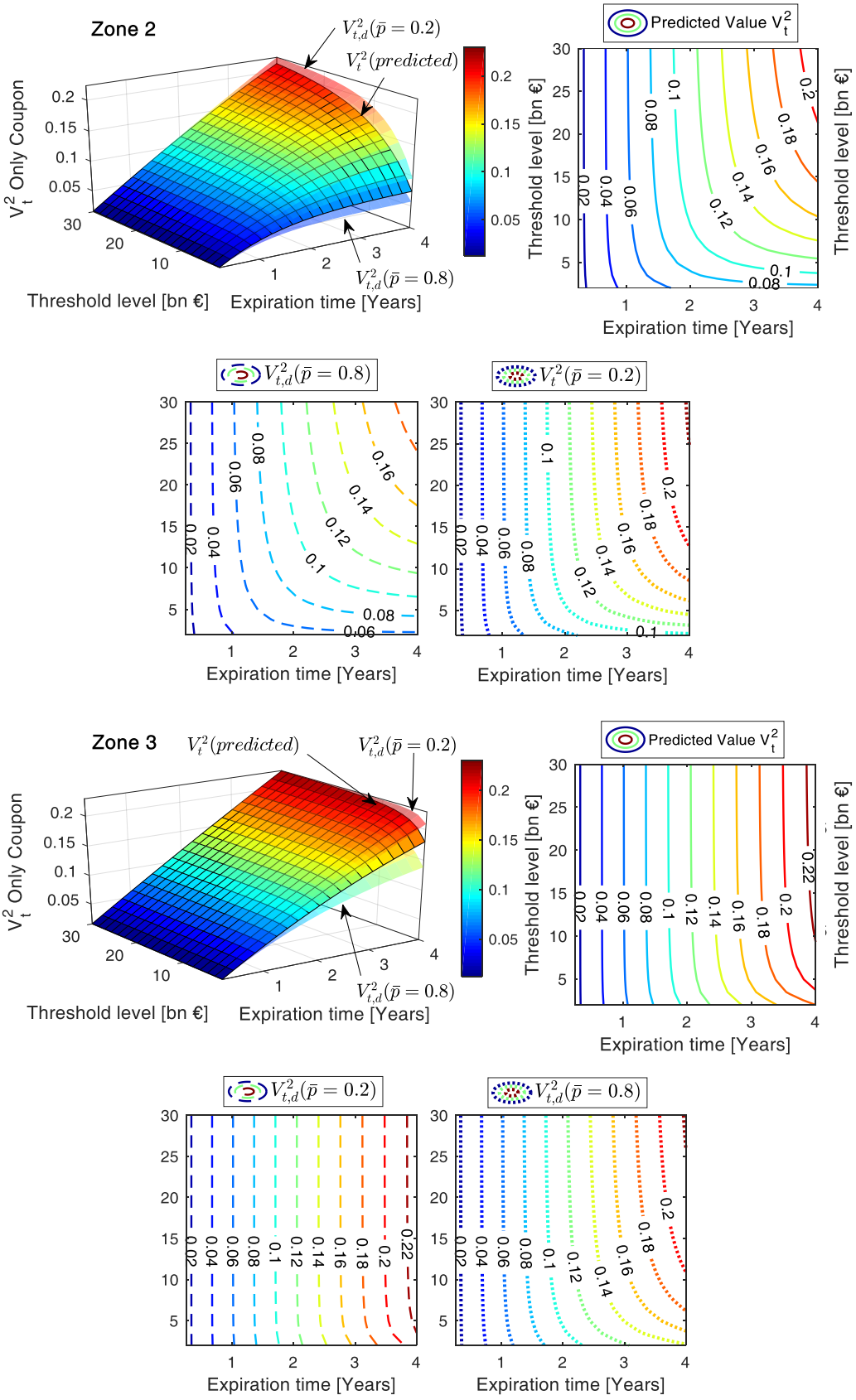

Figure 5.8: Only coupon CAT bond price for the three zones.

Finally, Figure 5.9 shows the *coupon* CAT bond pricing surfaces. The overall trend is similar to the *zero-coupon* one, but in this case results are the combination of the *zero-coupon* case and *only-coupon* case. For a set expiration time *T*, the price of *coupon* CAT bond increases as the threshold *D* increases, while increasing *T* leads generally to lower *coupon* CAT bond price since the chance of receiving more coupons is greater but at the same time the possibility of loosing the principal of the bond increases. As for the *zero-coupon* CAT bond surfaces, also the *coupon* CAT bond price reflects the different seismic risk-levels of the three zones. For a set *T-D* combination, the price for a bond in Zone 1 is the lowest, while price in Zone 3 is the highest. Table 5.3 reports, as example, *coupon* CAT bond values, approached when *T* = 2 years and *D* = 20 *bn €*.

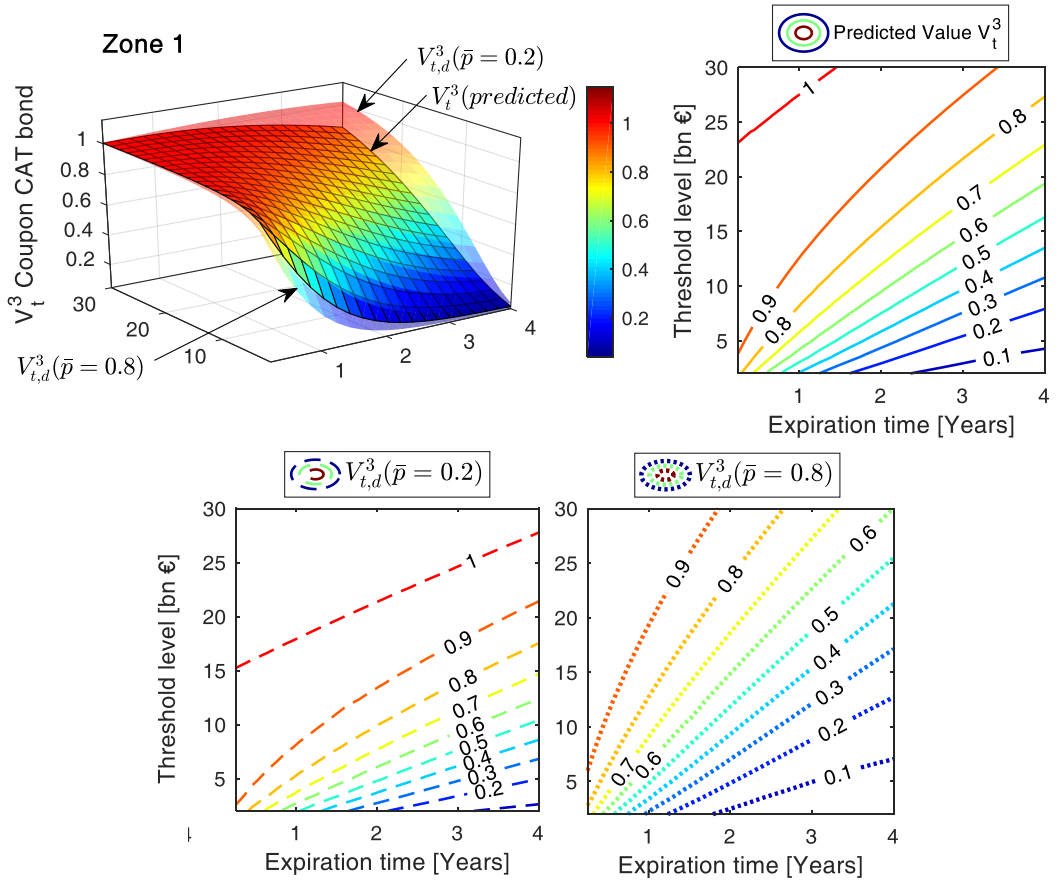

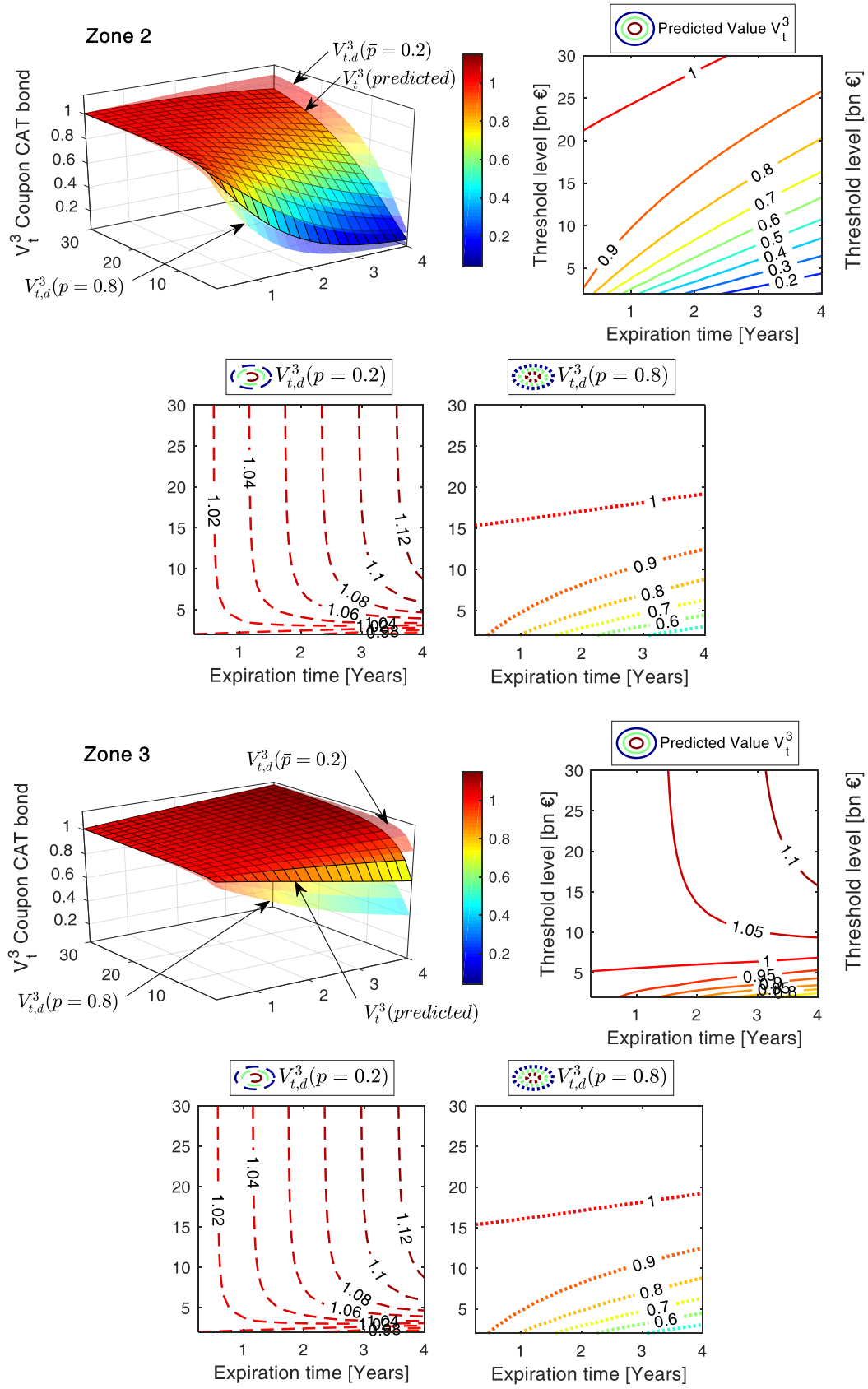

Figure 5.9: Coupon CAT bond price for the three zones

Table 5.3: Coupon CAT bond price [€] for T = 2 years and D = 20 bn €

Zone	*Coupon CAT bond price [€]*		
	$V_{t,d}^{3}\left(\overline{p}=0.20\right)$	V_{t}^{3}	$V_{t,d}^{3}\left(\overline{p}=0.80\right)$
1	0.975	0.875	0.725
2	1.017	0.925	0.80
3	1.07	1.06	1.01

5.3 Conclusions

This Chapter shows the application of the CAT bond pricing theory, developed in Chapter 4, in a more general context, in which CAT bonds can be used as risk-transfer financial method for areas exposed to potential huge seismic losses. The application framework is general, and can be applied to different natural hazards (e.g., earthquakes, flooding, hurricanes). The two main model inputs are the loss distributions, and parameters characterizing the occurrence frequency of events.

This method is able to represent every type of losses for which data for calibrating the distributions are available. In particular, this Chapter focused on a possible CAT bond-based coverage configuration against earthquake-induced losses for Italy. Italy has been therefore divided in three Zones and for each one a CAT bond has been priced.

The adopted subdivision provided CAT bonds associated to three different level of default risk. Zone 1 is characterized by the highest probability of failure since more events with bigger losses are expected; on the contrary, Zone 3 has the lowest probability of failure. For all the three zones, *zero coupon* and *coupon* CAT bonds have been priced.

As expected, results showed that for a fixed *T*-D domain, CAT bond of Zone 1 is at the same time the most convenient, but also the most risky. In this way, for a set *T-D* combination, three possible investment levels are proposed to the financial market.

6 Conclusions

This work focuses on some specific aspects related to the seismic risk assessment on local and regional scale. In particular, it gives a deep insight and contribution about some topics, still poorly treated in literature, but particularly current and important. A model able to compute indirect losses due to business interruption was firstly developed and applied to a real case study. The model is particularly indicated for performing a seismic risk analysis of a productive process, referring to its indirect potential losses due to production downtime. In Italy, especially the 2012 Emilia Earthquake, showed the need of study in detail this type of losses. The proposed model considered all aspects that influencing the response of system to the seismic shaking. In particular, a set of fragility curves was used for describing the structural seismic behaviour of each process component. Each process component was also characterized in terms of recovery time, by using recovery curves. These curves represent the expected time that each process element needs for recovering its functionality, depending on the state of the damage it has suffered. The productive process functional scheme was then used for linking together all the process components, allowing to compute the recovery curve for the entire process, conditioned on a given ground shaking (PGA). An economic formulation was then proposed for computing the monetary losses starting from the process downtime and the firm's balance sheet. Using as input PGA values of a seismic hazard curve, it was possible to perform a complete seismic risk analysis for the productive process. Results of the case study, showed how indirect losses due to business interruption become bigger than the direct ones for small values of Annual Exceedance Probability, so for higher ground shaking. This model allowed assessing the "*As-Built*" condition of the productive process, but it is also an important tool for quantitatively evaluating the best solution for reducing expected losses. The proposed model allowed to assess elements

that mostly influence the process, and to compute the benefit associated to possible retrofit or mitigation interventions.

A financial method for optimizing the retrofit strategy was thus proposed, and applied to the case study. The procedure is able to find the most profitable interventions' order and the optimal amount of initial investment. The case study showed how in case of multiple retrofit interventions, the total benefit is not the sum of single benefits; in particular, in order to obtain the exact total benefit, the analysis has to be done for every specific combination of possible mitigation strategies.

Regarding seismic risk on regional level, first an analysis of the Italian territory was performed, aimed to compute the seismic risk map for Italy and calculate the national *Expected Annual Loss*. Vulnerability and exposure were calculated at municipality level, on the basis of data provided by the National Institute of Statistics (ISTAT). For each municipality the built-area of eight different structural categories was calculated, in order to well represent fragility and exposure of the Italian building stock. Results showed that in most of Italian municipalities, masonry buildings are the most diffused structural typology; among all masonry structures, for a relevant number of municipalities, old masonry buildings (built before 1919) are a not negligible fraction. By considering the reconstruction cost per square meter, the exposure map was thus computed. Losses in each municipality due to all earthquakes of the historical national catalogue, were calculated by using seismic scenario analysis. From loss data, *Loss Exceedance Probability Curve* was computed for each Italian municipality and for the entire Italy. The integral of the curve is the *Expected Annual Loss* and it represents a synthetic indicator of hazard, vulnerability and exposure. A comparison between the hazard and risk map was performed, showing additional important information that the only hazard map is not able to show. In particular, areas with similar hazard may have totally different risk levels; this is particularly evident in the

Emilia-Romagna Region where the seismic risk is relatively high when compared with areas with a similar hazard level.

Lastly, the thesis focused on CAT bond, as risk-transferring method for possible high losses from natural hazard. Despite their growing importance, different and relatively few researches on CAT bond pricing can be found in scientific literature. Usually, natural disasters pose a set of challenging problems because they involve potentially high losses that are extremely uncertain. For this reason, the thesis proposes a mathematical framework for pricing CAT bonds, able to consider uncertainties in model parameters. Neglecting such uncertainties might lead to assuming risks that are higher than intended. The proposed mathematical derivation was first applied to a benchmark case study, showing the influence of the knowledge level on the final distribution of the CAT bond price. In particular, less uncertainties on model input parameters lead to a low spread price distribution and vice versa. With the proposed model it is possible to derive the CAT bond price corresponding to a given quantile of the price distribution.

Finally, the developed CAT bond pricing theory was included in the wider context of bond-design for financially covering a region exposed to potential high losses. The thesis illustrated a possible CAT bond-based coverage configuration, against earthquake-induced losses, for the Italian territory. Italy was divided into three zones and CAT bond was priced for every zone. The CAT bond price reflects the susceptibility and frequency to the high losses of the considered zone: the price is low in highly seismic areas, and it is high in less seismic areas.

6.1 Further studies

Models proposed in this works are useful tools and starting points for further studies and developments. The developed model for the

computation of losses from business interruption, can be integrated in a more general framework, able to consider possible functional relationships between firms; in this way it is possible to include other sources of indirect losses. This model allows performing scenario analysis, and seismic risk analysis at regional level, with clear reference to indirect losses due to business interruption.

The procedure used for obtaining the Italian seismic risk map can be extended for the risk assessment of other types of structures or losses. From risk maps and loss exceedance probability curves, insurance companies, but also national authorities, can determine types and location of buildings they would like to insure, what coverage to offer, and what price to charge.

In this context, CAT bond represents a possible tool for transferring the risk and avoid the insolvency risk. The proposed formulation is general, such that the loss distribution can be calibrated on different types of losses coming from different natural hazards. The proposed CAT bond pricing theory uses indemnity-based trigger, with possible problems of transparency for investors and moral hazard. Further researches are needed for developing a more transparent and physically based trigger.

7 Aknowledgments

At the end of this work, I would like to express my deepest gratitude to some people who have guided and helped me during these years of study.

First and foremost, I offer my sincerest gratitude to my supervisor, *Prof. Ing. Carlo Pellegrino* of the University of Padova. For me, it is really a pleasure to work with him; in particular, his guidance, dedication and human and scientific advices have been fundamental not only during this doctorate years, but since a I was an undergraduate student.

I would like to thank Eng. *Mariano Angelo Zanini* for guiding me, for his patience and the thoughtful support of my work. His competence and devotion to research have been an example for me.

My sincere gratitude to *Prof. Paolo Gardoni*, of the University of Illinois in Urbana-Champaign, for welcoming me in his research group. His enthusiasm for research, availability, scientific and human support, made my American staying extremely formative and unforgettable.

I would like to acknowledge and express my appreciation to *Eng. Flora Faleschini*, always present during these three years. Every discussion with her, her advices and time spent together have been important for me.

A special thank to all the friends and colleagues of the University of Padova and the University of Illinois in Urbana-Champaign.

Finally my deepest gratitude goes to my parents, my family and my friends; I will be forever grateful for all their ceaseless support, inspiration and encouragement of which I'm still a beneficiary, hence forever their debtor.

8 References

Ahmad, N., Crowley, H., Pinho, R., 2011, *Analytical fragility functions for reinforced concrete and masonry buildings aggregates of Euro-Mediterranean regions – UPAV methodology*. Internal report, Syner-G Project, 2009/2012.

Applied Technology Council (ATC), 2011, *Guidelines for Seismic Performance Assessment of Buildings*, ATC-58, Redwood City, California.

Asprone, D., Jalayer, F., Simonelli, S., Acconcia, A., Prota, A., Manfredi, G., 2013, *Seismic insurance model for the Italian residential building stock*, 2013, 44:70-79.

Ayyub, B. M. (2015). *Practical resilience metrics for planning, design, and decision making*, ASCE-ASME Journal of Risk and Uncertainty in Engineering Systems, Part A: Civil Engineering, 1(3): -1-1.

Bai, J.W., Hueste, M.B.D., Gardoni P., 2009, *Probabilistic Assessment of Structural Damage due to Earthquakes for Buildings in Mid-America*, Journal of Structural Engineering – ASCE, 135(10): 1155-1163.

Baryshnikov, Y., A. Mayo, and D. Taylor, (2001), *Pricing of CAT Bonds*, Preprint.

Bindi, D., Pacor, F., Luzi, L., Puglia, R., Massa, M., Ameri, G., Paolucci, R. (2011). *Ground motion prediction equations derived from the Italian strong motion database*. Bulletin of Earthquake Engineering, 9: 1899–1920.

Biondini, F., Camnasio, E., Titi, A. (2015). *Seismic resilience of concrete structures under corrosion.* Earthquake Engineering and Structural Dynamics, 44(14): 2445-2466.

Bournas, D. A., Negro, P., Taucer, F. F. (2014). *Performance of industrial buildings during the Emilia earthquakes in Northern Italy and*

recommendations for their strengthening. Bulletin of Earthquake Engineering, 12:2383-2404.

Bozza, A., Asprone, D., Jalayer, F., Manfredi, G., 2015, *National-level prediction of expected seismic loss based on historical catalogue*, Bulletin of Earthquake Engineering, 15(7):2853-2877.

Braun, A., (2016), *Pricing in the Primary Market for Cat Bonds: New Empirical Evidence*, The Journal of Risk and Insurance, 83(4): 811-847.

Broccardo, M., Galanis, P., Esposito, S., & Stojadinovic, B. (2015). *Resilience-based risk assessment of civil systems using the PEER framework for seismic hazard*. In European Safety and Reliability Conference ESREL 2015.

Bruneau, M., Chang, S. E., Eguchi, R. T., Lee, G. C., O'Rourke, T. D., Reinhorn, A. M., Shinozuka, M., Tierney, K., Wallace, A. W., von Winterfeldt, D. (2003). *A framework to quantitatively assess and enhance the seismic resilience of communities.* Earthquake Spectra, 19(4):733–752.

Burnecki, K., and G. Kukla, (2003), *Pricing of Zero-Coupon and Coupon CAT Bonds*, Applied Mathematics, 30: 315-324.

Burnecki, K., G. Kukla, and D. Taylor, (2005), *Pricing Catastrophe Bond*, in: P. Cizek, W. Härdle, R. Weron (eds.), Statistical Tools for Finance and Insurance (Berlin: Springer).

Burton, H.V., Deierlein, G., Lallemant, D., Lin, 457 T. (2015). *Framework for incorporating probabilistic building performance in the assessment of community seismic resilience*. Journal of Structural Engineering-ASCE, 142(8): -1—1.

Calvi G.M. (2013). *Choices and Criteria for Seismic Strengthening*. Journal of Earthquake Engineering, 17:769-802.

Cardone D., Flora A. (2014). *Direct displacement loss assessment of existing RC buildings pre and post-seismic retrofitting: a case study*. Soil Dynamics and Earthquake Engineering, 64:38-49.

Catenacci, V., *Dissesto geologico e geoambientale in Italia dal dopoguerra al 1990*, 1992, Istituto poligrafico e Zecca dello Stato.

Cimellaro, G. P., Reinhorn, A. M., Bruneau, M. (2006). *Quantification of seismic resilience*. Proceedings of the 8th US National Conference on Earthquake Engineering, 18th-22nd April 2006, San Francisco, California, Paper #1094.

Cimellaro, G. P., Reinhorn, A. M., Bruneau, M. (2010a). *Framework for analytical quantification of disaster resilience*. Engineering Structures, 32: 3639-3649.

Cimellaro, G. P., Reinhorn, A. M., Bruneau, M. (2010b). *Seismic resilience of a hospital system*. Structure and Infrastructure Engineering, 6(1–2):127–144.

"COMFOLIGNO" L'attività del Centro Operativo Misto Intercomunale di Foligno nell'Emergenza Sisma del 26/9/1997, 1998, https://www.slideshare.net/GianmarioGnecchi/com-foligno-questa-pubblicazione-stata-realizzata-dallo-staff-che-ha-diretto-e-coordinato-il-com-di-foligno-durante-lemergenza-del-terremoto-umbriamarche-del-1997, accessed October 16, 2017.

Commissariato per la Ricostruzione. *Ricostruzione: Stato di attuazione e programmazione.* Aggiornamento al 31 maggio; 2012. Available from: www.commissarioperlaricostruzione.it [in Italian], accessed October 16, 2017.

Cornell, C. (1968). *Engineering seismic risk analysis*. Bulletin of Seismological Society of America, 58(5):1583-1606.

Cornell, C.A., Krawinkler, H. (2000) *Progress and challenges in seismic performance assessment*, PEER Centre News,

http://peer.berkeley.edu/news/2000spring/index.html, accessed January 8, 2018.

Corriere della Sera, 2017. Day: August 24, 2017. http://archivio.corriere.it/Archivio/interface/slider_pagine.html#!/24-08-2017/24-08-2017/NobwRAdghgtgpmAXGAJlALlMAaMAzAJwHsYkwAmAFgHoAGADmvNoEYB2HMdIsqux5uzABfbOGjwyAazgBPAO5ECKTujgAPdGREBdIA, accessed October 16, 2017.

CRESME, Fondazione Housing Sociale (2011), *Il mercato delle costruzioni 2012*. XIX Rapporto Congiunturale e previsionale CRESME. Lo scenario di breve periodo, 2015.

Crowley, H., Silva, V., 2013, *OpenQuake Engine Book: Risk v1.0.0*, GEM Foundation, Pavia, Italy.

Cummins, J.D., (2008), *CAT Bonds and Other Risk-Linked Securities: State of the Market and Recent Developments*, Risk Management and Insurance Review, 11(1): 23-47.

Cutler, H., Shields, M., Tavani, D., & Zahran, S. (2016). *Integrating engineering outputs from natural disaster models into a dynamic spatial computable general equilibrium model of Centerville*. Sustainable and Resilient Infrastructure, 1(3-4), 169-187.

Daniell, J.E., Khazai, B., Wenzel, F., Vervaeck, A., 2011, *The CATDAT damaging earthquakes database*, Nat. Hazards Earth Syst. Sci., 11, 2235–2251.

Daniell, J.E, Vervaeck, A., 2012. CEDIM earthquake loss estimation series research report 2012-01. Karlsruhe: CEDIM; 2012.

Der Kiureghian, A., (1989). *Measures of structural safety under imperfect states of knowledge*. Journal of Structural Engineering, 115(5), 1119–1140.

Der Kiureghian, A., (2005). *Non-ergodicity and PEER's framework formula*. Earthquake Engineering and Structural Dynamics, 34:1643–1652.

DM 65 (2017) *Sisma Bonus – Linee guida per la classificazione del rischio sismico delle costruzioni e relativi allegati*. Modifiche all'articolo 3 del Decreto Ministeriale n° 58 del 28/02/2017. Ministero delle Infrastrutture e dei Trasporti, Roma.

Dolce, M., Manfredi, G. (2015). *White book on private 480 reconstruction outside the historical centers in the municipalities hit by the 6th April 2009 Abruzzo earthquake*. Retrieved online at <https://www.cineas.it/> (Dec. 27, 2016).

Dosanjh, K. (2011). Japan's economy after the quake. *The Economist Intelligence Unit*. The Economist, <https://www.eiu.com/public/topical_report.aspx?campaignid=japanquake> (Dec. 27, 2016).

Ellingwood, B.R., Celik, O.C., Kinali, K. (2007). *Fragility assessment of building structural systems in Mid-America*. Earthquake Engineering and Structural Dynamics, 36: 1935-1952.

Fischer, E. P. (2014). *Learning from earthquakes: 2014 Napa Valley earthquake reconnaissance report*. Lyles School of Civil Engineering Graduate Student Reports. Paper 1. <http://docs.lib.purdue.edu/civlgradreports/1> (Dec. 27, 2016).

Franco, G., (2010), *Minimization of trigger error in Cat-in-a-Box parametric earthquake catastrophe bonds with an application to Costa Rica*. Earthquake Spectra, 26(4): 983-998.

Fujita, S., Nakamura, I., Furuya, O., Watanabe, T., Minagawa, K., Morishita, M., Kamada, T., Takahashi, Y. (2012). *Seismic damage of mechanical structures by the 2011 Great East Japan Earthquake*. 15th World Conference on Earthquake Engineering WCEE, 24-28 September 2012, Lisbon, Portugal.

Galeotti, M., M. Gürtler, and C. Winkelvos, (2013), *Accuracy of Premium Calculation Models for CAT Bonds – An Empirical Analysis*, Journal of Risk and Insurance, 80(2): 401-421.

Gardoni, P., A. Der Kiureghian, and K.M. Mosalam, (2002), *Probabilistic Capacity Models and Fragility Estimates for Reinforced Concrete Columns based on Experimental Observations*, Journal of Engineering Mechanics, 128(10): 1024-1038.

Gardoni P., Guevara-Lopez F., Contento A. (2016). *The Life Profitability Method (LPM): a financial approach to engineering decisions*. Structural Safety, 63: 11-20.

Gardoni, P., and J. LaFave, (Eds.), (2016), *Multi-hazard Approaches to Civil Infrastructure Engineering*, Springer.

Gardoni, P., C. Murphy, and A. Rowell, (Eds.), (2016), *Societal Risk Management of Natural Hazards*, Springer.

Goda, K., 2013, Basis risk of earthquake catastrophe bond trigger using scenario-based versus station intensity-based approaches: a case study for southwestern British Columbia. Earthquake Spectra, 29(3): 757-775.

Goda, K., Atkinson, G.M., 2009, *Interperiod dependence of ground-motion prediction equations: a copula prospective*, Bulletin of the Seismological Society of America, 2009, 99(2A):922-927.

Goda, K., Atkinson, G.M., 2010, *Intraevent spatial correlation of ground-motion parameters using SK-net data*, Bulletin of the Seismological Society of America, 2009, 100(6):3055-3067.

Goda, K., Hong, H.P., 2008, *Spatial correlation of peak ground motions and response spectra*, Bulletin of the Seismological Society of America, 2008, 98(1):354-365.

Gonzalez, E., Almazan, J., Beltran, J., Herrera, R., Sandoval, V. (2013). *Performance of stainless steel winery tanks during the 02/27/2010 Maule Earthquake*. Engineering Structures, 56: 1402-1418.

Guidoboni, E., Ferrari, G., Mariotti, D., Comastri, A., Tarabusi, G., Valensise, G., 1997, *CFTI4med – Catalogue of Strong Earthquakes in Italy 461 B.C. – 1997 and Mediterranean Area 760 B.C. – 1500, An advanced Laboratory oh Historical Seismology*. http://storing.ingv.it/cfti4med/, accessed October 16, 2017.

HAZUS-MR4 (2003) *Multi-hazard loss estimation methodology – Earthquake Model* – Technical Manual.

Härdle, W. K., and B.L. Cabrera, (2010), *Calibrating CAT Bonds for Mexican Earthquakes*, The Journal of Risk and Insurance, 77(3): 625-650.

Hofer, L., Zanini, M.A., Faleschini, F., Pellegrino, C. (2018a). *Profitability analysis for assessing the optimal seismic retrofit strategy of industrial productive processes with business interruption consequences.* ASCE – Journal of Structural Engineering, 144(2): 04017205

Hofer L., Gardoni P., Zanini M.A., (2018b) *Reliability-based CAT bond pricing considering parameter uncertainties.* Insurance: mathematics and economics (submitted).

Holzer, T.L, Savage, J.C., 2013. *Global earthquake fatalities and population*. Earthquake Spectra, 29(1): 155-175.

Istituto Nazionale di Statistica (2011) *15-esimo Censimento Generale della popolazione e delle abitazioni*, 2011. Postel Editore, Roma.

Italian Anticorruption Authority. (2017). *Guidelines for the selection of a financial project assessment model: the Public Sector Comparator method and the economic analysis of the costs*. <https://www.anticorruzione.it/portal/public/classic/AttivitaAutorita/Pubblicazioni/RapportiStudi/_PSC/#_Toc236745905> (May 2, 2017).

Italian Ministry of Infrastructures (2008). *Technical Standards for Constructions*, NTC-2008-1-14 (in Italian).

Jacques, C. C., McIntosh, J., Giovinazzi, S., Kirsch, T. D., Wilson, T., Mitrani-Reiser, J. (2014). *Resilience of the Canterbury hospital system to the 2011 Christchurch earthquake*. Earthquake Spectra, 30(1): 533-554.

Jaeger, L., S. Mueller, and S. Scherling, 2010, Insurance-Linked Securities: What Drives Their Returns?, *Journal of Alternative Investments*, 13(2): 9-34.

Kostov, M., Vaseva, E., Kaneva, A., Koleva, N., Verbanov, G., Stefanov, D., Darvarova, E., Salakov, D., Simeonova, S., Cristoskov, L., *Application to Sofia*. RISK-UE WP13, 2004.

Kumar, R., and Gardoni, P., (2013). *Second-order logarithmic formulation for hazard curves and closed-form approximation to annual failure probability*. Structural Safety, 45, 18-23.

Kumar, R., D.B.H. Cline, and P. Gardoni, (2015), *A stochastic framework to model deterioration in engineering systems*, Structural Safety, 53: 36-43.

Kunreuther, H., (2001), *Mitigation and financial risk management for natural hazards*, The Geneva papers on risk and insurance, 26(2): 277-296.

Kunreuther, H., Pauly, (2001), *Insuring against catastrophes. The known, the unknown, and the unknowable in financial risk management: measurement and theory advancing practice*, Princeton University Press, Pages: 210-238.

Lanzano, G., Salzano, E., Santucci de Magistris, F., Fabbrocino, G. (2012). *An observational analysis of seismic vulnerability of industrial pipelines*. Chemical Engineering Transactions, 26: 567-572.

Legge 2 febbraio 1974, n. 64. *Provvedimenti per le costruzioni con particolari prescrizioni per le zone sismiche*.

Liu, J., Shi, Z., Lu, D., Wang, Y. (2017). *Measuring and characterizing community recovery to earthquake: the case of 2008 Wenchuan*

earthquake, China. Natural Hazards and Earth System Sciences, doi:10.5194/nhess-2017-72.

Mander, J. B., Sircar, J., Damnjanovic, I. (2012). *Direct loss model for seismically damaged structures*. Earthquake Engineering and Structural Dynamics, 41: 571-586.

McAllister, T. (2013). *Developing Guidelines and Standards for Disaster Resilience of the Built Environment: A Research Needs Assessment.* Gaithersburg, MD.

Meletti, C., Montaldo, V. (2007). *Stime di pericolosità sismica per diverse probabilità di superamento in 50 anni: valori di ag*. Progetto DPC-INGV S1, Deliverable D2, <http://esse1.mi.ingv.it/d2.html> (Dec. 27, 2016).

Meletti, C., Galadini, F., Valensise, G. (2008). *A seismic source zone model for the seismic hazard assessment of the Italian territory*. Tectonophysics, 450:85–108.

Mian, M.A. (2002). *Project Economics and Decision Analysis. Volume 1: Deterministic Models*, Tulsa Oklahoma: PennWell Books; 2002.

Mieler, M., Stojadinovic, B., Budnitz, R., Comerio, M., Mahin, S. (2014). *A framework for linking community-resilience goals to specific performance targets for the built environment*. Earthquake Spectra, 31(3): 1267-1283.

Ministro dei LL.PP di concerto con il Ministro dell'Interno, Decreto Ministeriale 19 giugno 1984. *Norme tecniche relative alle costruzioni in zone sismiche.*

Munich Re, NatCatSERVICE (2011) NATHAN *World Map of Natural Hazards*, version 2011. Munchener Ruckversicherungs-Gesellschaft, Geo Risks Research, NatCatSERVICE.

Munich RE, 2017, *Natural catastrophes 2016 - Analyses, assessments, positions*, 2017 Issue.

Norme Tecniche per le Costruzioni (2008) Decreto Ministeriale 14 gennaio 2008 – *Norme Tecniche per le Costruzioni NTC 2008*. Supplemento ordinario n°30 Gazzetta Ufficiale 4 febbraio 2008, n° 29.

OECD (2014). Economic Outlook No. 95 – *Long-term baseline projections*, 2014.

OPCM3274 (2003) *Primi elementi in materia di criteri generali per la classificazione sismica del territorio nazionale e di normative tecniche per le costruzioni in zona sismica*, G.U.R.I. n. 72 del 08/05/2003.

OPCM3362 (2004) *Modalità di attivazione del fondo per interventi straordinari della Presidenza del consiglio dei ministri istituito ai sensi dell'articolo 32-bis del decreto legge 30 settembre 2003*, n. 269, convertito, con modificazioni, dalla legge 24 novembre 2003, n. 326, G.U.R.I. n. 165 del 16/07/2004.

OPCM3376 (2004) *Modalità di attivazione del fondo per interventi straordinari della Presidenza del consiglio dei ministri istituito ai sensi dell'articolo 32-bis del decreto legge 30 settembre 2003*, n. 269, convertito, con modificazioni, dalla legge 24 novembre 2003, n. 326, G.U.R.I. n. 225 del 24/09/2004.

OPCM 3519 del 28 aprile 2006. All. 1b, *Pericolosità sismica di riferimento per il territorio nazionale*. Available from: http://zonesismiche.mi.ingv.it/, accessed October 16, 2017.

Pace, B., Peruzza, G., Lavecchia, G., Boncio, P. (2006). *Layered seismogenic source model and probabilistic seismic-hazard analyses in Central Italy*. Bulletin of Seismological Society of America, 96(1): 107-132.

Phan, H. N., Paolacci, F., Corritore, D., Akbas, B., Uckan, E., Shen, J. J. (2016). *Seismic vulnerability mitigation of liquefiedgas tanks using concave sliding bearings*. Bulletin of Earthquake Engineering, 14: 3283-3299.

Porter, K.A., Beck, J.L., Shaikhutdinov, R., 2004, *Simplified Estimation of Economic Seismic Risk for Buildings*, Earthquake Spectra, 20(4): 1239−1263.

Regione Basilicata, Eventi sismici, Rosa: intervenire subito dopo gravi ritardi, 2011, http://www.regione.basilicata.it/giunta/site/giunta/detail.jsp?sec=100133&otype=1012&id=292873&value=consiglioInforma, accessed October 16, 2017.

Regione Emilia Romagna, 2012, *Sei mesi dal sisma: un primo bilancio*, http://www.regione.emilia-romagna.it/terremoto/sei-mesi-dal-sisma/approfondimenti/il-documento-completo , accessed October 16, 2017.

Regione Molise – *Struttura Commissariale. Il percorso della ricostruzione; 2010.* Available from: http://www.regione.molise.it/web/grm/sis.nsf [in Italian], accessed October 16, 2017.

Rose, A. (2004). *Defining and measuring economic resilience to disasters.* Disaster Prevention and Management, 13(4):307–314.

Rovida, A., Locati, M., Camassi, R., Lolli, B., Gasparini, P., 2016, *CPTI15, the 2015 version of the Parametric Catalogue of Italian Earthquakes*, Istituto Nazionale di Geofisica e Vulcanologia, doi:http://doi.org/ 10.6092/ INGV.IT-CPTI15.

Saha, S. K., Sepahvand, K., Matsagar, V. A., Jain, A. K., Marburg, S. (2016). *Fragility analysis of base-isolated liquid storage tanks under random sinusoidal base excitation using generalized polynomial chaos expansion-based simulation*. Journal of Structural Engineering-ASCE,142(10):-1-1.

Shao, J., (2015), *Modelling Catastrophe Risk Bond*, PhD Thesis in Mathematical Science – University of Liverpool.

Sharma, N., Tabandeh, A., Gardoni, P. (2017). *Resilience analysis: a mathematical formulation to model resilience of engineering system,*

Sustainable and Resilient Infrastructure, doi: 10.1080/23789689.2017.1345257

Swan, S. W., Miller, D. D., Yanev, P. I. (1977). *The Morgan Hill Earthquake of April 24, 1984 – Effects on industrial facilities, building, and other facilities*. Earthquake Spectra, 1(3): 457-568.

Takahaschi, Y., (2017), *Innovative Derivatives to Drive Investment in Earthquake Protection Technologies.* In Gardoni, P., (Ed.) Risk and Reliability Analysis: Theory and Applications, Springer.

Tokui, J., Kawasaki, K., Miyagawa, T. (2017) *The economic impact of supply chain disruptions from the Great East-Japan earthquake.* Japan and the World Economy, 41: 59-70.

Xu, N., Guikema, S. D., Davidson, R. A., Nozick, L. K., Çağnan, Z., Vaziri, K. (2007). *Optimizing cheduling of post-earthquake electric power restoration tasks.* Earthquake Engineering and Structural Dynamics, 36(2):265–284.

Williams, R. J., Gardoni, P., Bracci, J.M. (2009). *Decision analysis for seismic retrofit of structures*. Structural Safety, 31(2): 188-196.

Zanini, M.A., Hofer, L., Faleschini, F., Pellegrino, C. (2017). *The seismic risk map of Italy.* 6th International Workshop on Design in Civil and Environmental Engineering, Cagliari, Italy, 9-11 November.

Zio, E. (2006). *An introduction to the basics of reliability and risk analysis. Series on Quality*, Reliability and Engineering Statistics, Vol.13, World Scientific Publishing Co. Pte. Ltd., 5 Toh Tuck Link, Singapore 596224.